A NUMERICAL SIMULATION OF MULTIPLE-SHAKER MODAL TESTING

by

Joseph F. Stafford

Thesis submitted to the Graduate Faculty of the
Virginia Polytechnic Institute and State University
in partial fulfillment of the requirements for the degree of

MASTER OF SCIENCE

in

Aerospace and Ocean Engineering

APPROVED:

W. L. Hallauer, Chairman

J. A. Schetz

T. A. Weisshaar

July, 1976

Blacksburg, Virginia

ACKNOWLEDGEMENTS

The author wishes to extend his thanks to Dr. William L. Hallauer for his many hours of guidance and support during the preparation of this thesis, and to committee members Doctors Joseph A. Schetz and Terry A. Weisshaar for their assistance. In addition, the author wishes to express his appreciation to the Langley Research Center of the National Aeronautics and Space Administration for their financial support of this project, (NASA Research Grant No. NSG 1276).

Thanks also go to Mr. Jan Crane for his assistance with the computer work, to Ms. Willie Hylton for her excellent typing, and to two very good friends, Miss Kathleen Stueber and Mr. Reginald Figard, for all the help they gave. Last, but certainly not least, a special word of thanks to the author's parents, Mr. and Mrs. Joseph G. Stafford, and to his sister, Jane, for their continuous interest and encouragement.

TABLE OF CONTENTS

LIST OF FIGURES

LIST OF FIGURES - continued

LIST OF FIGURES - continued

LIST OF FIGURES - continued

LIST OF TABLES

LIST OF TABLES - continued

NOMENCLATURE

$[A]$	Transfer function matrix
$[A_R]$	Coincident response matrix
$[A_I]$	Quadrature response matrix
a_{max}	Matrix element with the largest absolute value in the matrix
$[C]$	Generalized damping matrix
$[c]$	Damping matrix
D	Determinant of the coincident response matrix
D'	Slope of determinant versus frequency curve
$\{F\}$	Force-amplitude vector
$\{f\}$	Force vector
$[g]$	Structural damping matrix
$[K]$	Generalized stiffness matrix
$[k]$	Stiffness matrix
$[M]$	Generalized mass matrix
$[m]$	Mass matrix
T	Kinetic energy
T_i	Kinetic energy of the i^{th} mode
T_{avg}	Average kinetic energy
U	Potential energy
U_i	Potential energy of the i^{th} mode
U_{avg}	Average potential energy
$\{X\}$	Response-amplitude vector
$\{x\}$	Response vector

α	Mass to damping proportionality constant
β	Stiffness to damping proportionality constant
$\{\xi\}$	Generalized response vector
$\{\bar{\xi}\}$	Generalized response amplitude vector
$[\Phi]$	Coordinate transform matrix
$\{\phi\}$	Mode shape vector
ω	Natural frequency
$[\ ]$	Square matrix
$\{\ \}$	Column vector
$\{\ \}^T$,	Row vector
$\{\ \}_i$	i^{th} vector of a set of n vectors
q_i	i^{th} element of vector q
Q_i	i^{th} diagonal element of diagonal matrix Q
$\{\ _i\}_j$	i^{th} element of the j^{th} vector of a set of n vectors
$[\searrow]$	Diagonal matrix

I. INTRODUCTION

One of the major difficulties encountered in the vibration testing of a structure is the tendency of the structure to respond simultaneously in several of its normal modes. This is especially true for structures which have modes with closely spaced natural frequencies*. This tendency to respond in several modes prevents the direct measurement of the natural frequency and mode shape of any single mode. One approach to the solution of the problem is to employ a procedure to predict the distribution of excitation which will cause the structure to respond in only one mode. Such a procedure is likely to be simpler, cheaper, and more accurate than the analytic filtering of vibration data required to separate the effects of a given mode from the response in several modes.

In predicting the distribution of excitation, both the positions and the relative force-amplitude distribution of the shakers should be defined. However, since there is at present no analytical method for determining optimum shaker locations, only the force-amplitude distributions can be determined. The actual positioning of the shakers is left to the judgment of the test engineers.

The basic objective of this study has been to develop and test the numerical implementation of an analytical method due to

---

* All standard concepts of structural vibration theory discussed in this thesis (e.g., natural frequencies, normal modes, hysteretic damping) are defined in detail by Meirovitch (Reference 4).

Traill-Nash (Reference 1) and Asher (Reference 2) for determining the force-amplitude distributions required to isolate individual vibration modes. Although the method is analytical, it employs only experimental transfer function data and therefore is fully suitable for hardware testing. Experimental data has been simulated numerically in this study.

II. TECHNICAL DISCUSSION

A. Modal Separation Theory

In order to evaluate the response characteristics of the structure, a method of modal separation first proposed by Traill-Nash (Reference 1) and Asher (Reference 2) was used in the development of the computational technique. This method is usually called "Asher's Method," even though that name does not properly account for the contribution of Traill-Nash. See the comment by Fraeijs de Veubeke and the reply by Craig and Su, (Reference 12).

For a structural system with hysteretic damping and many degrees of freedom, the matrix equation of motion is given by

$$[m]\{\ddot{x}\} + (1/\omega)[c]\{\dot{x}\} + [k]\{x\} = \{f\} . \qquad (1)$$

This equation is valid for systems with sinusoidal excitation and response at frequency ω. Therefore, the force, $\{f\}$, and the response, $\{x\}$, are denoted by

$$\{f\} = \{F\} e^{i\omega t} \quad \text{and} \quad \{x\} = \{X\} e^{i\omega t} , \qquad (2)$$

and the equation of motion reduces to

$$-\omega^2 [m]\{X\} + i[c]\{X\} + [k]\{X\} = \{F\} . \qquad (3)$$

The natural frequencies, ω_n, of the system can be determined using the equation of motion for undamped, free vibration,

$$-\omega_n^2 [m]\{\phi\}_n + [k] \{\phi\}_n = \{0\} . \quad (4)$$

The eigenvalues of Equation 4 define the natural frequencies of the structure, and the eigenvectors are the natural mode shapes, $\{\phi\}_n$. The mode shapes are used to develop a coordinate transformation which is useful in the solution of the damped problem.

Using a displacement coordinate transformation described by Bisplinghoff, Ashley and Halfman (Reference 3), the mode shapes are used to define a matrix, $[\Phi]$, in which each mode shape forms a column. Then, the coordinate transformation for a system with n degrees of freedom is given by

$$X_i = \sum_{j=1}^{n} \{\phi_i\}_j \xi_j , \text{ or } \{X\} = [\Phi] \{\xi\} . \quad (5)$$

Substitution of Equation 5 into Equation 3, and premultiplication of the result by $[\Phi]^T$ yields an equation of motion in the form

$$[\Phi]^T ([k] - \omega^2 [m] + i [c]) [\Phi] \{\xi\} = [\Phi]^T \{F\}. \quad (6)$$

The use of the independent mode shapes as the transform matrix in the coordinate transformation uncouples the equations both inertially and elastically. The result of the matrix multiplications in Equation 6 is the production of diagonal mass and stiffness matrices as described by Meirovitch (Reference 4). Using the nomenclature of "generalized matrices", the diagonal generalized mass matrict is defined by

$$[M] = [\Phi]^T [m] [\Phi] , \tag{7}$$

and the diagonal generalized stiffness matrix is given by

$$[K] = [\Phi]^T [k] [\Phi]. \tag{8}$$

In addition, the restriction of the type of damping to proportional damping, defined by

$$[c] = \alpha[m] + \beta[k] , \tag{9}$$

where α and β are constants, results in the generation of a diagonal generalized damping matrix described by

$$[C] = [\Phi]^T [c] [\Phi]. \tag{10}$$

Substituting Equations 7, 8, and 10 into Equation 6 yields an equation of motion in uncoupled form,

$$([K] - \omega^2 [M] + i [C]) \{\xi\} = [\Phi]^T \{F\} . \tag{11}$$

Solving the above equation for the generalized response, $\{\xi\}$,

$$\{\xi\} = [([K] - \omega^2[M] + i[C])]^{-1} [\Phi]^T \{F\} , \tag{12}$$

or, defining each element of the vector,

$$\xi_i = \frac{\{\phi\}_i^T \{F\}}{M_i(\omega_i^2 - \omega^2) + iC_i} . \tag{13}$$

With the generalized response determined by Equation 13, the displacement response, X, is found by applying the coordinate transformation defined in Equation 5.

$$\{X\} = \sum_{i=1}^{n} \frac{\{\phi\}_i \{\phi\}_i^T}{M_i (\omega_i^2 - \omega^2) + iC_i} \{F\} . \qquad (14)$$

The portion of Equation 14 under the summation defines the transfer function matrix, [A]. It is clear that this matrix is complex, and therefore the response will have both coincident (in-phase) and quadrature (out-of-phase) portions. Using the transfer function matrix, the response equation, Equation 14, becomes

$$\{X\} = [A_R + A_I] \{F\} , \qquad (15)$$

where $[A_R]$ is the coincident response matrix, and $[A_I]$ is the quadrature response matrix. These matrices correspond to the real and imaginary parts of the transfer function matrix, respectively.

Bishop and Gladwell (Reference 5, p. 270) proved that: "A necessary and sufficient condition for the response to be in an undamped natural mode is that (all) response be in quadrature with the exciting forces." Therefore, for the case of resonant response in a true mode, Equation 15 becomes

$$[A_R] \{F\} = \{0\} , \qquad (16)$$

and,

$$i\,[A_I]\,\{F\} = \{X\} \quad . \tag{17}$$

The frequencies, ω, for which the determinant of the coincident response matrix has a value of zero are the natural frequencies, and the eigenvectors of that matrix are the amplitudes of the forces at the respective degrees of freedom which will cause the system to vibrate in a given mode.

Manipulation of the real part of the summation term of Equation 14 shows the coincident response matrix used in Equations 15 and 16 to be

$$[A_R] = \sum_{j=1}^{n} \frac{M_j\,(\omega_j^2 - \omega^2)}{M_j^2\,(\omega_j^2 - \omega^2)^2 + C_j^2}\,\{\phi\}_j\,\{\phi\}_j^T \quad . \tag{18}$$

Note that Equation 18 is valid only for the case of proportional hysteretic damping. For other types of damping, different expressions are used to define the coincident response matrix.

In order to determine the natural frequencies, the proper procedure is to plot the determinant of the coincident response matrix as a function of frequency,

$$D(\omega) = \text{Det}\quad [A_R] \tag{19}$$

Such a plot will have certain points where the line will intersect the zero-determinant axis, and the frequencies corresponding to

these zero-crossings are the natural frequencies of vibration. To determine the exact value of these frequencies, a numerical convergence procedure should be performed starting with frequency values in the region of the zero-crossing. A more complete description of the root-finding procedure is found in Appendix B.

Once the natural frequency has been determined and the corresponding force eigenvector has been calculated, the displacement response shape, {X}, may be determined from Equation 14. This vector will be complex, with the real part representing the coincident response, and the imaginary part representing the quadrature response.

In cases where all of the degrees of freedom of the structure are excited by a shaker, the frequencies determined for the zero-determinant values will always be the natural frequencies of the system, and the modes of vibration excited by the shakers will be the true natural modes. However, in cases where the number of shakers is less than the number of degrees of freedom, zero-crossings will often be found at certain non-resonant frequencies, which are called false resonances. Forced response at a false resonance does exhibit partial quadrature response, but the motion does not approximate any natural vibration mode of the system. In addition, exciting some but not all degrees of freedom will result at best in approximations of true modes, as only the degrees of freedom which are being shaken will exhibit purely quadrature response.

B. Modal Quality Determination

For the case of exciting a reduced number of degrees of freedom, it is necessary to evaluate the quality of each mode generated. Not only is it essential to determine the false modes, but some determination must be made of whether the approximate true modes are sufficiently close to the natural modes to be of value.

The identification of false modes is relatively simple since the plot of the coincident response determinant versus frequency will provide an indication of which of the zero-crossings correspond to false modes. If the damping is small, the slope of the curve at a zero-crossing which corresponds to a true resonant frequency will be nearly vertical. This is referred to as a "sharp crossing." If the slope at any crossing is much gentler than the slopes at the sharp crossings, this crossing is likely to be a false resonance. This slope test is a less accurate indication of the false modes in the case of large values of damping. Since the increase in damping causes the determinant plot to be somewhat gentler in slope, large values of damping may cause the slope at a true resonance to appear quite small.

Another test used in the locating of false resonances is an examination of a plot of the coincident response versus the quadrature response resulting from any forced excitation. It was shown by Kennedy and Pancu (Reference 6) that the coincident-quadrature response for a true resonant condition will form a perfect circle

when the response of the system at a narrow band of frequencies centered on the resonant frequency is plotted in the Argand plane. This test will not only identify false modes, but also provide a good measure of the quality of the approximate modes. The deviation from the circular shape will be small in the case of approximately true modes, due to the presence of modes other than the desired mode. The extent of deviation indicates the amount of modal distortion caused by other modes. Therefore, the best approximate modes are those for which the response will most closely approximate a circle in an Argand plane plot.

Perhaps the best and simplest test of an indicated resonant frequency and corresponding mode is to evaluate the kinetic and potential energy of the structure in that vibration mode. For a system of n degrees of freedom, the kinetic energy, T, of the structure is

$$T = \tfrac{1}{2} \{\dot{x}\}^T [m] \{\dot{x}\} \quad , \tag{20}$$

where

$$\{x\} = [\Phi] \{\xi\} \tag{21}$$

Using the above equation as a transformation, and using the definition of the generalized mass matrix found in Equation 7, the kinetic energy expression in Equation 20 reduces to

$$T = \tfrac{1}{2} \{\dot{\xi}\}^T [M] \{\dot{\xi}\}. \tag{22}$$

The diagonal nature of the generalized mass matrix reduces Equation 22 to a simple summation which sums the effect of each vibration mode in the total vibration. For each mode, j, of the n degree of freedom system, the kinetic energy of the mode, T_j, is given by

$$T_j = \tfrac{1}{2} M_j \dot{\xi}_j^2 \tag{23}$$

and the total kinetic energy of the system is

$$T = \sum_{j=1}^{n} T_j \quad , \quad \text{or} \quad T = \tfrac{1}{2} \sum_{j=1}^{n} M_j \dot{\xi}_j^2 \tag{24}$$

For these expressions, the generalized response amplitude, $\bar{\xi}_j$, is given by

$$\bar{\xi}_j = \frac{\{\phi\}_j^T \{F\}}{M_j (\omega_j^2 - \omega^2) + iC_j} \tag{25}$$

and manipulation in complex algebra yields the average value,

$$\text{Avg } (\dot{\xi}_j^2) = \tfrac{1}{2} \omega^2 \left| \bar{\xi}_j \right|^2 \quad . \tag{26}$$

Substituting this equation into Equation 24 yields an expression for the average kinetic energy, T_{avg}, of the system,

$$T_{avg} = \tfrac{1}{4} \sum_{j=1}^{n} M_j \omega^2 \left| \bar{\xi}_j \right|^2 = \sum_{j=1}^{n} (T_j)_{avg} \tag{27}$$

For the potential energy, U, the system equation is similar to the kinetic energy expression,

$$U = \tfrac{1}{2} \{x\}^T [k] \{x\} \quad . \tag{28}$$

Using the same basic procedure as was used in the kinetic energy derivation, the potential energy expression of Equation 28 becomes

$$U_j = \tfrac{1}{2} M_j \omega_j^2 \xi_j^2 \quad , \tag{29}$$

and

$$U = \sum_{j=1}^{n} U_j \ , \quad \text{or} \quad U = \tfrac{1}{2} \sum_{j=1}^{n} M_j \omega_j^2 \xi_j^2 \quad . \tag{30}$$

Again using Equation 25 to define the generalized response amplitude, algebraic manipulation provides an average value,

$$\text{Avg } (\xi_j^2) = \tfrac{1}{2} \left| \bar{\xi}_j \right|^2 \quad , \tag{31}$$

so that the average potential energy, U_{avg}, of the system is

$$U_{avg} = \tfrac{1}{4} \sum_{j=1}^{n} M_j \omega_j^2 \left| \bar{\xi}_j \right|^2 = \sum_{j=1}^{n} (U_j)_{avg} \tag{32}$$

Evaluation of the energy expressions reveals that a system vibrating in a given mode will have energy contributions only from that particular mode. This means that a structure vibrating purely in the i^{th} mode will have energy ratios,

$$(T_i/T)_{avg} = 1 \quad , \qquad (U_i/U)_{avg} = 1, \tag{33}$$

and

$$(T_j/T)_{avg} = 0, \ (U_j/U)_{avg} = 0, \quad \text{for all } j \neq i. \tag{34}$$

For vibration response which is not in a true mode of vibration, the energy will have contributions from more than one mode, and therefore none of the energy ratios, $(T_i/T)_{avg}$, $(U_i/U)_{avg}$, will be equal to 1. If all of the energy ratios are significantly different from a value of 1, either the frequency for which the response was calculated is not a true resonant frequency, or the mode under study has not been isolated from interfering modes.

III. COMPUTATIONS AND RESULTS

A. Software System

The theoretical analysis described in Section II was developed into a computer software package. This package was written in the FORTRAN IV programming language for use with the IBM Conversational Monitoring System. All of the program compilation and calculations were performed on the IBM 370 computer at Virginia Polytechnic Institute and State University. The programming package is briefly described in Appendix A.

B. Structural Model

The computational study of the procedure and the program package was performed on a grid structure with five lumped masses. Figure 1 is a diagram of the structure.

The beams of the structure are all solid circular aluminum ($E = 10^7$ psi) rods, 10 inches in length, and ¼ inch in diameter. The beams each have a bending stiffness, EI, of 1.917×10^3 lb-in^2, and a torsional stiffness, GJ, of 1.534×10^3 lb-in^2.

It is assumed that the structure experiences only out-of-plane motions, so that it has a total of 15 degrees of freedom, one translation and two rotations at each of the five mass nodes. The 15 x 15 stiffness matrix was developed using the direct stiffness method. With the complete stiffness matrix, a reduced stiffness matrix for

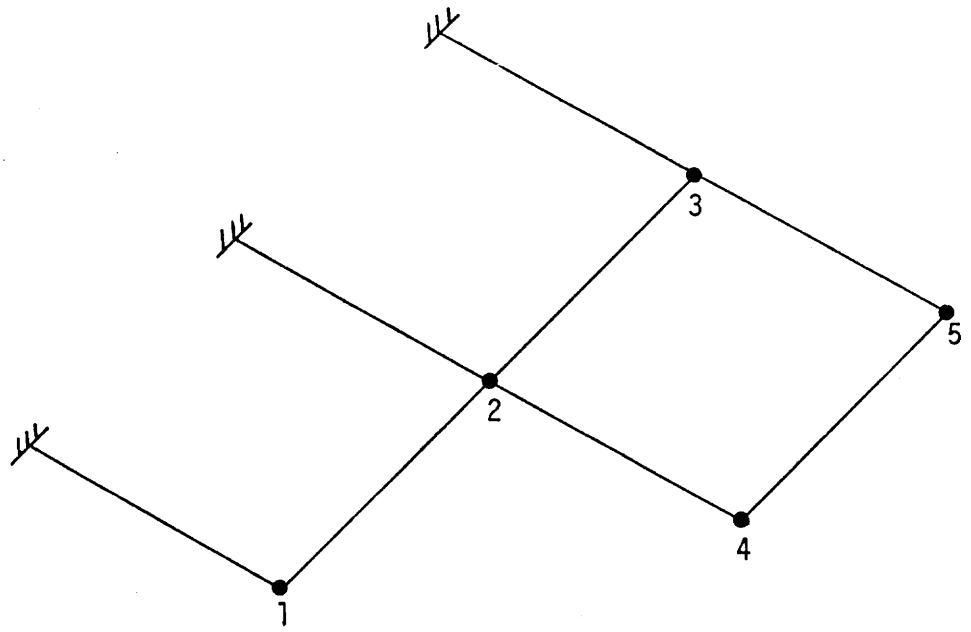

Beam properties:

material: Aluminum ($E = 10^7$ psi)

length: 10 inches

geometry: solid circular; ¼ inch diameter

bending stiffness: 1.917×10^3 psi.

torsional stiffness: 1.534×10^3 psi.

Figure 1. Structural Test Model.

only the translational degrees of freedom was generated using the matrix condensation method described by Przemieniecki (Reference 7). This reduction is appropriate because the structure is subjected to translational forces only. The generation of the 15 x 15 stiffness matrix and the condensation of this matrix to a 5 x 5 matrix was done through the use of the program KMAT, and the resulting symmetric stiffness matrix is shown in Table I.

For this structure, it was assumed that the damping is proportional to the stiffness matrix only, that is, that the mass proportionality constant, α, seen in Equation 9, is assumed to be equal to zero. The stiffness proportionality constant, β in Equation 9, was chosen, somewhat arbitrarily, to be 3.473×10^{-2}, so that

$$[c] = 3.473 \times 10^{-2} [k] . \tag{35}$$

The value of the mass elements was determined by first establishing an upper bound on the value of the first natural frequency. The value of this frequency was set at two (2) Hertz, which was considered to be realistic for possible experimental work, and which would not require overly large masses. With this limiting frequency, a simple Rayleigh-Ritz analysis was performed with the mass as the dependent variable. At this point, the mass was assumed to be the same at all mass nodes. From the Rayleigh-Ritz analysis, the common lumped mass value was set at 6.939×10^{-3} lb-sec^2/in, which corresponds to a weight of 2.678 lb. This mass value is shown as mass set 1 in

Table 1

Symmetric Stiffness Matrix

14.0240	-9.4063	3.0259	-1.1374	0.3803
-	48.5540	-13.2800	-11.6860	3.6392
-	-	36.4260	4.0634	-12.2320
-	-	-	8.0814	-4.5574
-	-	-	-	7.8623

Table II.

An analysis of the structure for the undamped free vibration modes, using the RMSYS program, revealed that the natural frequencies are widely spaced. These frequency values are listed in Table III as frequency set 1.

Since the structure did not exhibit any closely spaced modes, and since closely spaced modes are of special interest, the program MODE was used in an interactive procedure to produce near coalescence of two adjacent resonant frequencies. The approximate change in a resonant frequency with mass variation was calculated from Equation C-11 developed in Appendix C. With this information, an iterative process of the mass change and exact mode calculations was implemented to produce the desired closely spaced modes. The result was a system which had two modes with natural frequencies separated by less than two (2) radians per second. The mass values for this structure appear in Table II as mass set 2, and the natural frequencies developed by the structure are listed in Table III as frequency set 2. All numerical results presented subsequently were developed for the model with mass set 2.

It was noted that the masses in this system do not simulate any realistic type of structure. However, since the model was intended to serve as a test and demonstration case for the analytic procedure, and not as a simulation of any specific structure, it was considered to be satisfactory.

Table II

Nodal Mass Values (lb-sec^2/in)

Mass node	1	2	3	4	5
Mass set 1	0.00694	0.00694	0.00694	0.00694	0.00694
Mass set 2	0.01952	0.06657	0.03206	0.00694	0.00694

Table III

Natural Frequencies (rad/sec)

Mode	1	2	3	4	5
Frequency set 1	10.7912	28.4030	44.7970	67.1368	95.6476
Frequency set 2	8.5741	18.6254	30.5385	31.9047	50.1099

The natural mode shapes of the structure, which are shown in Table IV, were used to develop the modal matrix, $[\Phi]$, which was defined in Section II. This matrix was then used in Equation 7 to generate the generalized mass matrix, $[M]$. As was stated in Section II, the generalized mass matrix is diagonal, which uncouples the system inertially, and the diagonal elements of the matrix are listed in Table V.

The $[\Phi]$ matrix was also used in Equation 10 to generate the generalized damping matrix, $[C]$. This matrix is also diagonal, and is related to the generalized mass matrix through the structural damping constant, g, as described by Bisplinghoff and Ashley (Reference 8). The generalized damping is related to the generalized stiffness matrix by

$$[C] = [g]\,[K] , \tag{38}$$

where the matrix [g] is a diagonal matrix of damping constants, and where the generalized stiffness matrix is related to the generalized mass matrix by

$$[K] = [\omega^2 M] \tag{37}$$

In this case, the structural damping constants are all equal to the value of the stiffness proportionality constant. Therefore, the value of the structural damping constant is 3.473×10^{-2}.

Table IV

Normal Mode Shapes

mass node	mode 1	mode 2	mode 3	mode 4	mode 5
1	0.2087	-0.7167	1.00	-0.0030	0.0409
2	0.3201	-0.3263	-0.2958	0.2369	-0.1654
3	0.3534	0.4518	0.9181	0.4128	0.4103
4	0.9377	-0.3360	-0.5326	-1.00	0.8682
5	1.00	1.00	0.4973	-0.4620	-1.00

Table V

Generalized Mass ($lb\text{-}sec^2\text{-}in$)

M_1	M_2	M_3	M_4	M_5
0.0247	0.0314	0.0303	0.0176	0.0194

C. Modal Response Calculations

The natural frequencies, mode shapes, and generalized modal data were used by the program VIBE, which calculated forced response. The data calculated by VIBE includes modal frequencies, optimum forcing vectors, coincident response determinant plots, and energy and co-quad response data for certain resonant frequencies.

The simulation of vibration testing was performed with various arrangements of shakers. Vibration states with two, three, four, and five mass nodes under excitation were simulated. In all cases, the wide-band frequency sweeps for the resonant search calculations were chosen to include the five natural frequencies of the system. In the simulation of five shakers, the analysis showed the system in resonance at the five natural frequencies, as would be expected. For simulations involving fewer than five shakers, certain false modes were predicted by the analysis.

All of the shaker simulations were evaluated to yield the exact values of the forced resonance frequencies, and the relative magnitudes of the forces required to cause these vibration conditions. In addition, all simulations predicted the presence of two closely spaced modes, with values of frequency close to the frequency values for the closely spaced natural modes. Since these two modes were of special interest because of the experimental problems in their isolation, an examination of the modal quality of the two closely spaced modes was performed in each case. This examination included

an analysis of the coincident and quadrature response characteristics of the structure in a narrow-band of frequencies centered on each resonant frequency. In this case, the response was evaluated for frequencies within plus or minus 0.5 radians per second of the resonant frequency. In addition, the kinetic and potential energies of these two modes in each simulation were examined as a numerical determination of the modal quality.

For the simulation of five shakers, the coincident response determinant plot shows five resonant frequencies, all of which correspond to true modes. The determinant plots for this simulation are shown in Figures 2 and 3, and the resonant frequencies and respective force-amplitude distributions are listed in Table VI. The plots show the zero-determinant axis is crossed at five locations, indicating the five resonant frequencies. The slopes at these crossings are very steep, indicating true modes. It should be noted that due to the resolution of the plotting device used, two determinant plots with different frequency ranges are necessary to show the location and nature of all resonant frequencies. Also each determinant plot here has been normalized to the maximum absolute value of the coincident response determinant in the frequency band covered by the plot. The normalization algorithm is discussed in Appendix B.

The force-amplitude distribution for the case of all mass nodes under excitation can be determined by another method. This method, which might be described as the standard method, determines the force vector as a function of the mass and stiffness matrices, and

Table VI

Resonance Data for System Excited at All Nodes

Mode	Frequency (rad/sec)	Force-amplitude Distribution				
		node 1	node 2	node 3	node 4	node 5
1	8.5741	0.1911	1.00	0.5317	0.3053	0.3256
2	18.6254	0.6439	1.00	-0.6668	0.1073	-0.3195
3	30.5385	0.9932	-1.00	0.3225	-0.1876	0.1751
4	31.9048	0.0038	-1.00	-0.8393	0.4401	0.2033
5	50.1099	0.0481	-0.8396	1.00	0.4572	-0.5269

the mode shapes. The expression for the force vector is given by

$$\{F\} = (a_1 [m] + a_2 [k]) \{\phi\}_j \quad , \tag{38}$$

where a_1 and a_2 are arbitrary constants. The standard method was used as a check of the force-amplitude distributions calculated for the five shaker simulation, and the numbers from the standard calculations were identical to the force vectors in Table VI.

The simulation of excitation at four nodes of the structure involved shakers at mass nodes 1, 3, 4, and 5 (see Figure 1). With this pattern of excitation, the determinant plots, shown in Figures 4 and 5, have six zero-crossings. The values of the indicated frequencies and corresponding force vectors appear in Table VII. With six resonant frequencies in a five degree of freedom system, it is clear that one of the frequencies must be a false mode. Examination of the determinant plots reveals a false crossing in the vicinity of 27 radians per second, where the gentle slope of the crossing indicates the spurious nature of the crossing. The actual value of the frequency at this crossing is 27.047 radians per second, and this frequency is noted with the letter "f" in Table VII to indicate that it corresponds to a false mode.

Testing the structure characteristics with three shakers was performed with excitation at nodes 1, 3, and 4. As in the four shaker simulation, and in both of the two shaker simulations to follow, the large central mass was not placed under excitation. The determinant

Table VII

Resonance Data for System Excited at Nodes 1, 3, 4, and 5

Mode	Frequency (rad/sec)	Force-amplitude Distribution				
		node 1	node 2	node 3	node 4	node 5
1	8.5743	0.4885	0.00	1.00	0.6848	0.2901
2	18.6277	1.00	0.00	-0.1443	0.5574	-0.4556
f	27.0475	0.7138	0.00	1.00	0.8824	-0.2736
3	30.5219	1.00	0.00	0.7729	0.4133	-0.0577
4	31.8904	0.4611	0.00	-0.1440	1.00	0.0114
5	50.1059	0.1149	0.00	1.00	0.4941	-0.5058

plots for the three shaker test, seen in Figures 6 and 7, reveal seven zero-crossings, with two of these being false crossings. The frequencies at the spurious crossings were 25.8760 and 34.5993 radians per second, as can be seen in the complete listing of the frequency and force-amplitude distribution data for this simulation in Table VIII.

Two different simulations of excitation using two shakers were performed on the structure. These tests involved one simulation with shakers at mass nodes 1 and 3, and another with shakers at nodes 4 and 5. The results of these tests were qualitatively similar in that both tests yielded eight resonant frequencies. Both simulations showed one false mode with a frequency close to the value of the false frequency found in the four shaker test, but both also revealed two false frequencies not found in the four shaker test. These two other false modes had different frequencies in each simulation.

The simulation of shakers at mass nodes 1 and 3, for which the determinant plots are found in Figures 8 and 9, reveals false modal frequencies at 16.3211, 27.3857, and 44.9903 radians per second. The value of 27.3857 radians per second is quite close to the frequency of the single false mode found in the four shaker test. Table IX contains all of the frequency and forcing data for this two shaker test.

Determinant plots for the simulation of forcing at nodes 4 and 5, shown in Figures 10 and 11, reveal the presence of false modes with frequencies of 20.9451, 27.9309, and 37.0219 radians per second.

Table VIII

Resonance Data for System Excited at Nodes 1, 3, and 4

Mode	Frequency (rad/sec)	Force-amplitude Distribution				
		node 1	node 2	node 3	node 4	node 5
1	8.5743	0.3032	0.00	1.00	0.5704	0.00
2	18.6303	1.00	0.00	-0.9476	0.2513	0.00
f	25.8760	1.00	0.00	-0.0536	0.6638	0.00
3	30.5228	1.00	0.00	0.4143	0.2397	0.00
4	31.8904	0.4486	0.00	-0.0312	1.00	0.00
f	34.5993	0.0532	0.00	1.00	0.4307	0.00
5	50.0840	0.0648	0.00	1.00	0.4516	0.00

Table IX

Resonance Data for System Excited at Nodes 1 and 3

Mode	Frequency (rad/sec)	Force-amplitude Distribution				
		node 1	node 2	node 3	node 4	node 5
1	8.5756	0.4568	0.00	1.00	0.00	0.00
f	16.3211	0.5466	0.00	1.00	0.00	0.00
2	18.6265	0.0754	0.00	-1.00	0.00	0.00
f	27.3957	0.4234	0.00	-1.00	0.00	0.00
3	30.5202	1.00	0.00	-0.2449	0.00	0.00
4	31.8753	0.1496	0.00	-1.00	0.00	0.00
f	44.9903	0.0104	0.00	1.00	0.00	0.00
5	49.9992	0.0225	0.00	1.00	0.00	0.00

Again, one of the values is close to the single false frequency found in the four shaker simulation. However, the other two frequencies found in this test are not at all similar to the false modal frequencies in the test with shakers at nodes 1 and 3. The complete data for the simulation of shakers at nodes 4 and 5 is listed in Table X.

The presence of an increasing number of false modes in the data seemed to indicate a pattern in which one false mode would appear in the system for each degree of freedom not under excitation. This was indeed the case for this particular series of tests. However, the results of similar studies by Bishop and Gladwell (Reference 5) and Craig and Su (Reference 9) showed that in some cases of reduced shaker simulation certain natural modes were absent, and for different location patterns of the same number of shakers, different numbers of false modes were found. It would seem then that the pattern of increasing numbers of false modes with decreasing numbers of shakers is not necessarily the general result.

The two closely spaced modes were of the most interest in this study because of the practical problems involved in experimental separation of close modes. Therefore, the analysis of the modal energy ratios and the coincident-quadrature response used to determine the modal purity was confined to the third and fourth natural modes in each simulation.

The approximate modes developed by each force-amplitude distribution were examined for their contributions to the total potential and kinetic energy of the response, and the energy contributions of

Table X

Resonance Data for System Excited at Nodes 4 and 5

Mode	Frequency (rad/sec)	Force-amplitude Distribution				
		node 1	node 2	node 3	node 4	node 5
1	8.5745	0.00	0.00	0.00	1.00	0.7229
2	18.6441	0.00	0.00	0.00	1.00	-0.3427
f	20.9451	0.00	0.00	0.00	1.00	0.0429
f	27.9309	0.00	0.00	0.00	0.0068	1.00
3	30.5081	0.00	0.00	0.00	0.3417	-1.00
4	31.8791	0.00	0.00	0.00	1.00	0.5680
f	37.0219	0.00	0.00	0.00	0.6276	-1.00
5	50.0858	0.00	0.00	0.00	0.7685	-1.00

the other modes participating in the response were examined.

The coincident and quadrature response characteristics of the modes were also used to determine the modal quality, since the response of a system in a pure mode will be purely in quadrature, and will match the natural mode shape. In the case of the approximate modes, the mass nodes not under excitation will have non-zero coincident response values, and the values of the quadrature will differ from the natural mode shape. As with the variations in the energy contributions, the deviation of the quadrature response from the natural mode shape is the result of the effect of modes other than the one approximately isolated.

The best use of the response data in the analysis of the modal quality is to examine the data in the form of plots of the coincident response versus the quadrature response, with the data plotted in the Argand plane.

With the coincident response plotted along the real axis and the quadrature response along the imaginary axis, the locus of several response points in the vicinity of the resonant frequency will appear as a circle which has its center on the imaginary axis and the origin as one of its points. As the mode becomes more approximate, the shape of the plot is distorted, and the center moves away from the axis. Therefore, an examination of the co-quad response plots in the Argand plane was used as a qualitative study of the modal purity, while the energy ratios provided a more quantitative result.

The response data for the five shaker simulation indicated that true modes are isolated in both the third and fourth modes, as was expected. The co-quad response values are shown in Tables XI and XII for the third and fourth modes, respectively. The small values of the coincident response shown in these tables is the result of the loss of accuracy which occurs in the use of single precision arithmetic.

Using a narrow band of frequencies near the resonant frequency, the co-quad response plots in the Argand plane for multiple-shaker excitation were developed and found to indicate the existence of true modes. For the third mode, Figure 12 shows the locally normalized determinant plot for the narrow frequency band. Figures 13, 14, and 15 show the response values in the Argand plane. All five response curves reveal the presence of purely quadrature response at the resonant frequency and demonstrate the exactly circular patterns indicating a pure mode. Those response plots noted with the letter "c" (for conjugate) are phase reversed with respect to the other response values.

Figure 16 shows the determinant values for the narrow frequency band around the resonant frequency for the fourth mode. Figures 17 and 18 reveal the presence of a true mode by the circular shape of the response plots and by the indication of pure quadrature response at the resonant frequency. In this mode, the response of the first mass node was very small and not included in these plots, or in any plots of the fourth mode response.

Table XI

Response Data for the Third Approximate Mode

Shakers Used 1 - 5		Frequency (rad/sec) 30.5385	
Mass node	Response		Normal Mode Shape
	Coincident	Quadrature	
1	0.0002	1.00	1.00
2	-0.0001	-0.2958	-0.2958
3	0.00	0.1981	0.1981
4	-0.0001	-0.5326	-0.5326
5	0.0001	0.4973	0.4973

Table XII

Response Data for the Fourth Approximate Mode

Shakers Used 1 - 5		Frequency (rad/sec) 31.9048	
Mass node	Response		Normal Mode Shape
	Coincident	Quadrature	
1	0.00	-0.0030	-0.0030
2	-0.0001	0.2369	0.2369
3	-0.0002	0.4128	0.4128
4	-0.0005	-1.00	-1.00
5	0.0002	-0.4620	-0.4620

The determinant plots of the narrow frequency bands for the other shaker simulations show the frequency ranges used in the multiple-shaker excitation response analyses. The determinant plots for the simulations with fewer than five shakers are found in Figures 19, 23, 26, 30, 33, 37, 40, and 44.

Figures 20, 21, and 22, which depict the response data for the third approximate mode of the simulation with shakers at nodes 1, 3, 4, and 5, show that the response of mass node 2 had a non-zero co-incident component at the resonant frequency. Also, the co-quad plots for all mass nodes are slightly distorted from the circular pattern, indicating the contribution of other modes to the response. Figures 24 and 25 show similar results for the fourth approximate mode. For the four shaker test, the actual distortions of the circular shapes is very small, indicating fairly good modal quality. The response values for the resonant frequencies of the third and fourth modes are shown in Tables XIII and XIV, respectively.

Analysis of Figures 27, 28, 29, 31, and 32 reveals that more loss of modal purity occurs in the simulation of shakers at mass nodes 1, 3, and 4. In this test, the co-quad plots show nodes 2 and 5 with some coincident response at resonance. The distortion of the circular shape is again apparent, although the amount of distortion is still small. Tables XV and XVI contain the numerical values of the resonant response for the third and fourth modes approximated by this simulation.

Table XIII

Response Data for the Third Approximate Mode

Shakers Used 1 3 4 5		Frequency (rad/sec) 30.5217	
Mass node	Response		Normal Mode Shape
	Coincident	Quadrature	
1	0.0003	1.00	1.00
2	-0.0445	-0.2930	-0.2958
3	0.0001	0.1911	0.1981
4	-0.0001	-0.5130	-0.5326
5	0.0001	0.5031	0.4973

Table XIV

Response Data for the Fourth Approximate Mode

Shakers Used 1 3 4 5		Frequency (rad/sec) 31.8903	
Mass node	Response		Normal Mode Shape
	Coincident	Quadrature	
1	0.00	0.0040	0.0030
2	-0.0496	0.2336	0.2369
3	-0.0002	0.4119	0.4128
4	0.0002	-1.00	-1.00
5	0.0002	-0.4549	-0.4620

Table XV

Response Data for the Third Approximate Mode

Shakers Used 1 3 4		Frequency (rad/sec) 30,5226	
Mass node	Response		Normal Mode Shape
	Coincident	Quadrature	
1	0.0002	1.00	1.00
2	-0.0400	-0.2984	-0.2958
3	0.0001	0.1896	0.1981
4	-0.0001	-0.5106	-0.5326
5	0.0254	0.5017	0.4973

Table XVI

Response Data for the Fourth Approximate Mode

Shakers Used 1 3 4		Frequency (rad/sec) 31.8903	
Mass node	Response		Normal Mode Shape
	Coincident	Quadrature	
1	0.0002	0.0040	-0.0030
2	-0.0485	0.2336	0.2369
3	0.0002	0.4113	0.4128
4	0.0004	-1.00	-1.00
5	-0.0069	-0.4546	-0.4620

Figures 34, 35, 36, 38, and 39, which detail the co-quad response for the third and fourth mode for the simulation with shakers at nodes 1 and 3, reveal a continuation of the pattern of the loss of modal quality. In these plots, three nodes have coincident response at resonance, and the distortion of the circular shape is again seen. The distortion in these plots is greater than resulted from the excitation with more shakers. This indicates contribution of other modes to the response in greater quantity than in previous tests, and therefore a deterioration in the modal quality. Figures 41, 42, 43, 45, and 46 reveal similar patterns in the response for the simulation of shakers at mass nodes 4 and 5. The numerical values of the resonant response for the two shaker tests are listed in Tables XVII through XX.

Graphical analysis of the response data gives a qualitative indication of the modal quality, but a numerical result is necessary in order to determine the extent of the deterioration of the modal quality with the removal of shakers. The numerical tests used in this study are the modal energy ratios, $(T_i/T)_{avg}$ and $(U_i/U)_{avg}$, defined by Equations 27 and 32.

The average kinetic energy ratios for the third mode of all tests are shown in Table XXI and the corresponding average potential energy ratios are contained in Table XXII. Both of these tables show the increase in the energy contributions of interfering modes as the number of shakers is decreased. Tables XXIII and XXIV show similar results for the kinetic and potential energy of the fourth mode. The energy data indicates the effects of the interfering modes is small, even for the cases with only two shakers.

Table XVII

Response Data for the Third Approximate Mode

Shakers Used 1 3		Frequency (rad/sec) 30.5208	
Mass node	Response		Normal Mode Shape
	Coincident	Quadrature	
1	0.0003	1.00	1.00
2	-0.0401	-0.3011	-0.2958
3	0.0001	0.1872	0.1981
4	0.0184	-0.5073	-0.5326
5	0.0851	0.5075	0.4973

Table XVIII

Response Data for the Fourth Approximate Mode

Shakers Used 1 3		Frequency (rad/sec) 31.8751	
Mass node	Response		Normal Mode Shape
	Coincident	Quadrature	
1	0.0003	0.0063	-0.0030
2	-0.0153	0.2325	0.2369
3	-0.0001	0.4137	0.4128
4	0.0185	-1.00	-1.00
5	0.0790	-0.4555	-0.4620

Table XIX

Response Data for the Third Approximate Mode

Shakers Used		Frequency (rad/sec)
4 5		30.5079
Mass node	Response	Normal Mode Shape
	Coincident / Quadrature	
1	-0.0752 / 1.00	1.00
2	0.0112 / -0.4234	-0.2958
3	0.0760 / 0.1815	0.1981
4	0.0001 / -0.4971	-0.5326
5	-0.0001 / 0.5216	0.4973

Table XX

Response Data for the Fourth Approximate Mode

Shakers Used		Frequency (rad/sec)
4 5		31.8789
Mass node	Response	Normal Mode Shape
	Coincident / Quadrature	
1	0.0810 / 0.0134	-0.0030
2	-0.0065 / 0.2300	0.2369
3	-0.0454 / 0.4121	0.4128
4	0.0004 / -1.00	-1.00
5	0.0020 / -0.4496	-0.4620

Table XXI

Kinetic Energy Ratios for the Third Approximate Mode

Shakers Used	Kinetic Energy Ratios				
	mode 1	mode 2	mode 3	mode 4	mode 5
1 - 5	0.00	0.00	1.00	0.00	0.00
1 3 4 5	0.0001	0.0004	0.9968	0.0014	0.0013
1 3 4	0.00	0.0005	0.9979	0.0013	0.0003
1 3	0.00	0.0008	0.9965	0.0027	0.00
4 5	0.0001	0.0079	0.9837	0.0069	0.0063

Table XXII

Potential Energy Ratios for the Third Approximate Mode

Shakers Used	Potential Energy Ratios				
	mode 1	mode 2	mode 3	mode 4	mode 5
1 - 5	0.00	0.00	1.00	0.00	0.00
1 3 4 5	0.0001	0.0004	0.9968	0.0014	0.0013
1 3 4	0.00	0.0005	0.9979	0.0013	0.0003
1 3	0.00	0.0008	0.9965	0.0027	0.00
4 5	0.0001	0.0079	0.9837	0.0069	0.0063

Table XXIII

Kinetic Energy Ratios for the Fourth Approximate Mode

Shakers Used	Kinetic Energy Ratios				
	mode 1	mode 2	mode 3	mode 4	mode 5
1 - 5	0.00	0.00	0.00	1.00	0.00
1 3 4 5	0.0009	0.0007	0.0007	0.9974	0.0003
1 3 4	0.0010	0.0007	0.0007	0.9972	0.0004
1 3	0.0006	0.0029	0.0013	0.9948	0.0005
4 5	0.0014	0.0001	0.0035	0.9950	0.0001

Table XIV

Potential Energy Ratios for the Fourth Approximate Mode

Shakers Used	Potential Energy Ratios				
	mode 1	mode 2	mode 3	mode 4	mode 5
1 - 5	0.00	0.00	0.00	1.00	0.00
1 3 4 5	0.0001	0.0002	0.0006	0.9983	0.0007
1 3 4	0.0001	0.0002	0.0006	0.9981	0.0009
1 3	0.00	0.0010	0.0012	0.9966	0.0012
4 5	0.0001	0.00	0.0035	0.9966	0.00

IV. SUMMARY AND CONCLUSIONS

This study has used Asher's method to determine the force-amplitude distributions required to isolate as completely as possible individual modes of vibration of the structure. The analytical structural model employed is a five-degree-of-freedom lumped-mass grid structure assumed to be linear and to have small proportional, hysteretic damping. Two of the model's five natural modes have closely spaced natural frequencies, and particular attention has been given to the separation of these two modes. Forced sinusoidal vibration tests consisting of two, three, four, and five shakers have been simulated on the structural model.

The simulation study used two different methods for evaluating the purity of the modes isolated by multiple-shaker excitation. The first method was the examination of the coincident-quadrature response in an Argand plane plot. The second method involved examining the energy contributions of the natural modes to the total energy of the system. The energy ratios were used for comparison of the results with different numbers of shakers, and the expected decline in modal purity with the decrease in the number of shakers was reflected by the energy ratios.

Since Craig and Su (Reference 9) previously conducted a similar study, it is appropriate to point out the new features of the present work. Whereas the study of Craig and Su considered only zero-crossings of the coincident response determinant, this study has generated and

examined the entire plot of the determinant versus frequency. It has been demonstrated that this plot can provide useful information. In contrast to the two through five shaker simulations on a five-degree-of-freedom model of the present study, Craig and Su examined only one through three shaker simulations on a nine-degree-of-freedom model. That is, this study has considered a simpler model but more thoroughly. Finally, this study has included a more detailed evaluation of the purity of partially isolated modes than Craig and Su presented. Whereas they examined the amplitude and phase of each mass node only at the approximate resonant frequency, the evaluation in this study consists of the entire co-quad plot for each mass node in a narrow band about the resonance. Also, a second evaluation of the analytical simulation by means of modal energy ratios has been presented.

On the basis of their simulation study, Craig and Su concluded that Asher's method can predict the force-amplitude distribution required to isolate a mode of vibration acceptably. Although the results of this study corroborate that conclusion, it should be emphasized that both studies considered only small, lumped-mass analytical structural models quite unlike most real continuous structures. The practical value of Asher's method has yet to be established for actual structures. Further theoretical and numerical studies are required. Should the method continue to appear promising after these studies, experimental research implementing Asher's method should be conducted.

REFERENCES

1. Traill-Nash, R. W., "On the Excitation of the Pure Modes in Aircraft Resonance Testing", Journal of Aero/Space Sciences, December 1958, pp. 775-778.

2. Asher, G. W., "A Method of Normal Mode Excitation Utilizing Admittance Measurements", Proceedings of the National Specialists Meeting on Dynamics and Aero-elasticity, Institute of Aerospace Sciences, Fort Worth, Texas, 1958, pp. 69-76.

3. Bisplinghoff, R. L., Ashley, H., and Halfman, R. L., Aeroelasticity, Reading, Massachusetts, Addison-Wesley Publishing Company, 1955.

4. Meirovitch, L., Elements of Vibration Analysis. New York, McGraw-Hill Book Company, 1975.

5. Bishop, R. E. D. and Gladwell, G. M. L., "An Investigation into the Theory of Resonance Testing", Philosophical Transactions of the Royal Society of London, Vol. 255, Series A. No. 1055, 1963, pp. 241-280.

6. Kennedy, C. C. and Pancu, C. D. P., "Use of Vectors in Vibration Measurement and Analysis", Journal of Aerospace Sciences, Vol. 14, No. 11, 1947, pp. 603-625.

7. Przemieniecki, J. S., Theory of Matrix Structural Analysis, New York, McGraw-Hill Book Company, 1968.

8. Bisplinghoff, R. L. and Ashley, H., Principles of Aeroelasticity, New York, Dover Publications, Inc., 1975.

9. Craig, R. R. and Su, Y.-W.T., "On Multiple-Shaker Resonance Testing", AIAA Journal, Vol. 12, No. 7, 1974, pp. 924-931.

10. Korn, G. A. and Korn, T. M., Mathematical Handbook for Scientists and Engineers, New York, McGraw-Hill Book Company, 1961.

11. Zarghamee, M. S., "Optimum Frequency of Structures," AIAA Journal, Vol. 6, No. 4, April 1968, pp. 749-750.

12. Fraeijs de Veubeke, Comment on "On Multiple-Shaker Resonance Testing." Craig, R. R. and Su, Y.-W.T., Reply by Authors to Fraeijs de Veubeke. AIAA Journal, Vol. 13, No. 5, 1975, pp. 703-704.

FIGURES 2 through 46

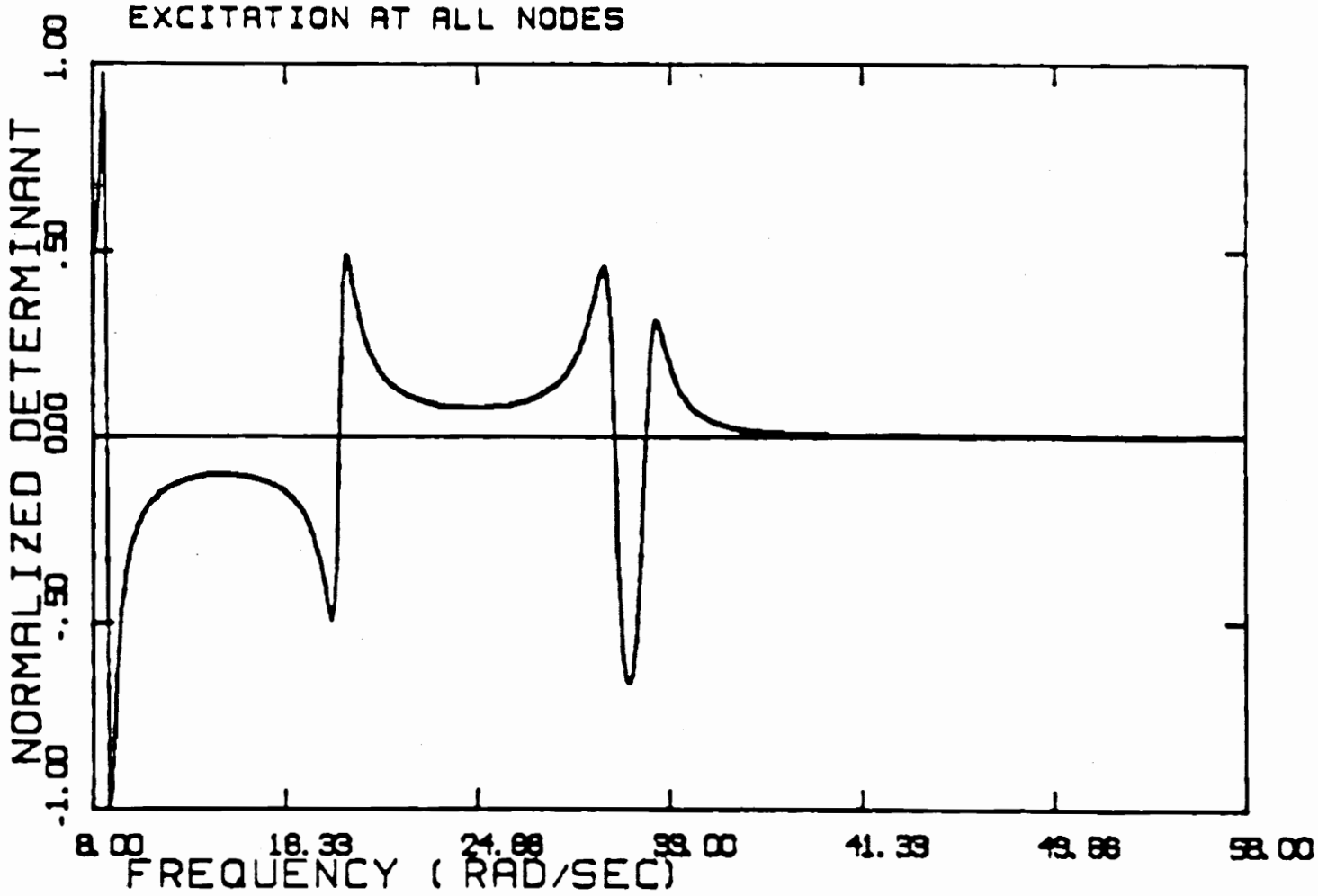

Figure 2. D(ω) for Excitation at All Nodes, 8.0 rps. to 58.0 rps.

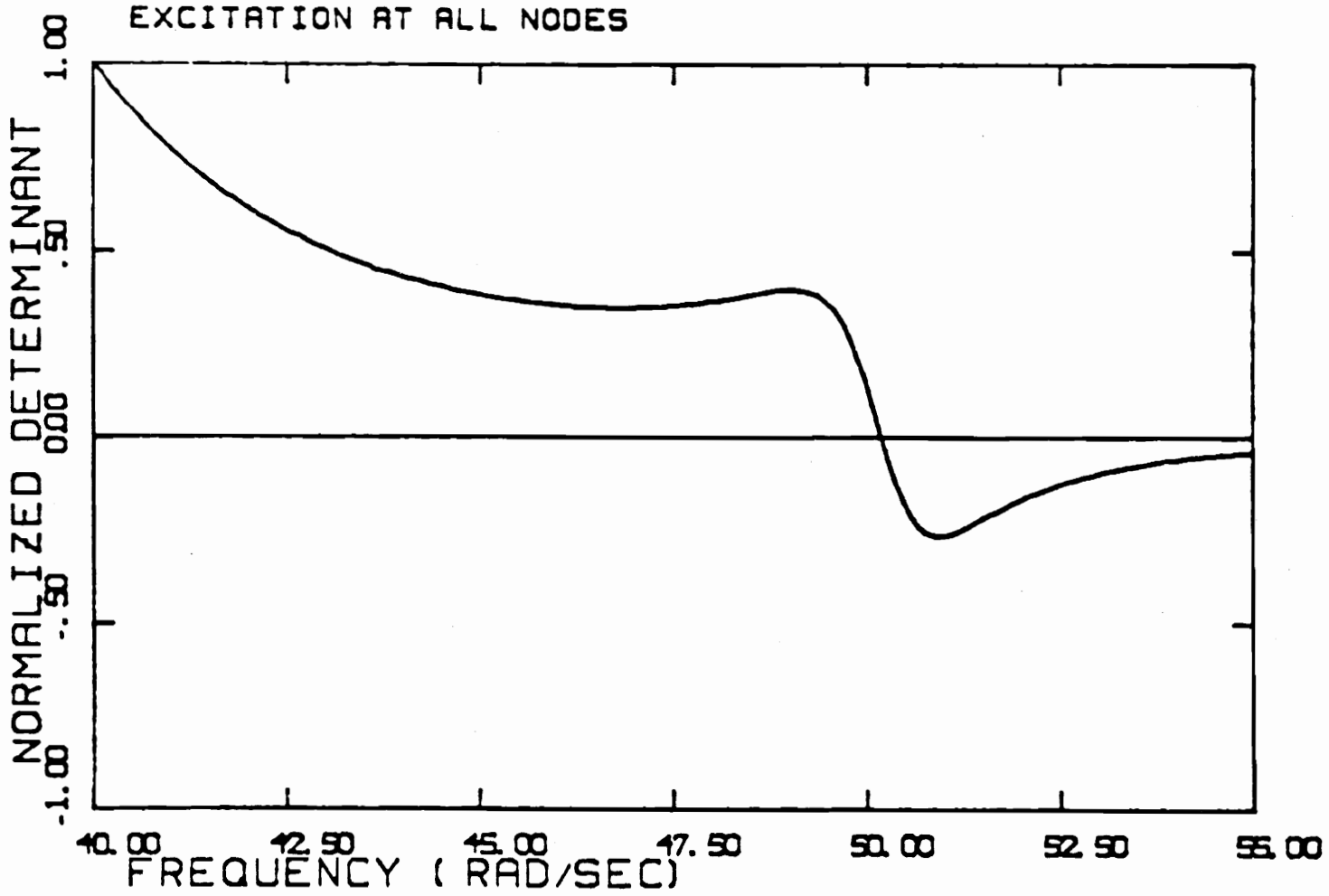

Figure 3. D(ω) for Excitation at All Nodes, 40.0 rps. to 55.0 rps.

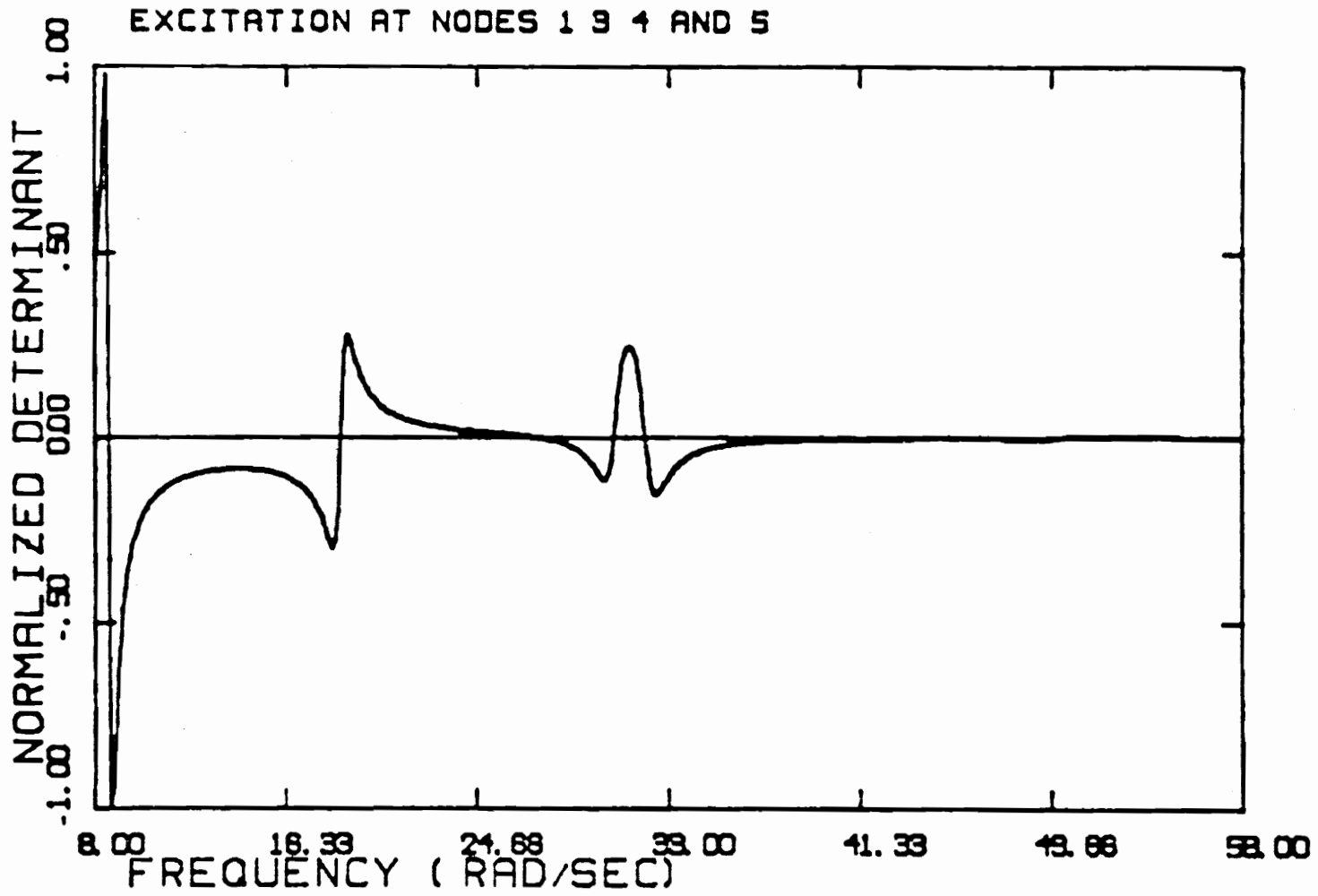

Figure 4. D(ω) for Excitation at Nodes 1, 3, 4, and 5, 8.0 rps. to 58.0 rps.

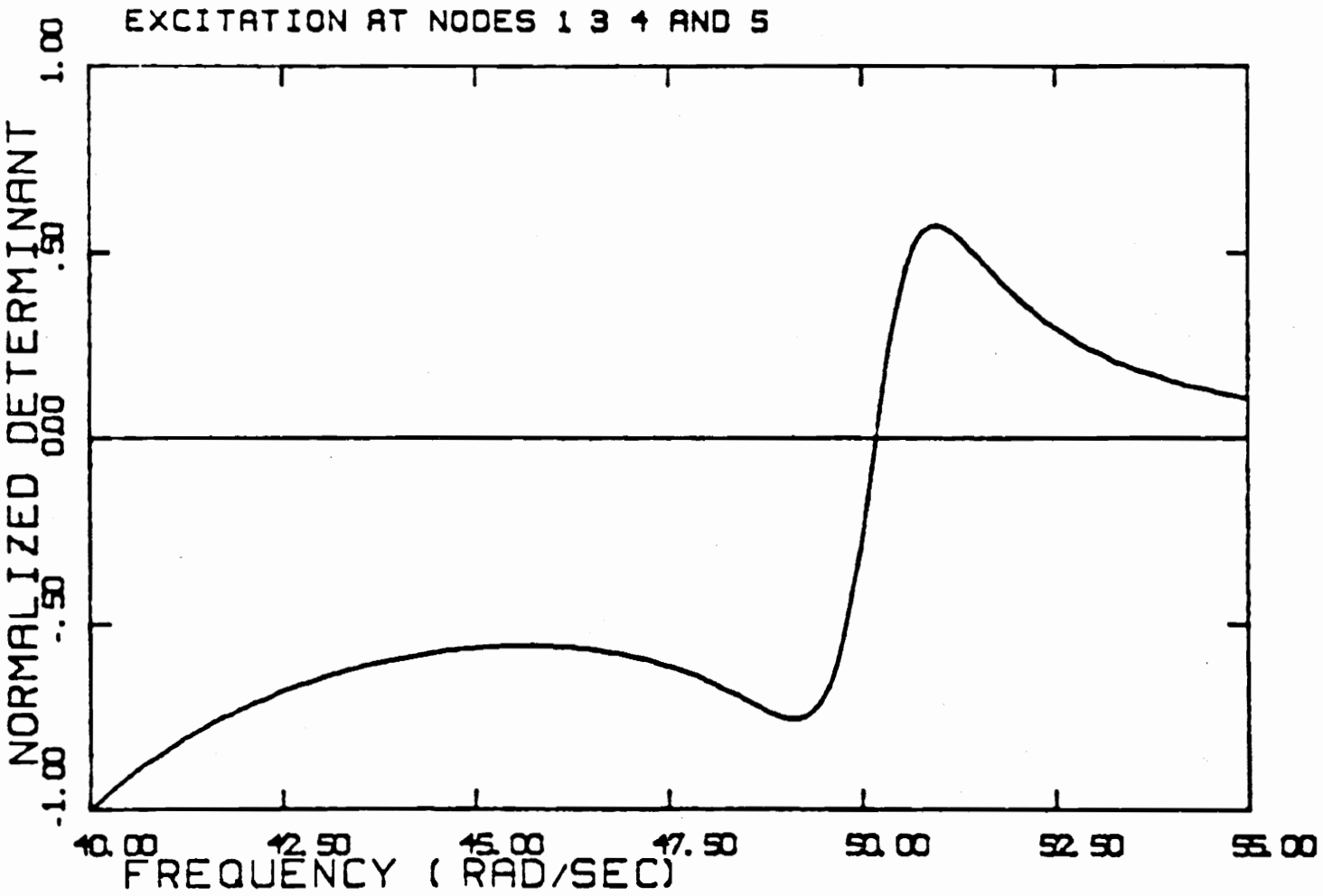

Figure 5. $D(\omega)$ for Excitation at Nodes 1, 3, 4, and 5, 40.0 rps. to 55.0 rps.

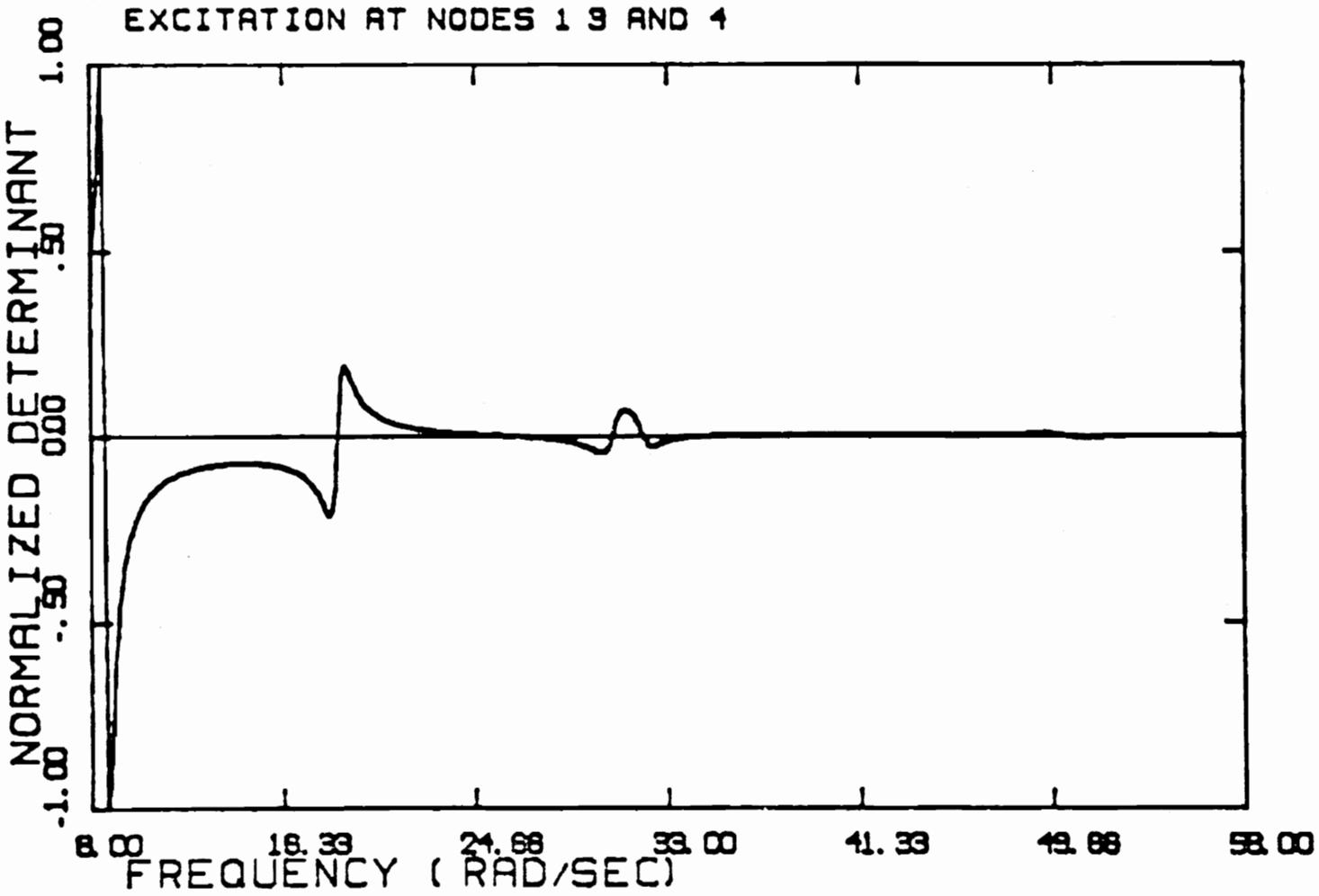

Figure 6. D(ω) for Excitation at Nodes 1, 3, and 4, 8.0 rps. to 58.0 rps.

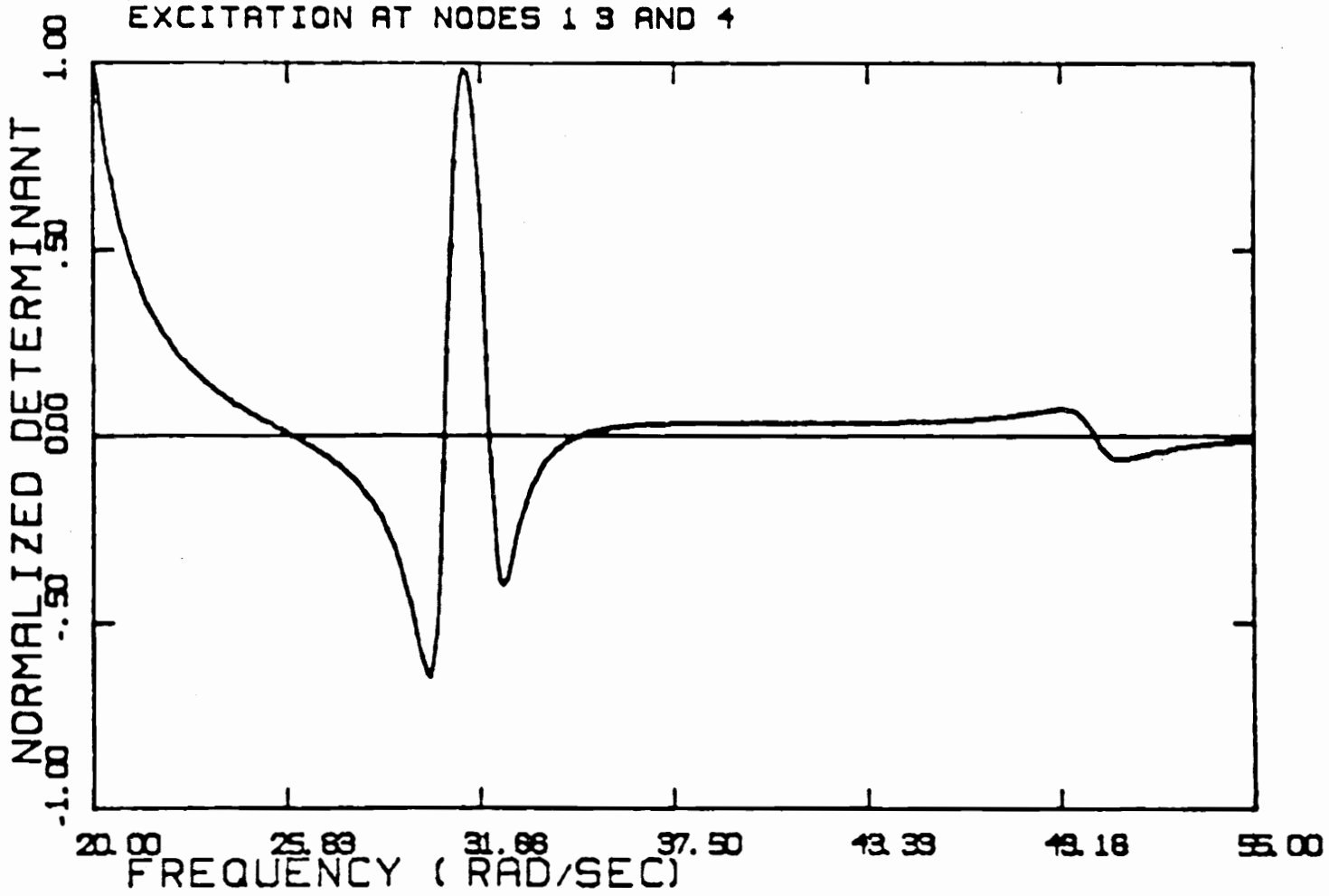

Figure 7. D(ω) for Excitation at Nodes 1, 3, and 4, 20.0 rps. to 55.0 rps.

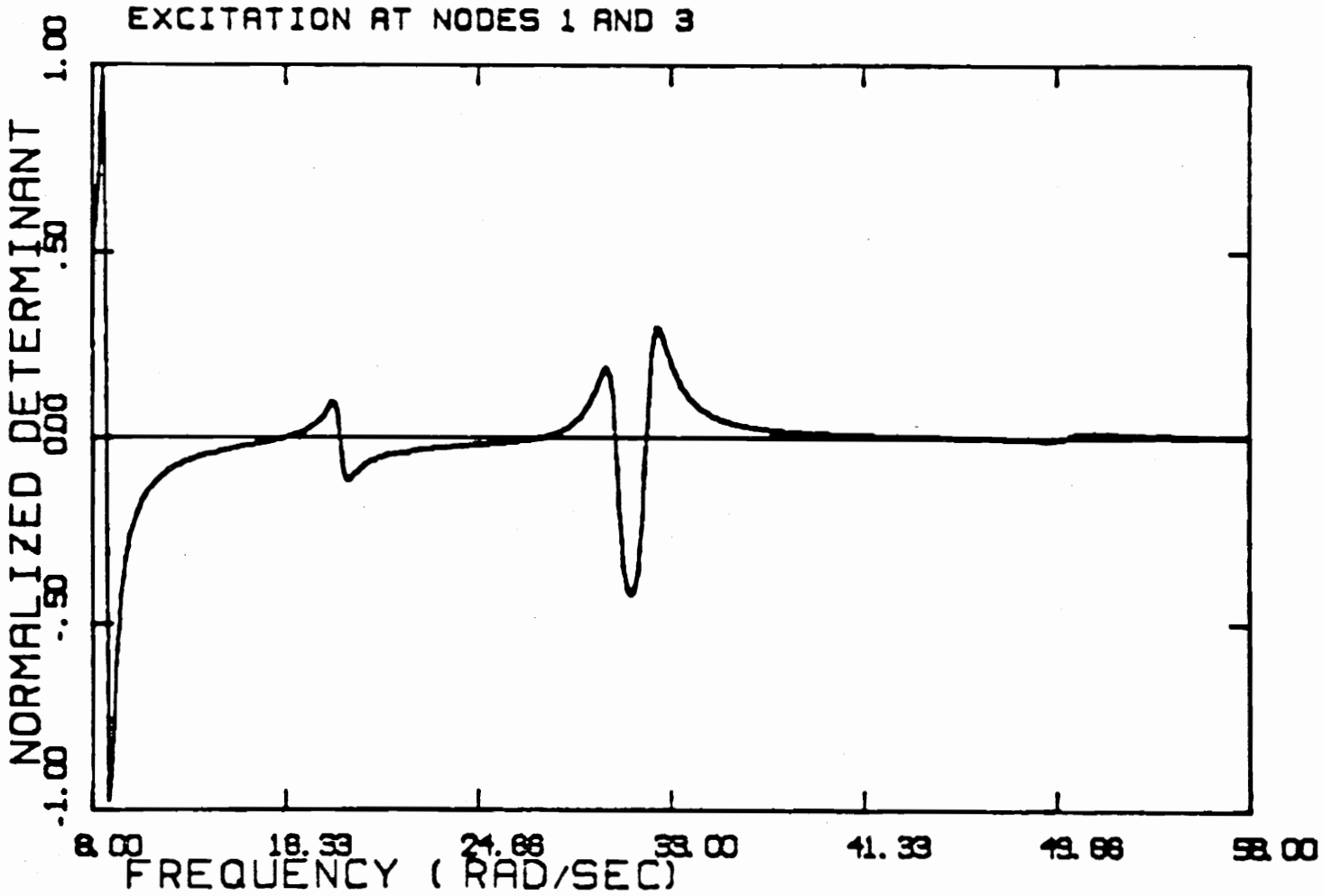

Figure 8. D(ω) for Excitation at Nodes 1 and 3, 8.0 rps. to 58.0 rps.

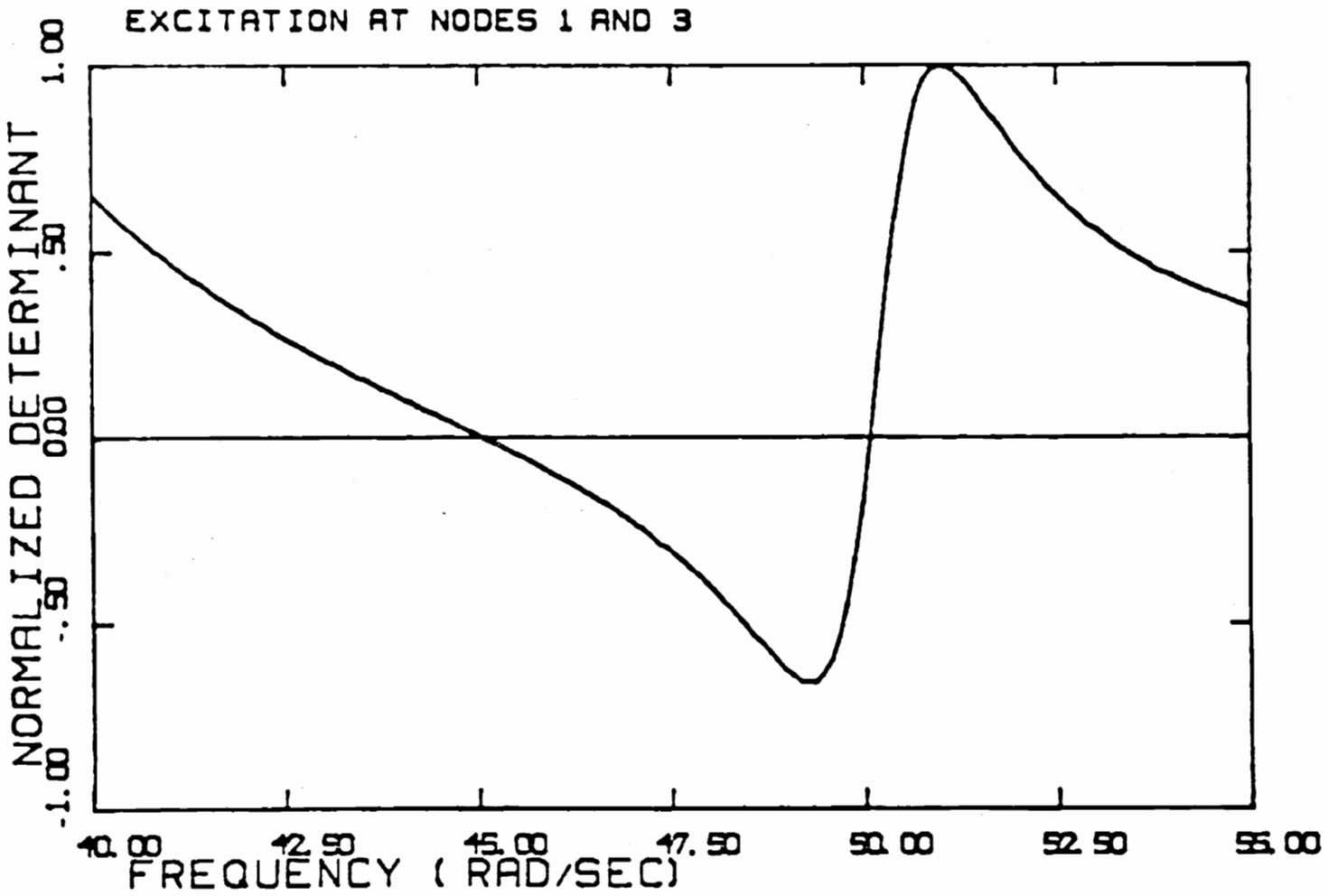

Figure 9. D(ω) for Excitation at Nodes 1 and 3, 40.0 rps. to 55.0 rps.

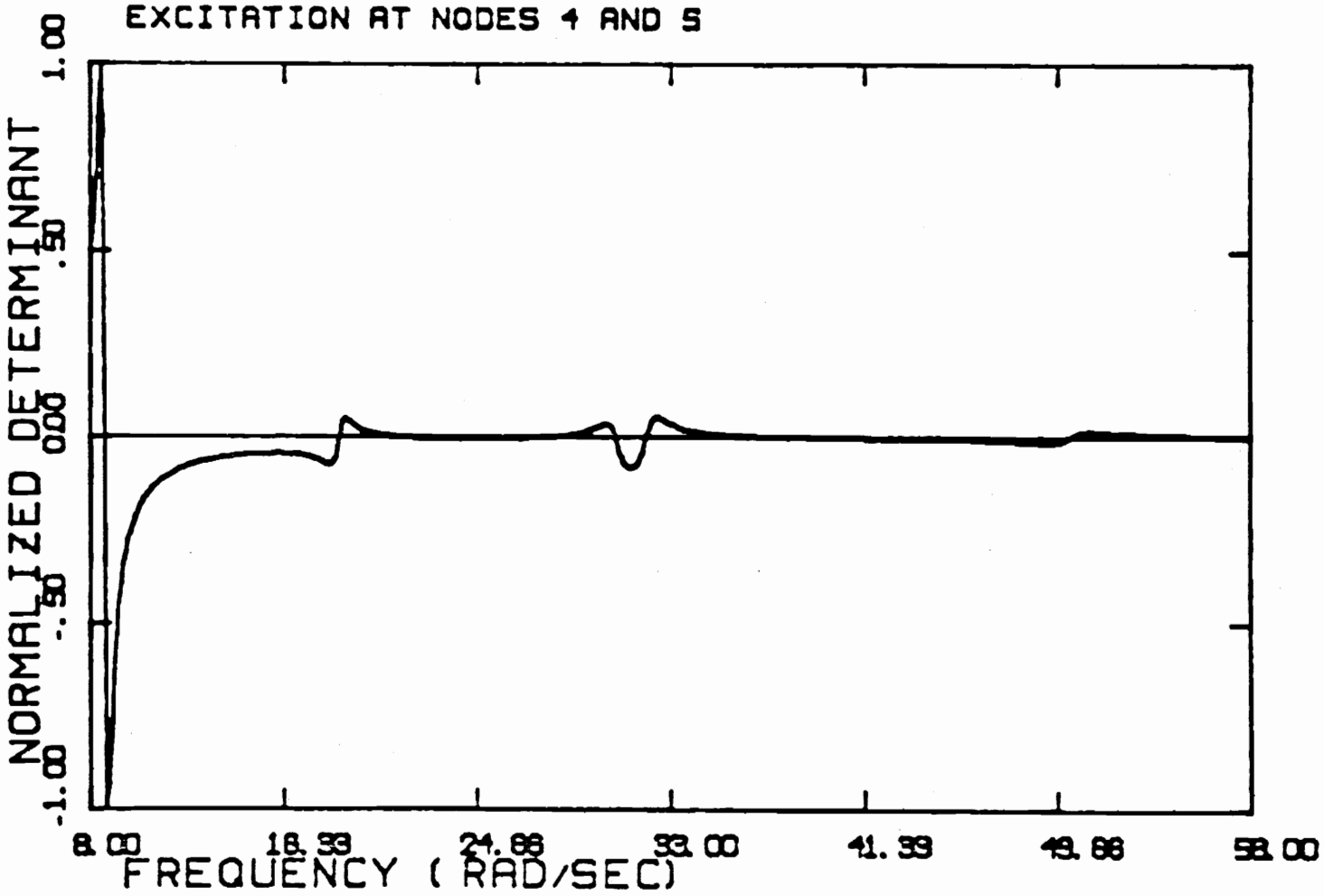

Figure 10. $D(\omega)$ for Excitation at Nodes 4 and 5, 8.0 rps. to 58.0 rps.

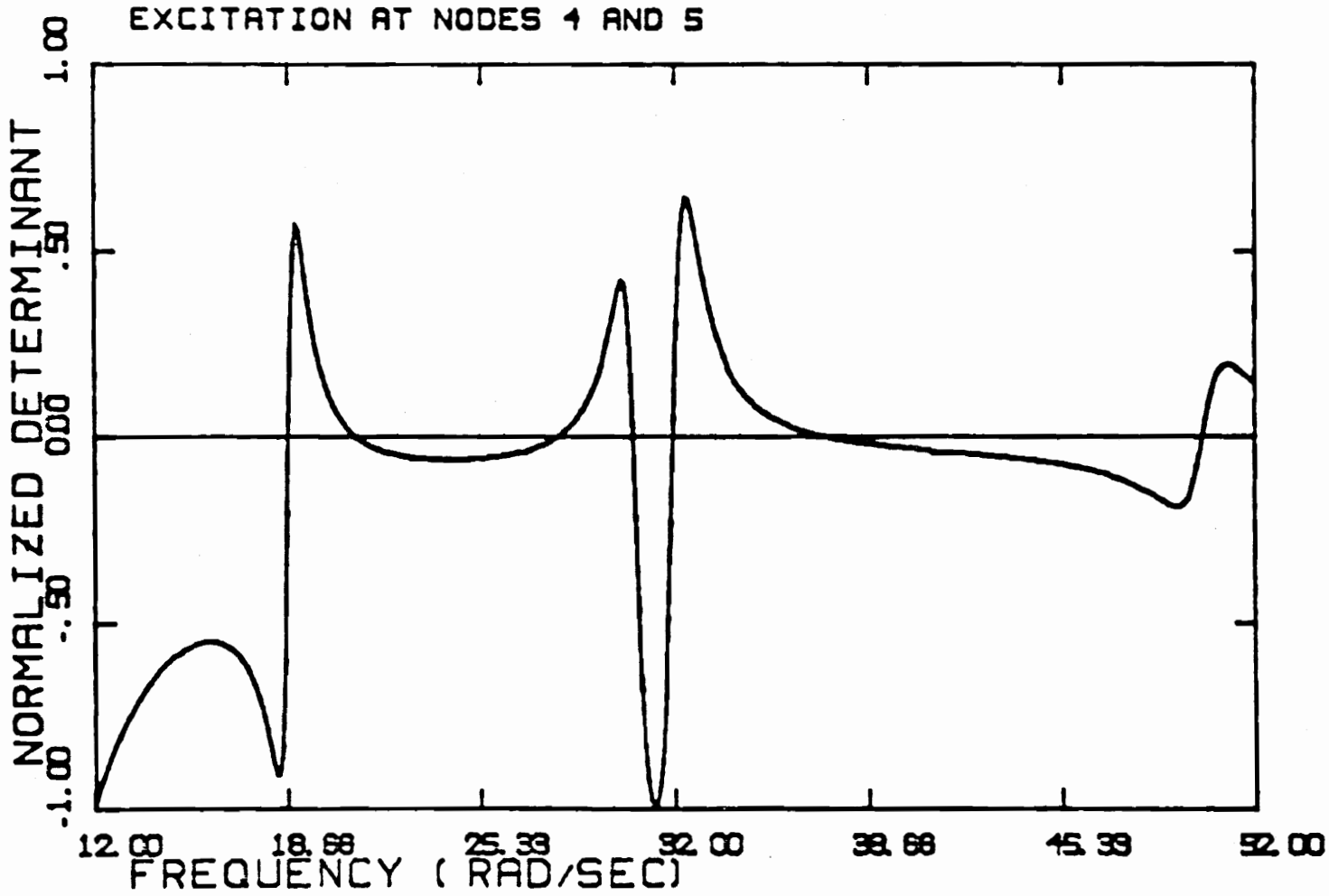

Figure 11. D(ω) for Excitation at Nodes 4 and 5, 12.0 rps. to 52.0 rps.

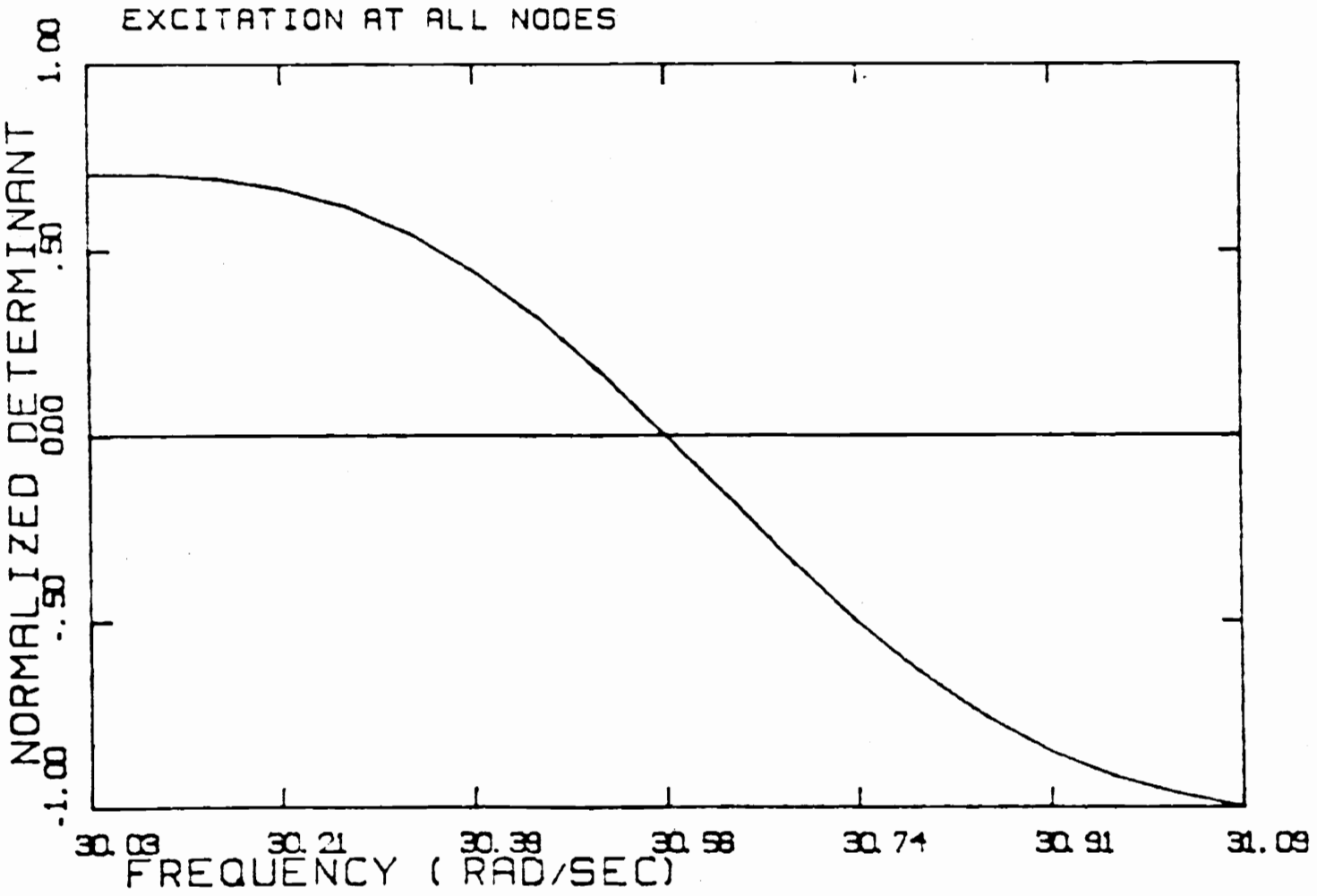

Figure 12. D(ω) for Excitation at All Nodes 30.03 rps. to 31.09 rps.

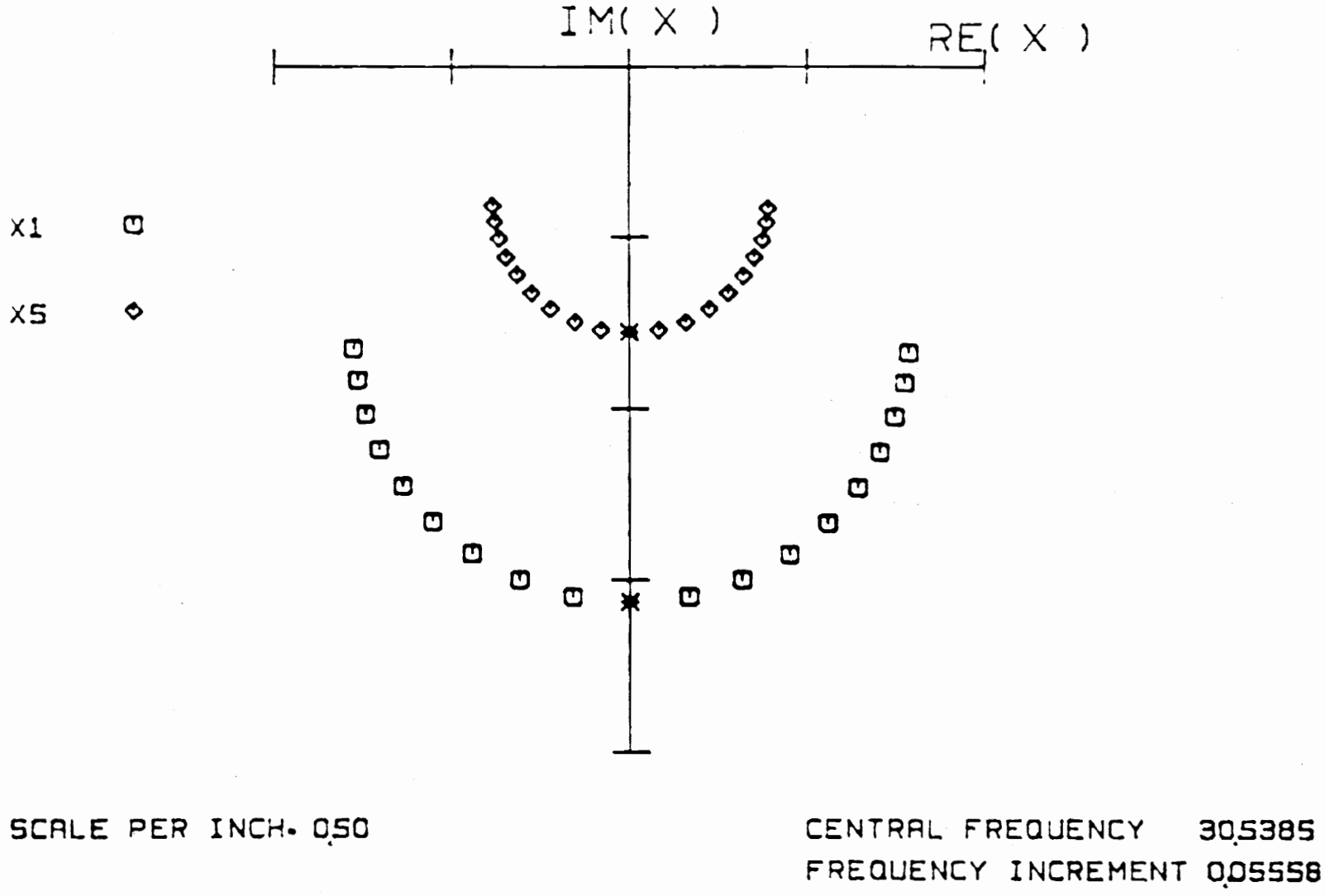

Figure 13. Co-quad Response in Mode 3 for Excitation at All Nodes

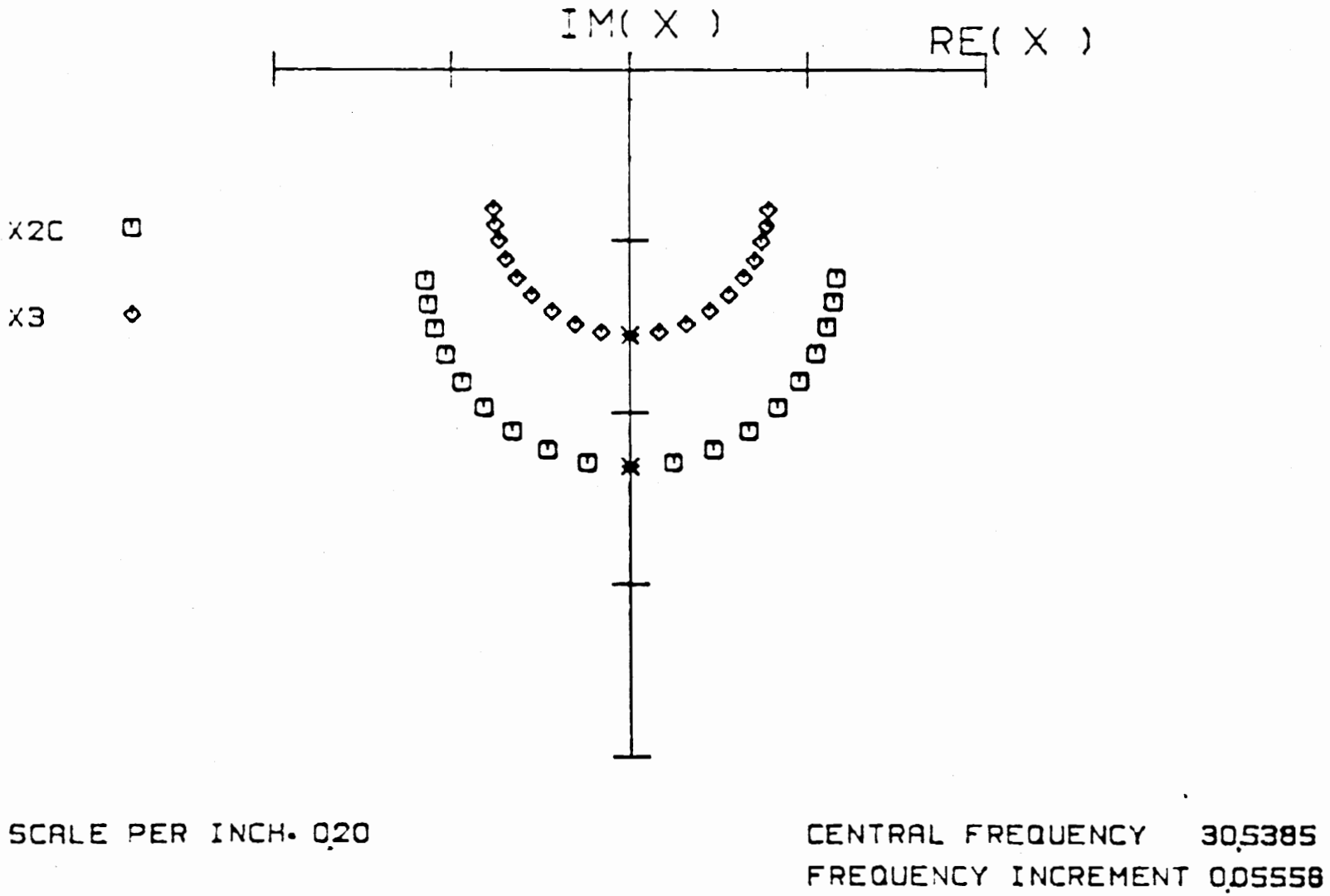

Figure 14. Co-quad Response in Mode 3 for Excitation at All Nodes

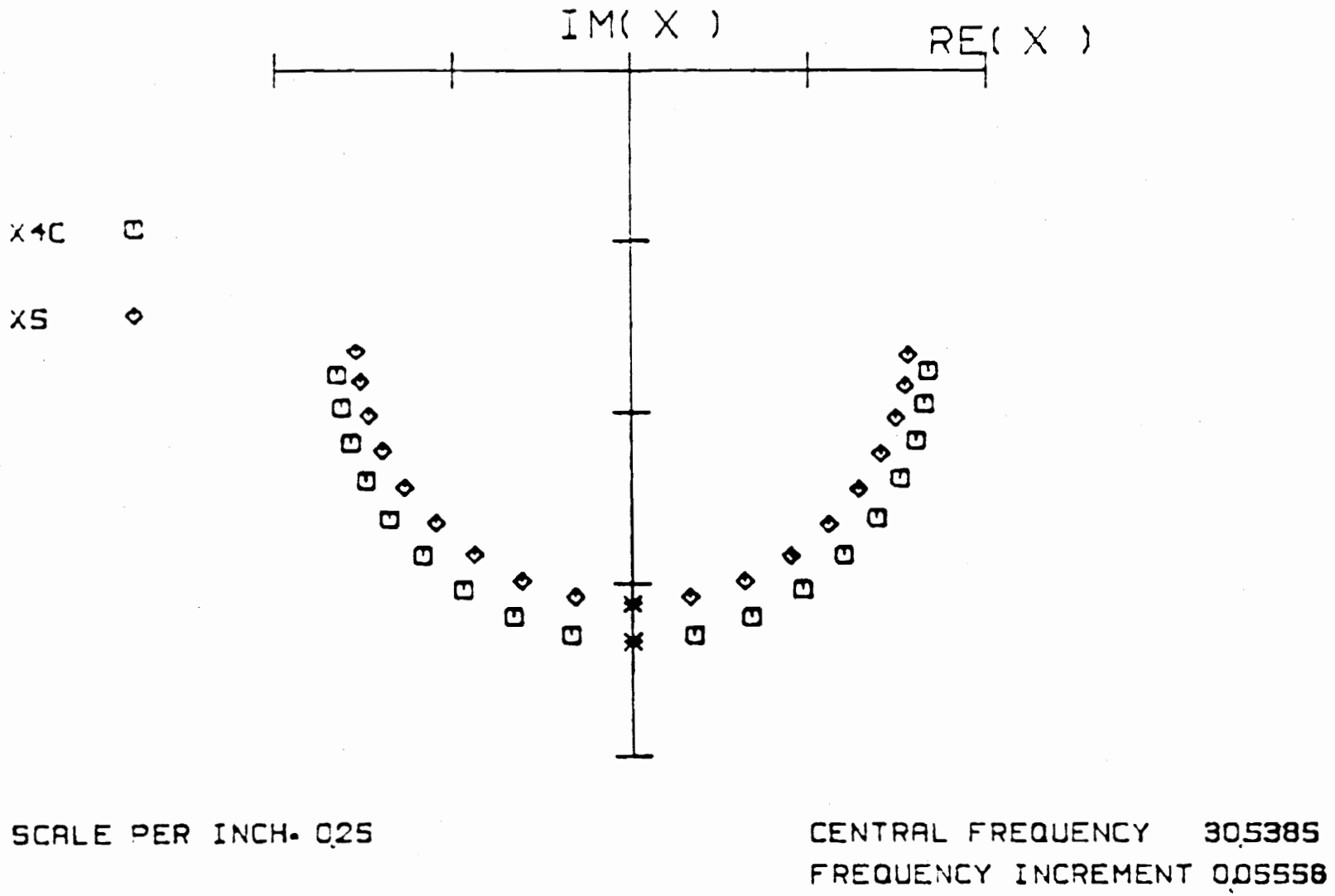

Figure 15. Co-quad Response in Mode 3 for Excitation at All Nodes.

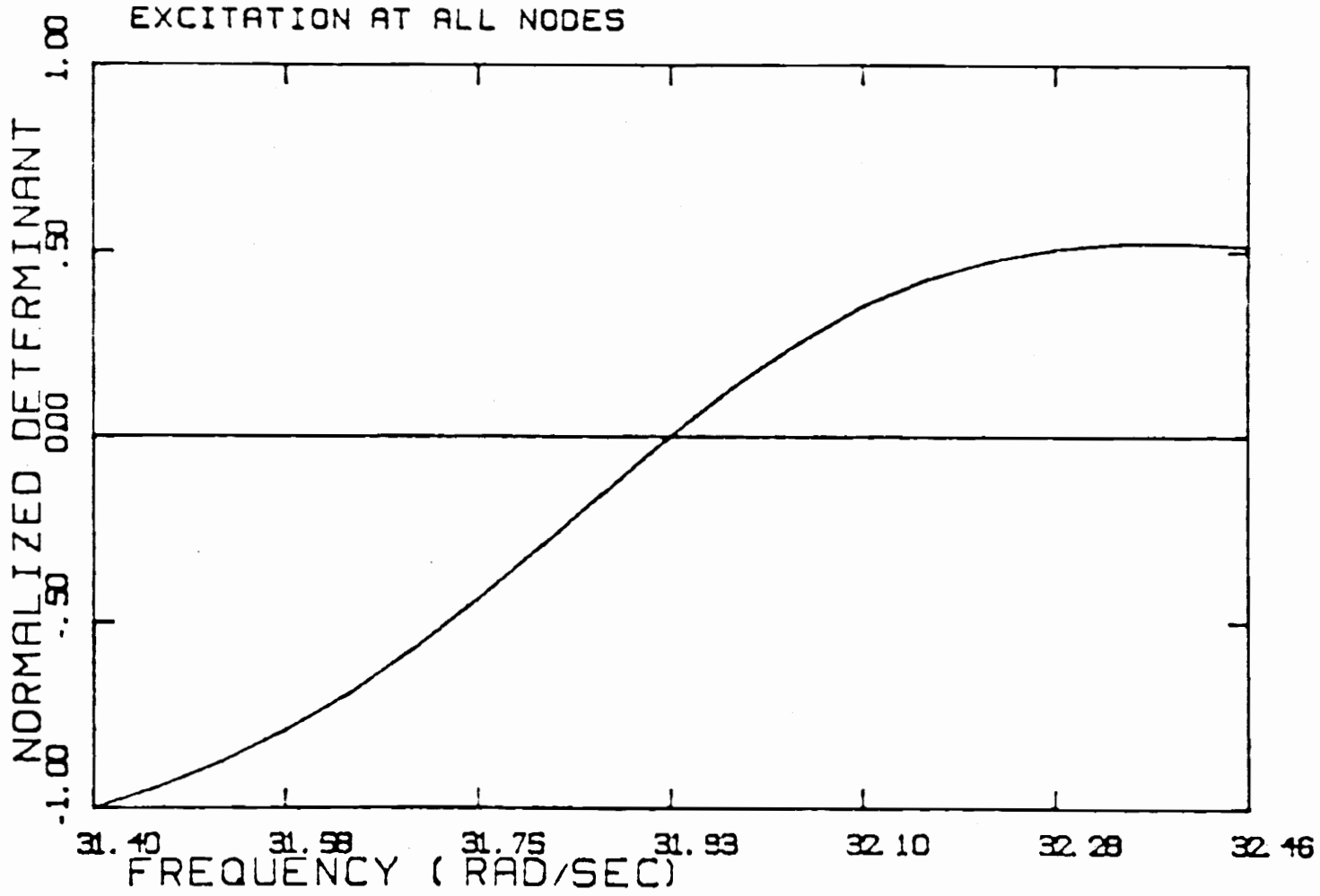

Figure 16. D(ω) for Excitation at All Nodes, 31.40 rps. to 32.46 rps.

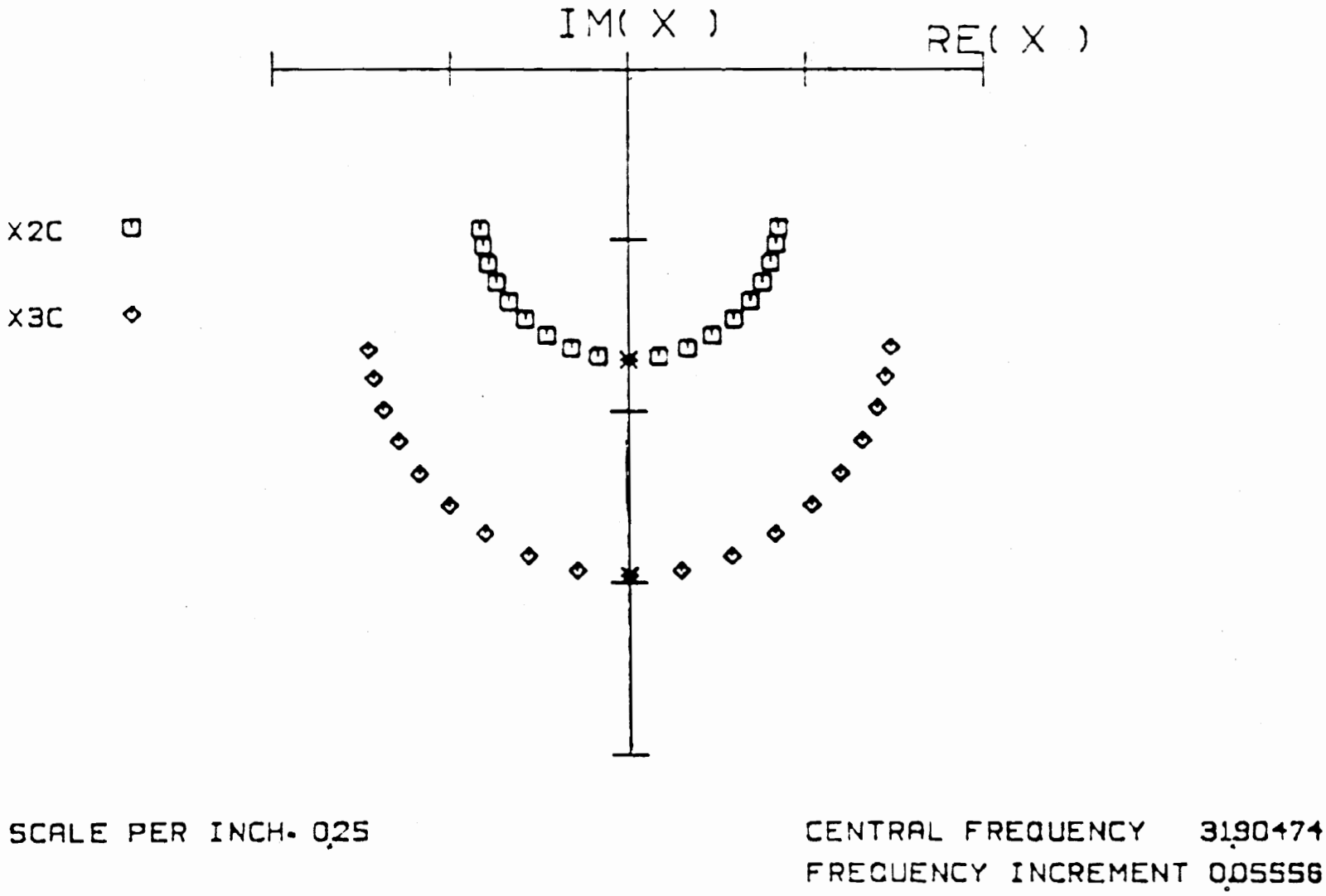

Figure 17. Co-quad Response in Mode 4 for Excitation at All Nodes

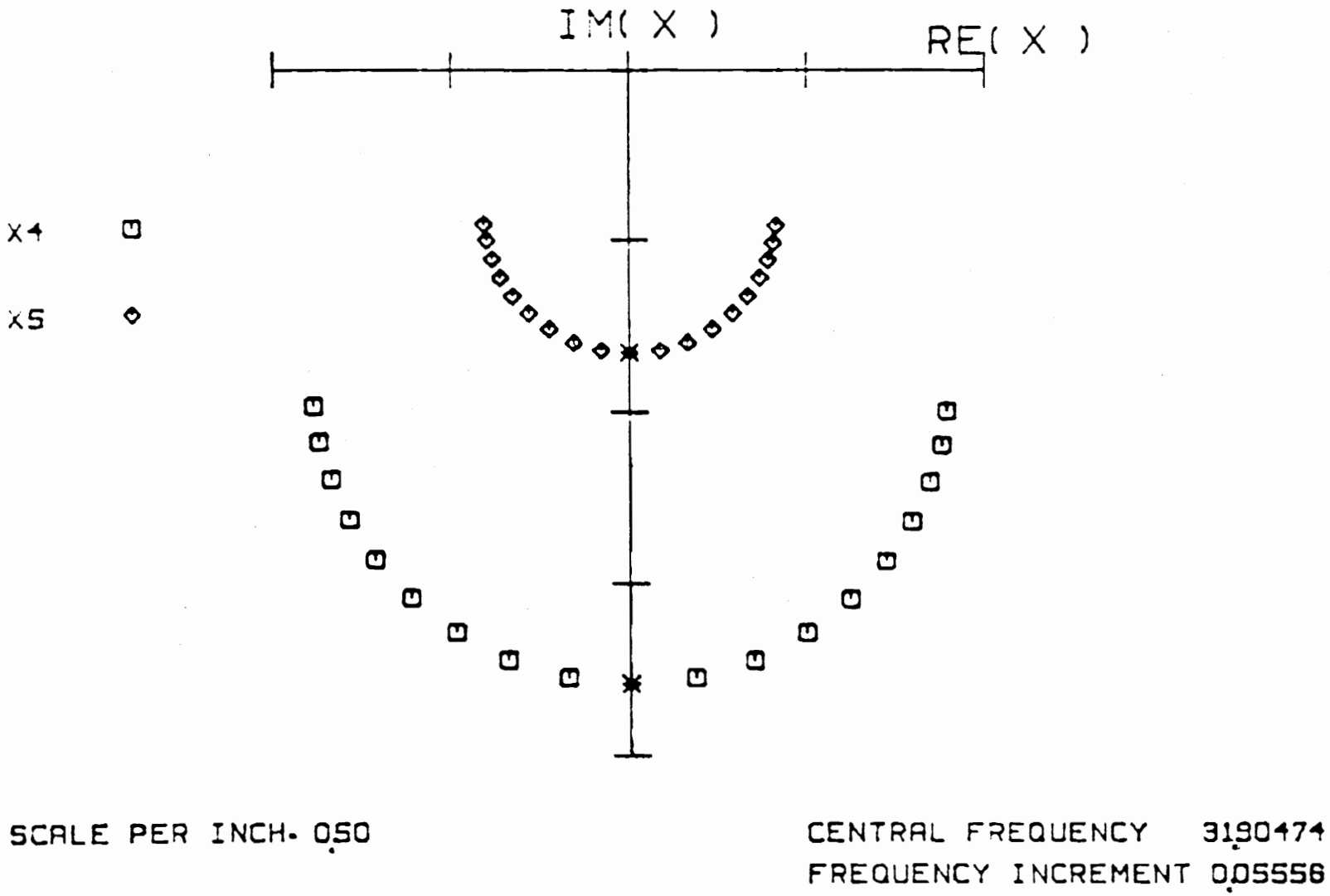

Figure 18. Co-quad Response in Mode 4 for Excitation at All Nodes.

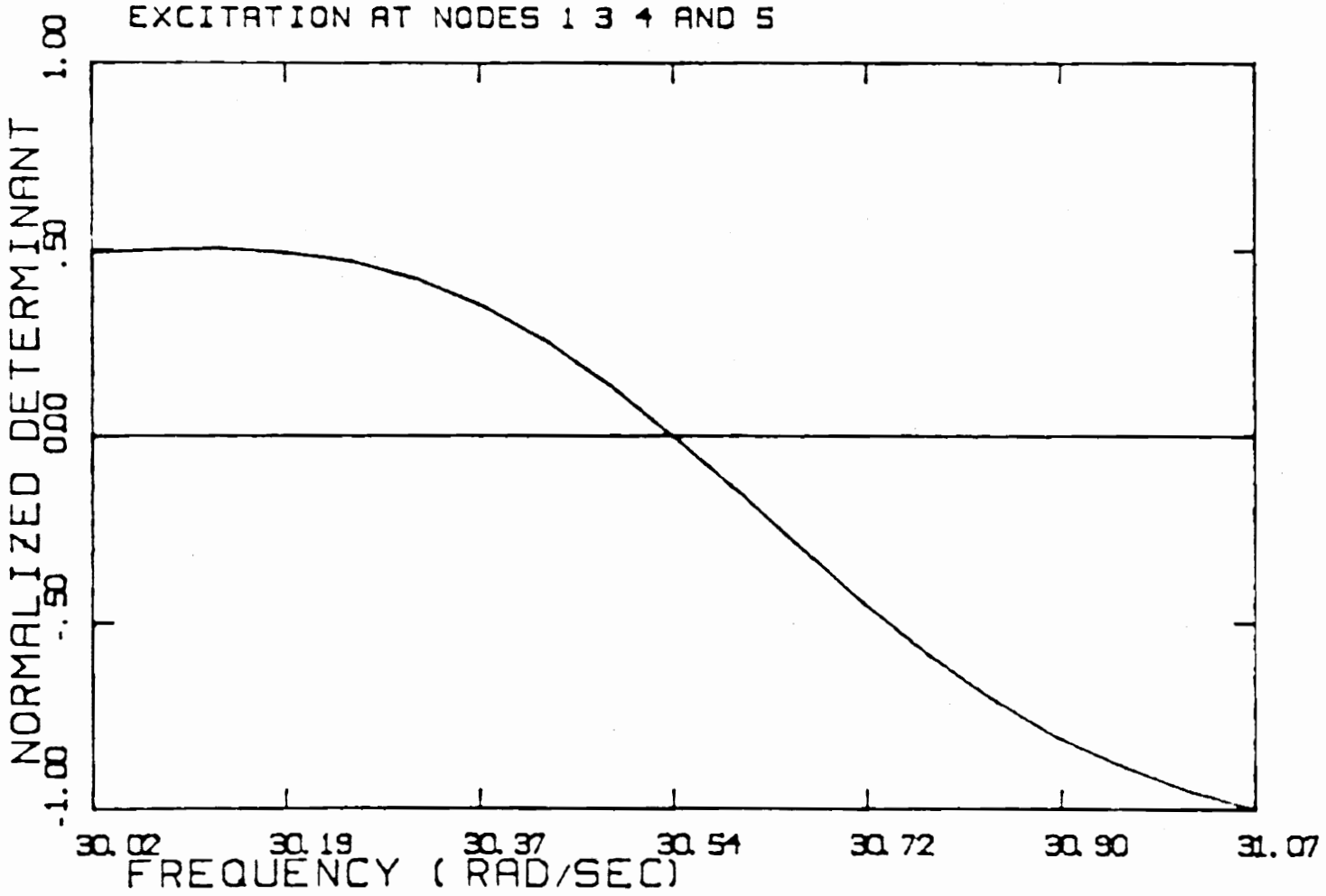

Figure 19. D(ω) for Excitation at Nodes 1, 3, 4, and 5 , 30.02 rps. to 31.07 rps.

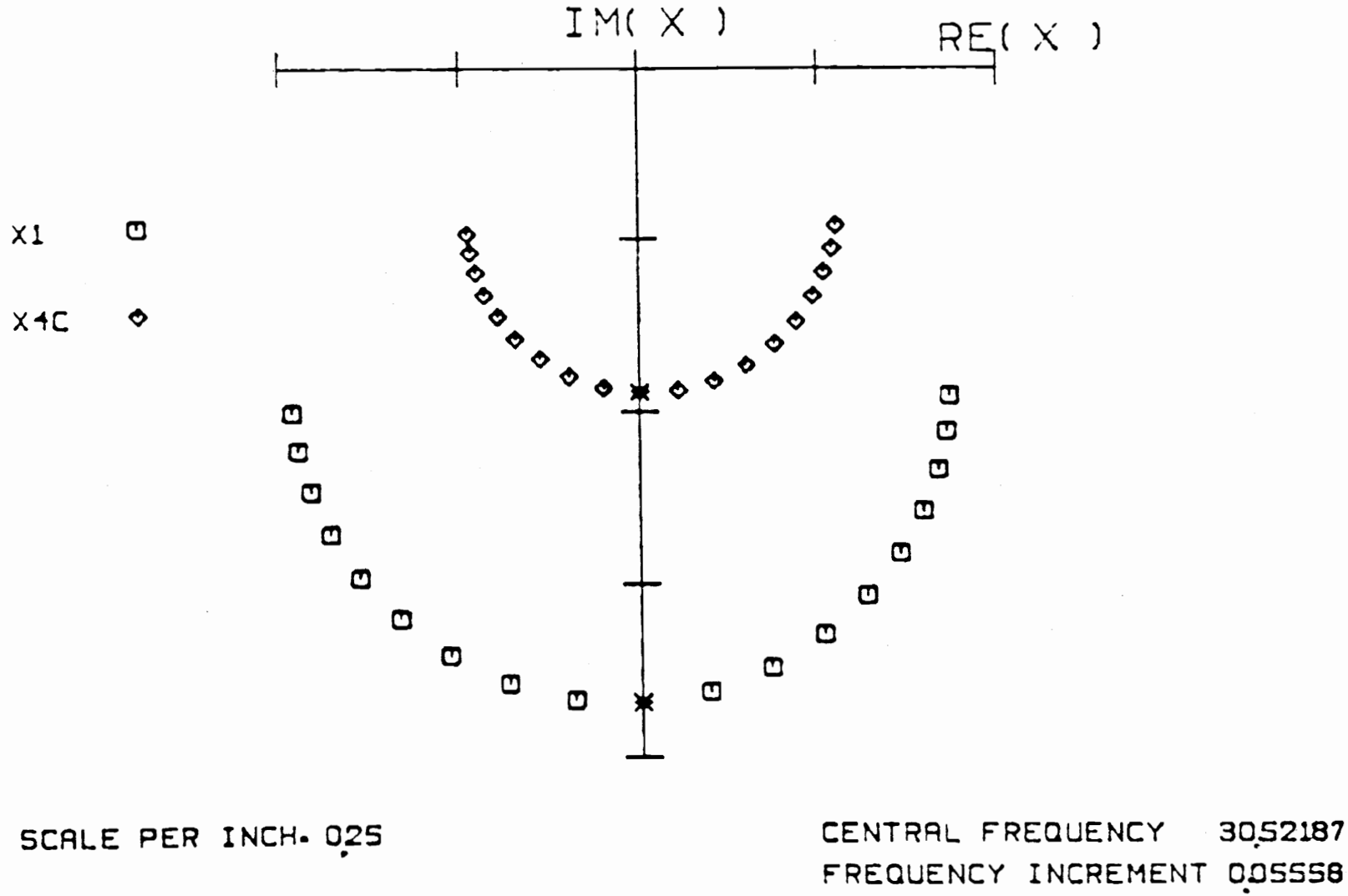

Figure 20. Co-quad Response in Mode 3 for Excitation at Nodes 1, 3, 4, and 5

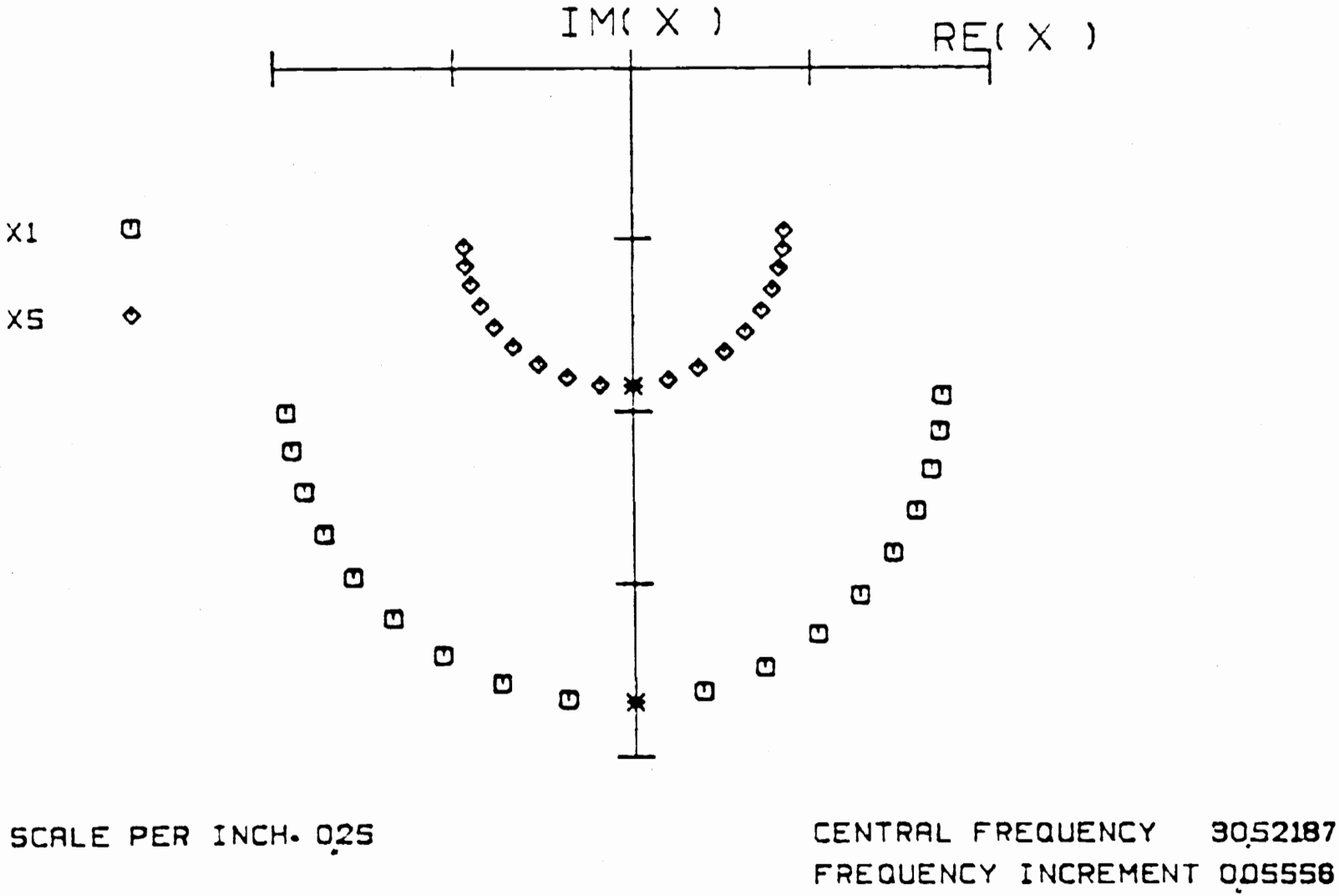

Figure 21. Co-quad Response in Mode 3 for Excitation at Nodes 1, 3, 4, and 5.

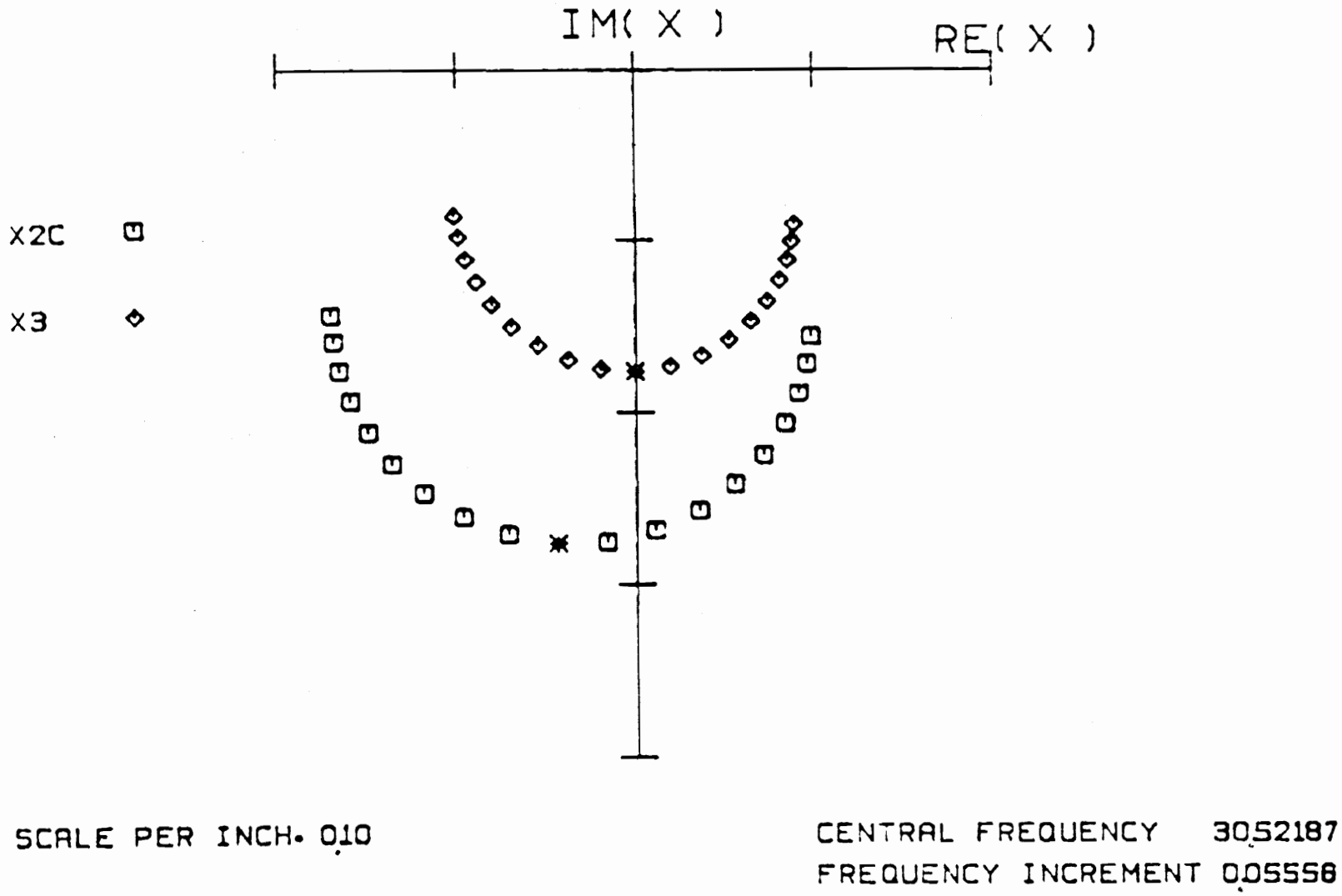

Figure 22. Co-quad Response in Mode 3 for Excitation at Nodes 1, 3, 4, and 5.

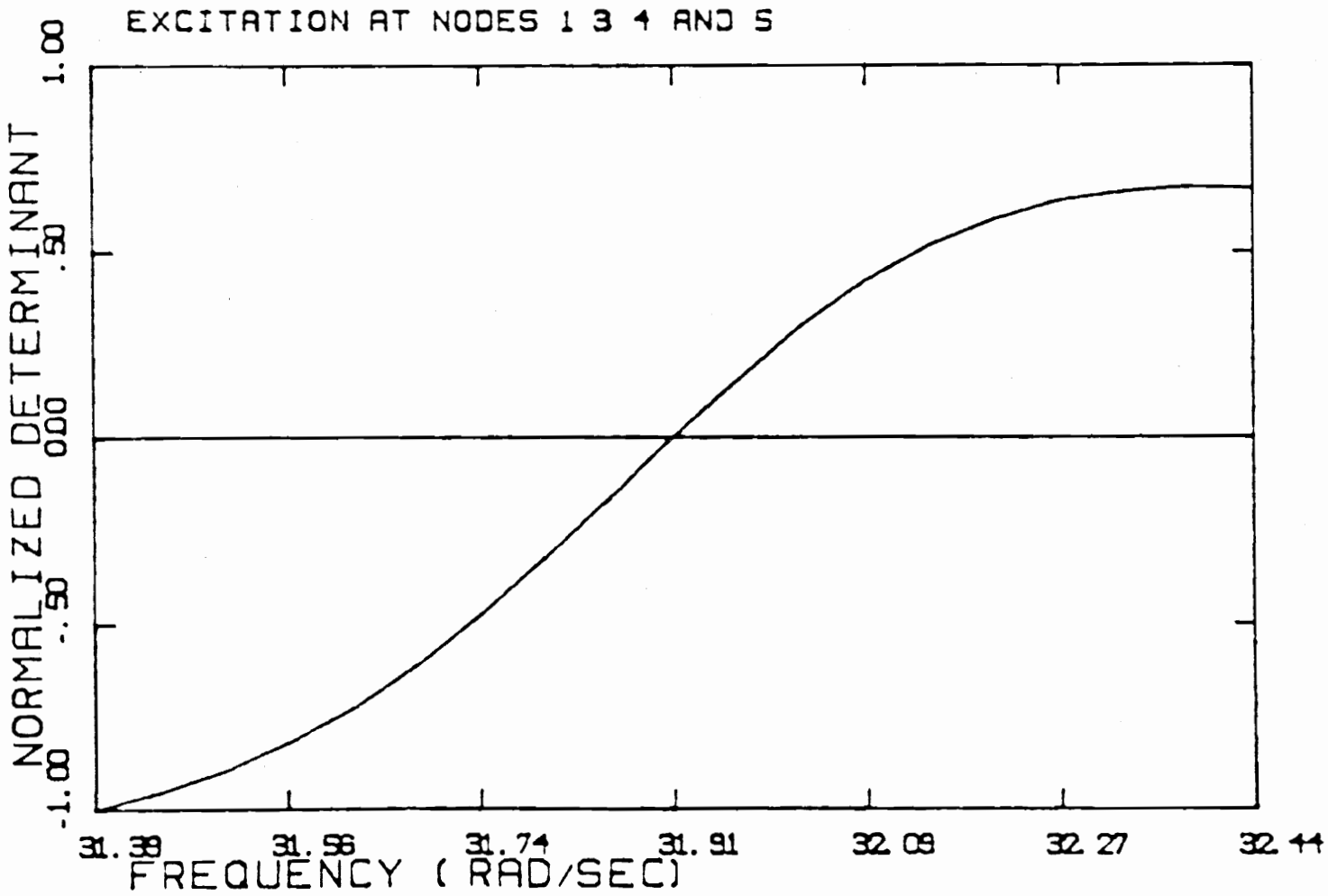

Figure 23. D(ω) for Excitation at Nodes 1, 3, 4, and 5, 31.39 rps. to 32.44 rps.

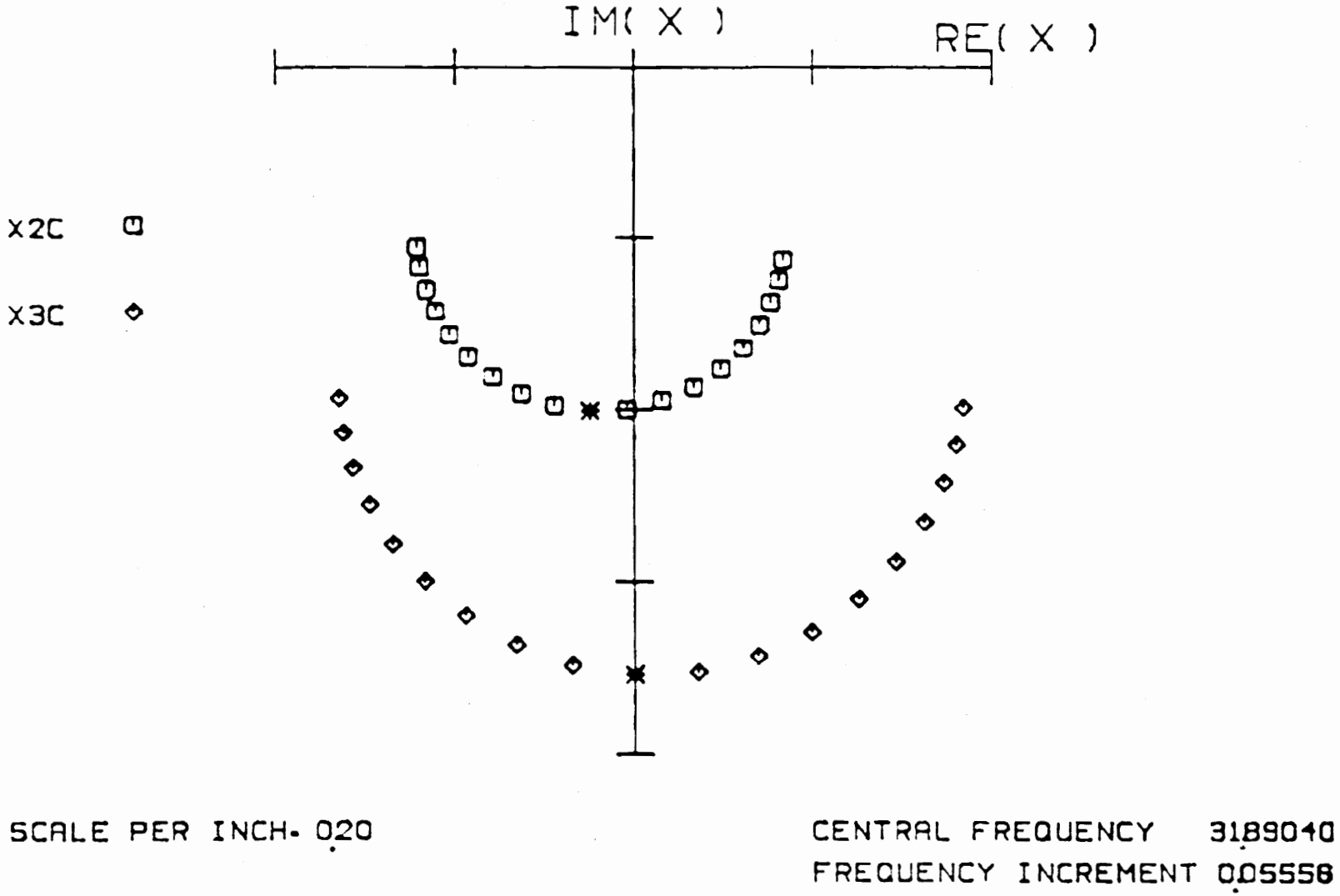

Figure 24. Co-quad Response in Mode 4 for Excitation at Nodes 1, 3, 4, and 5.

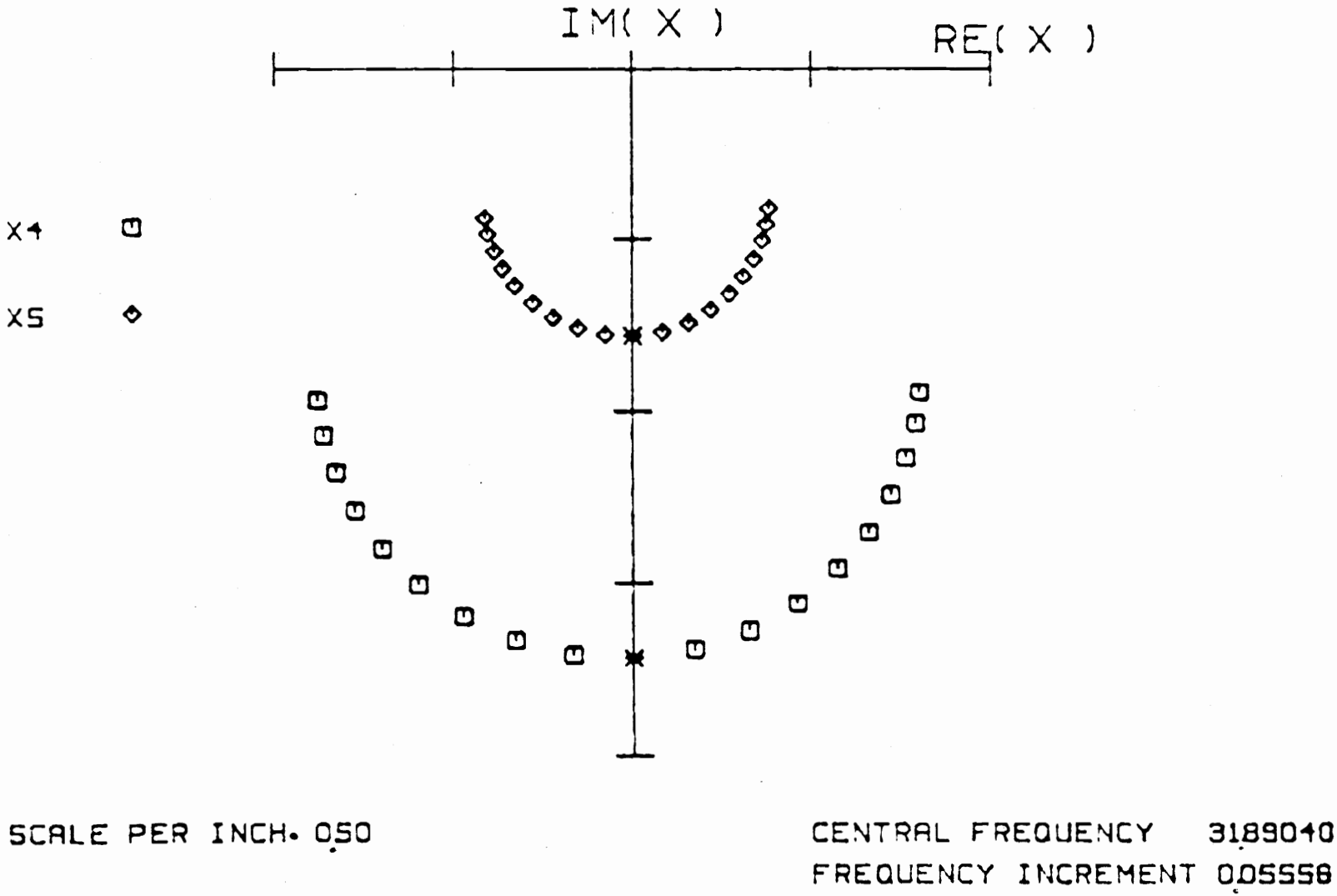

Figure 25. Co-quad Response in Mode 4 for Excitation at Nodes 1, 3, 4, and 5.

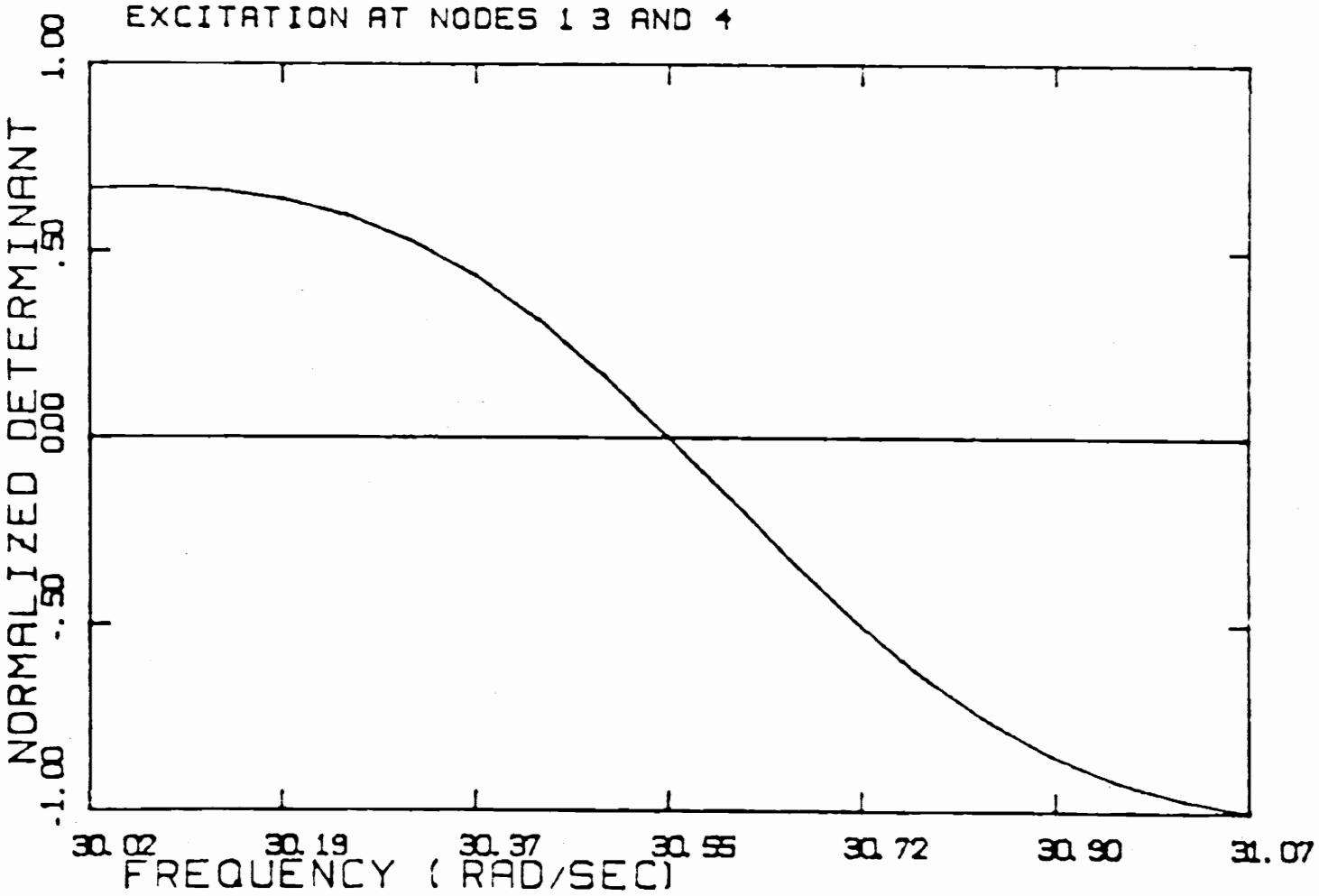

Figure 26. D(ω) for Excitation at Nodes 1, 3, 4, 30.02 rps. to 31.07 rps.

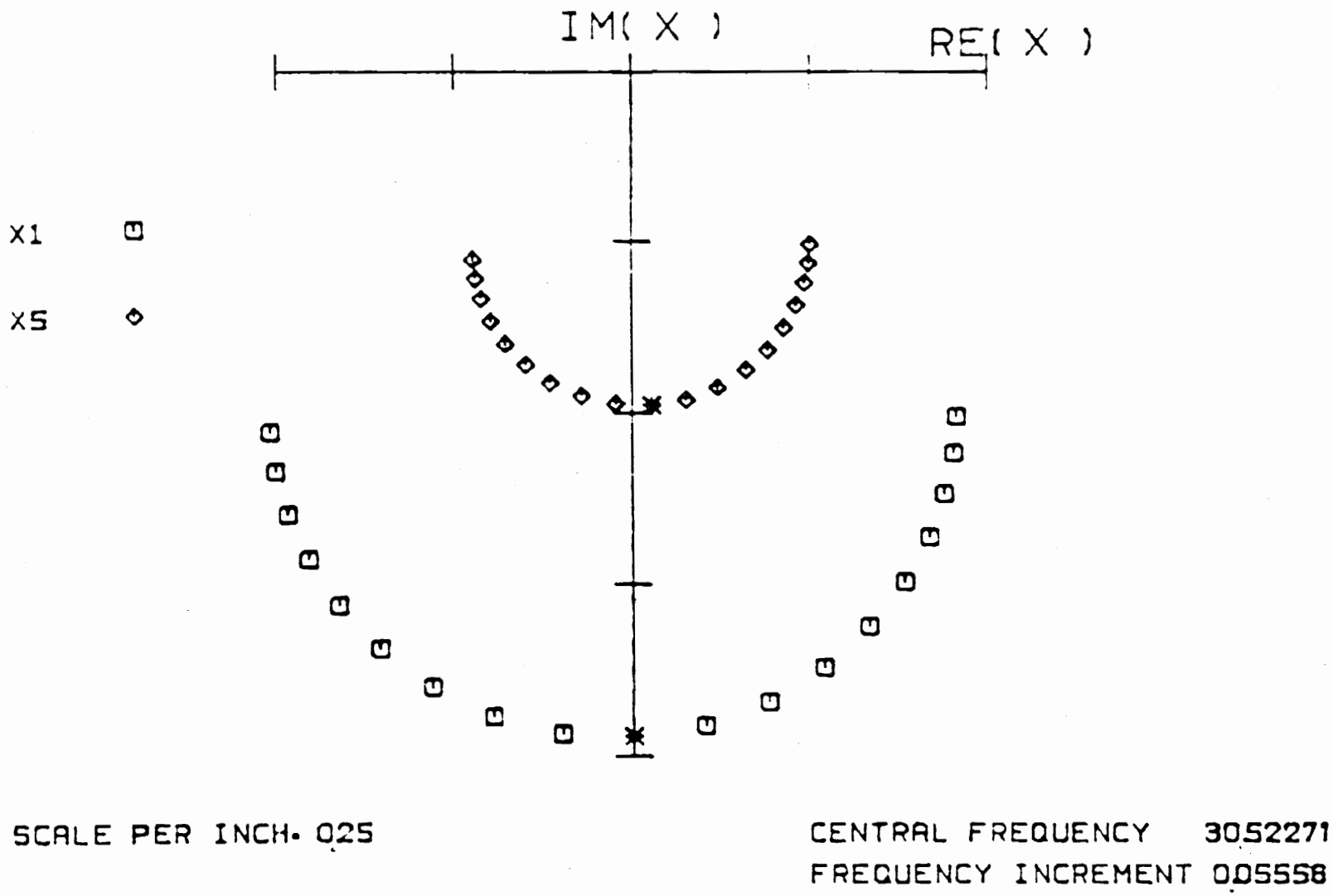

Figure 27. Co-quad Response in Mode 3 for Excitation at Nodes 1, 3, and 4.

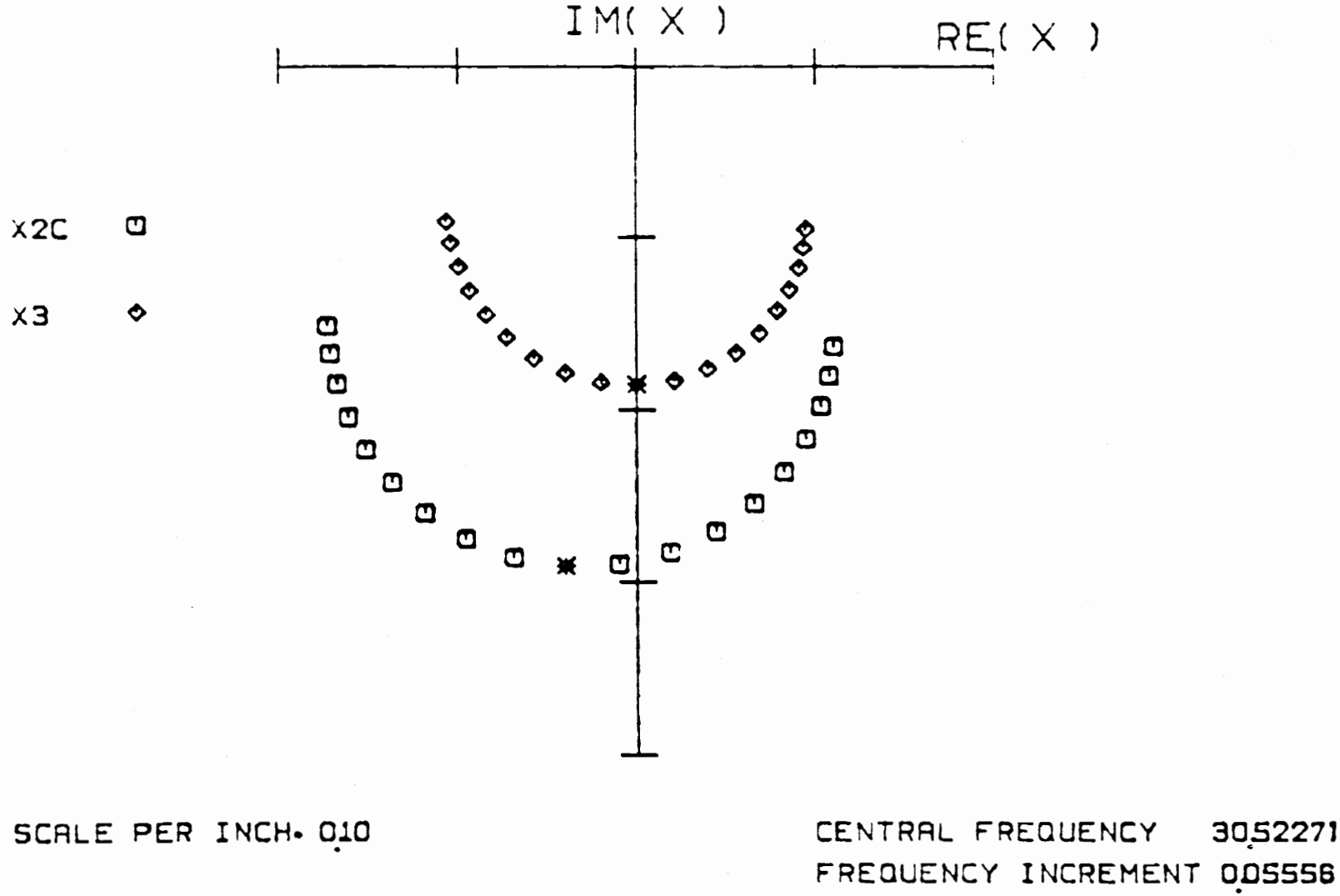

Figure 28. Co-quad Response in Mode 3 for Excitation at Nodes 1, 3, and 4.

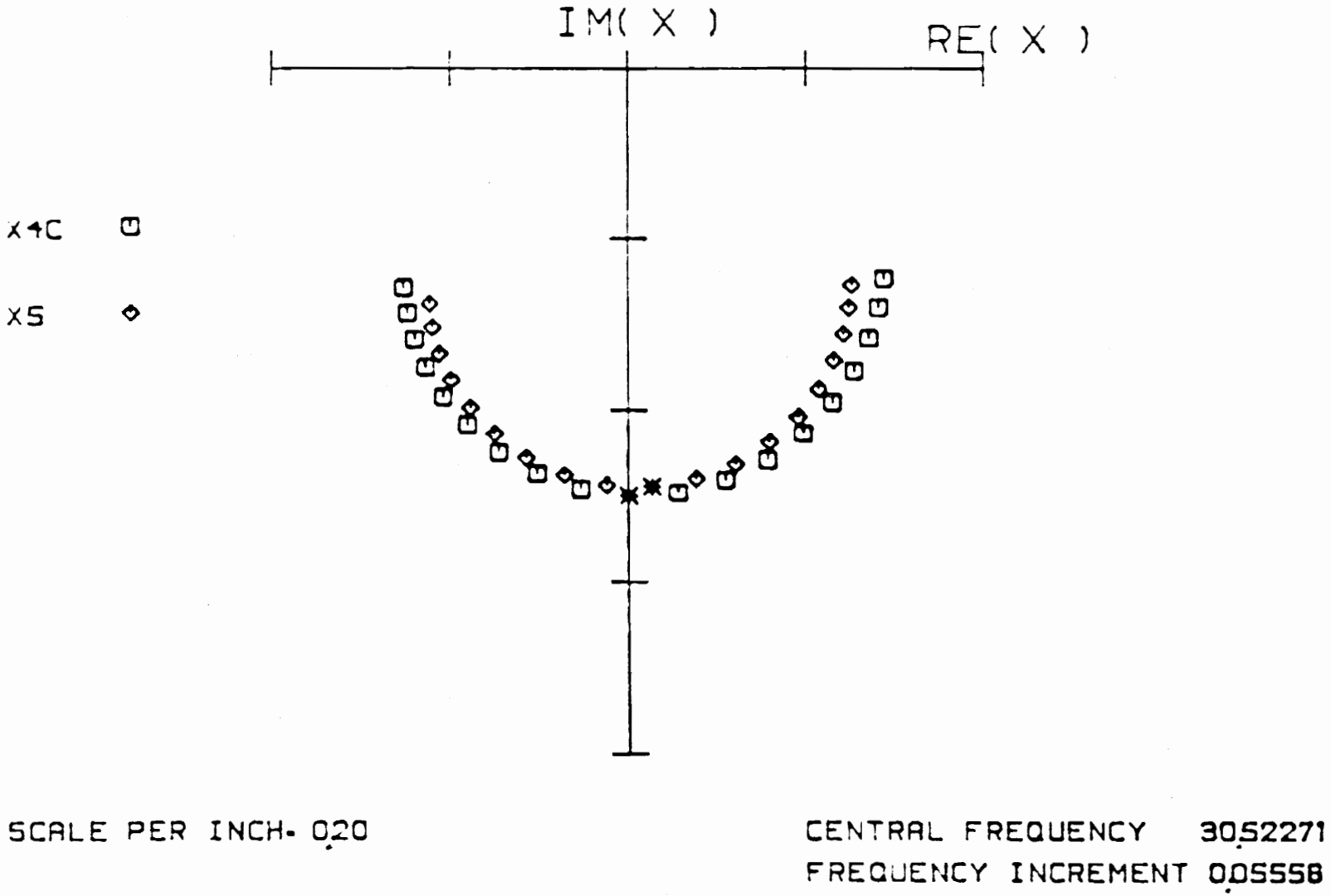

Figure 29. Co-quad Response in Mode 3 for Excitation at Nodes 1, 3, and 4.

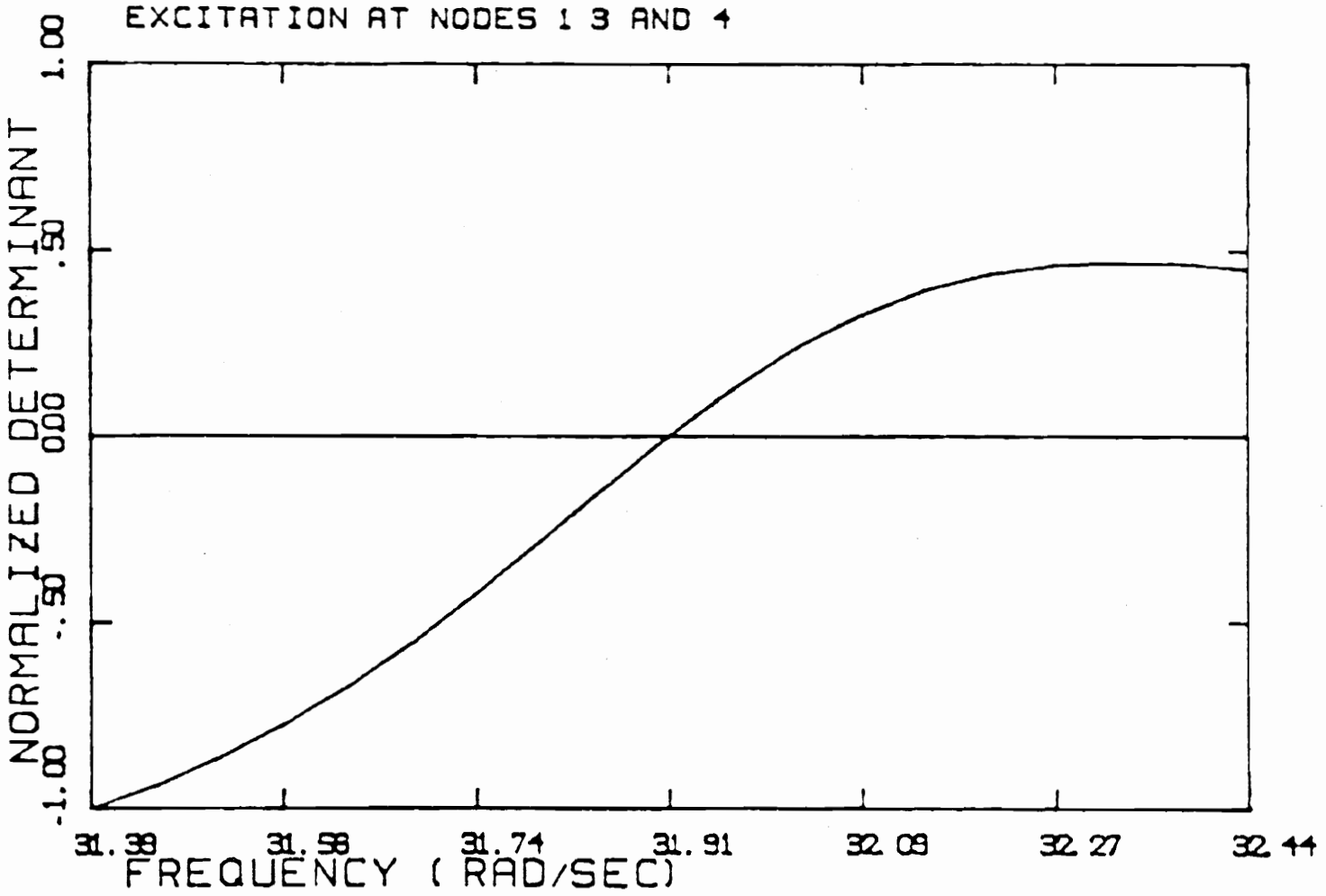

Figure 30. D(ω) for Excitation at Nodes 1, 3, and 4, 31.38 rps. to 32.44 rps.

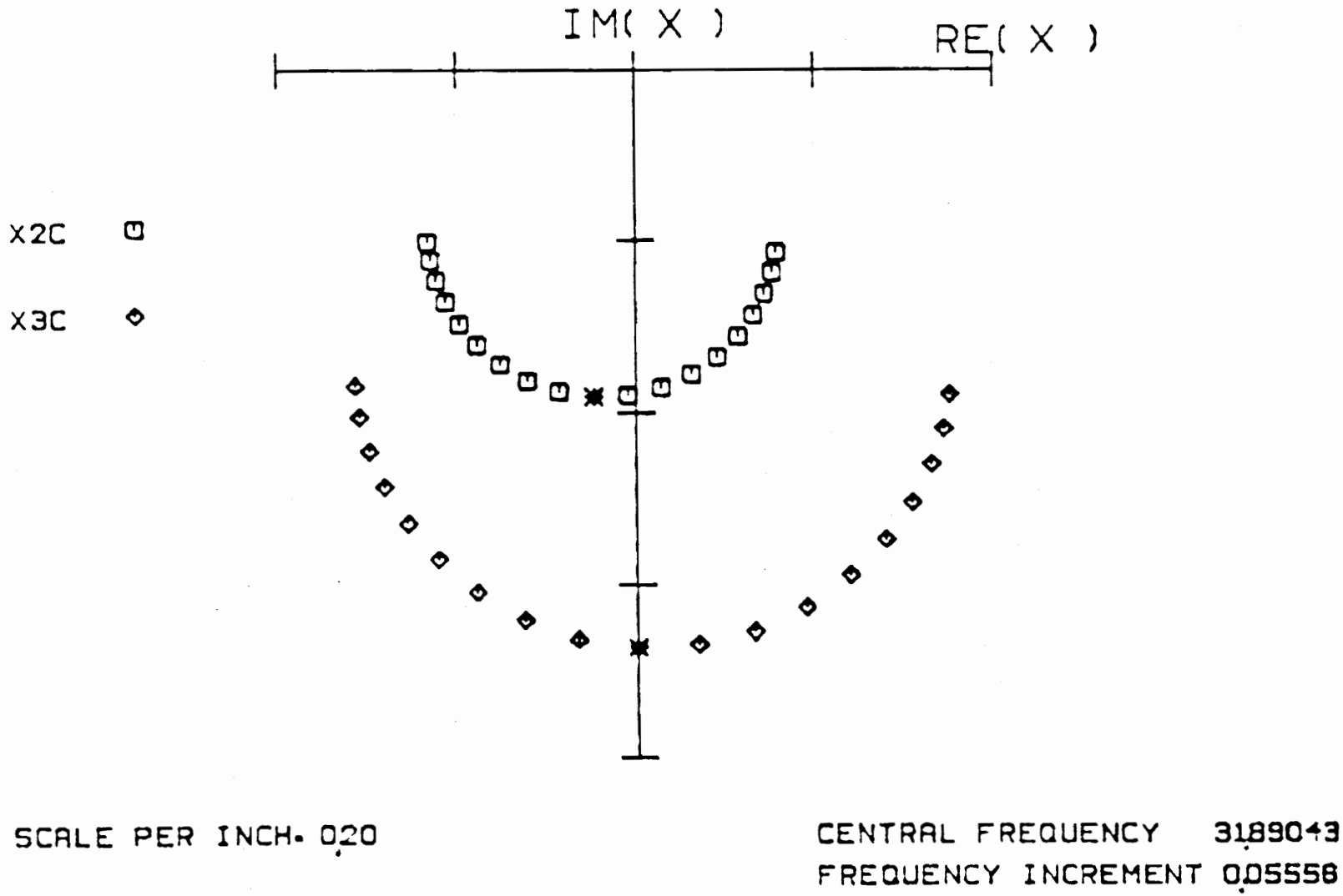

Figure 31. Co-quad Response in Mode 4 for Excitation at Nodes 1, 3, and 4.

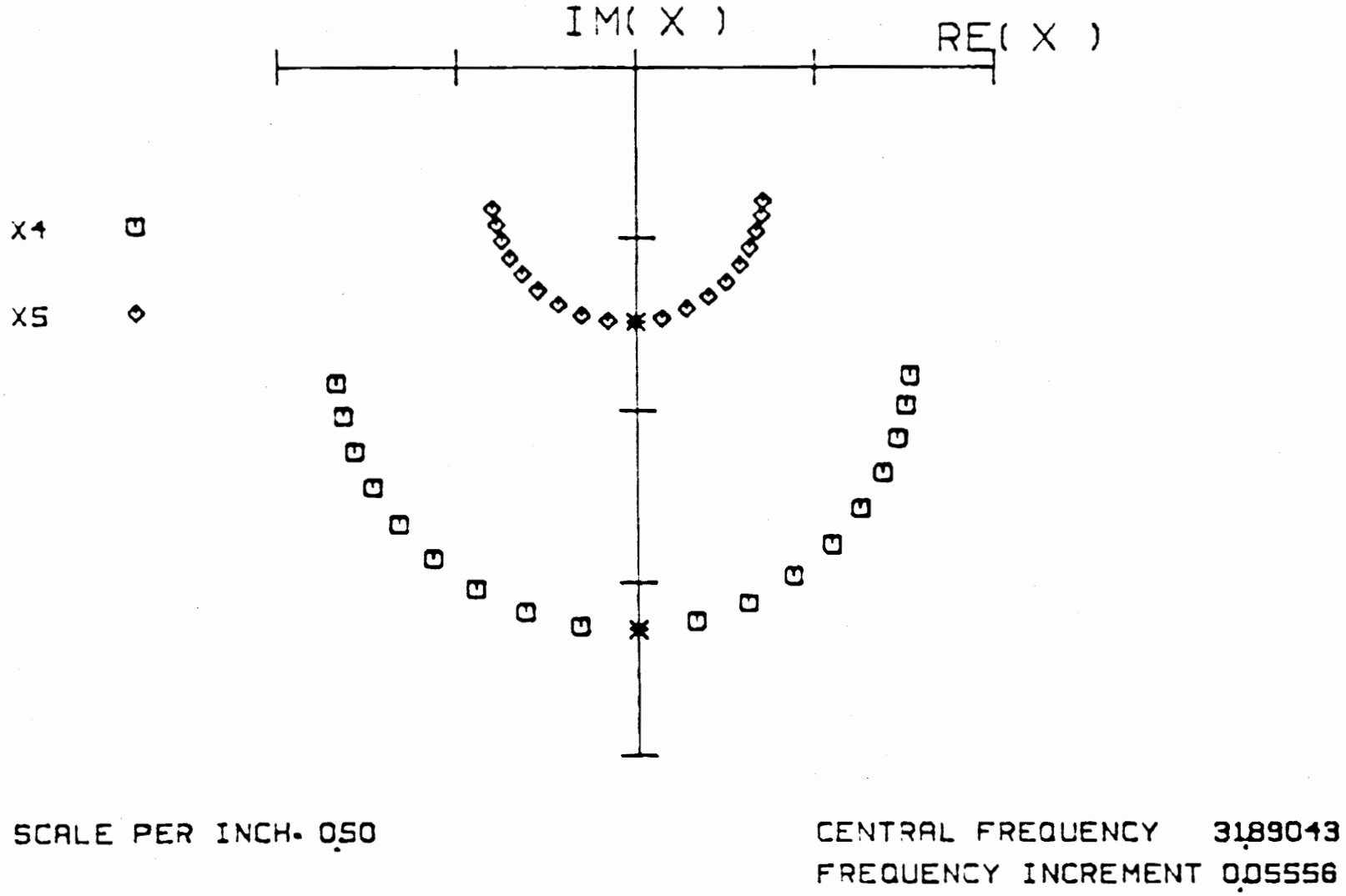

Figure 32. Co-quad Response in Mode 4 for Excitation at Nodes 1, 3, and 4.

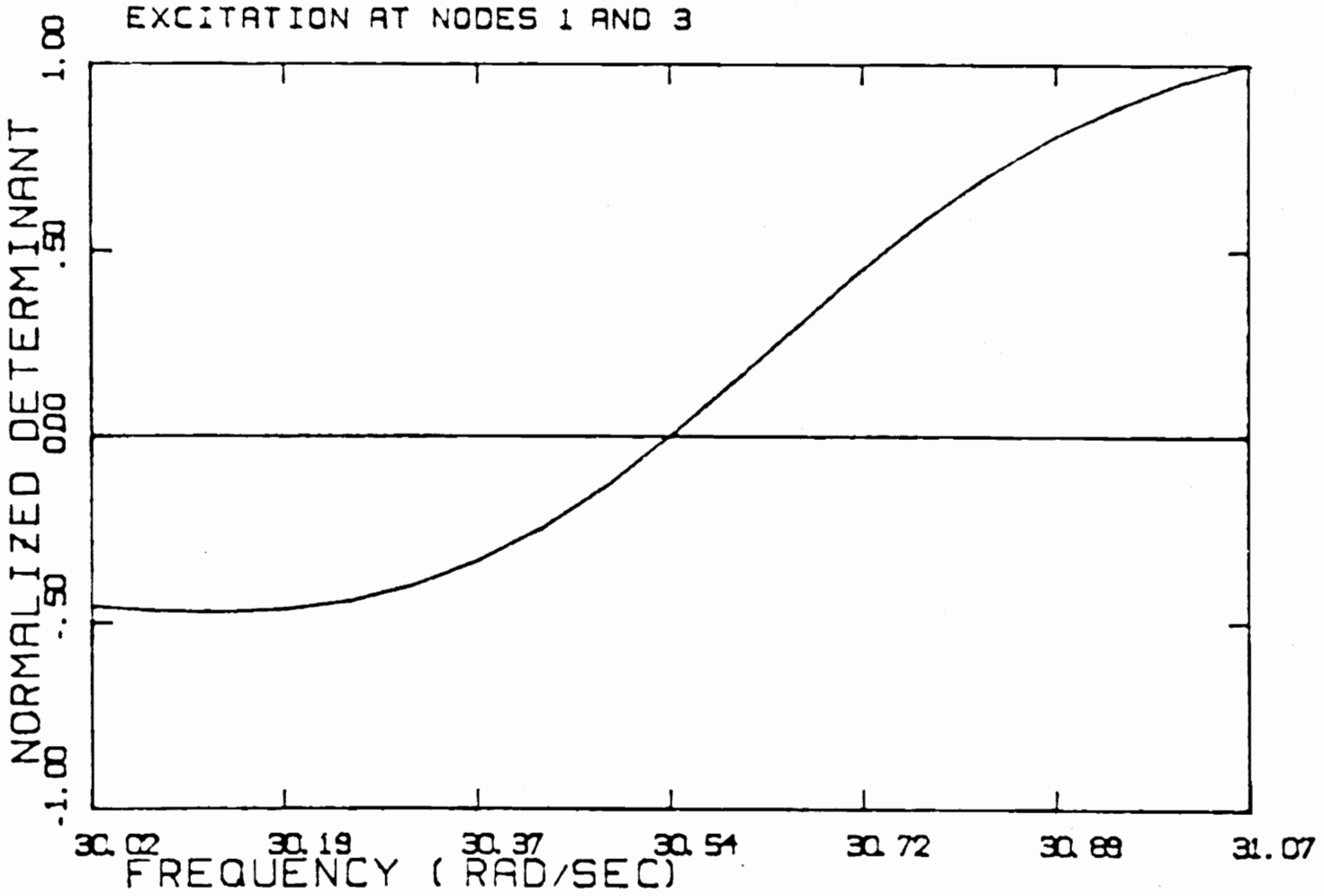

Figure 33. D(ω) for Excitation at Nodes 1 and 3, 30.02 rps. to 31.07 rps.

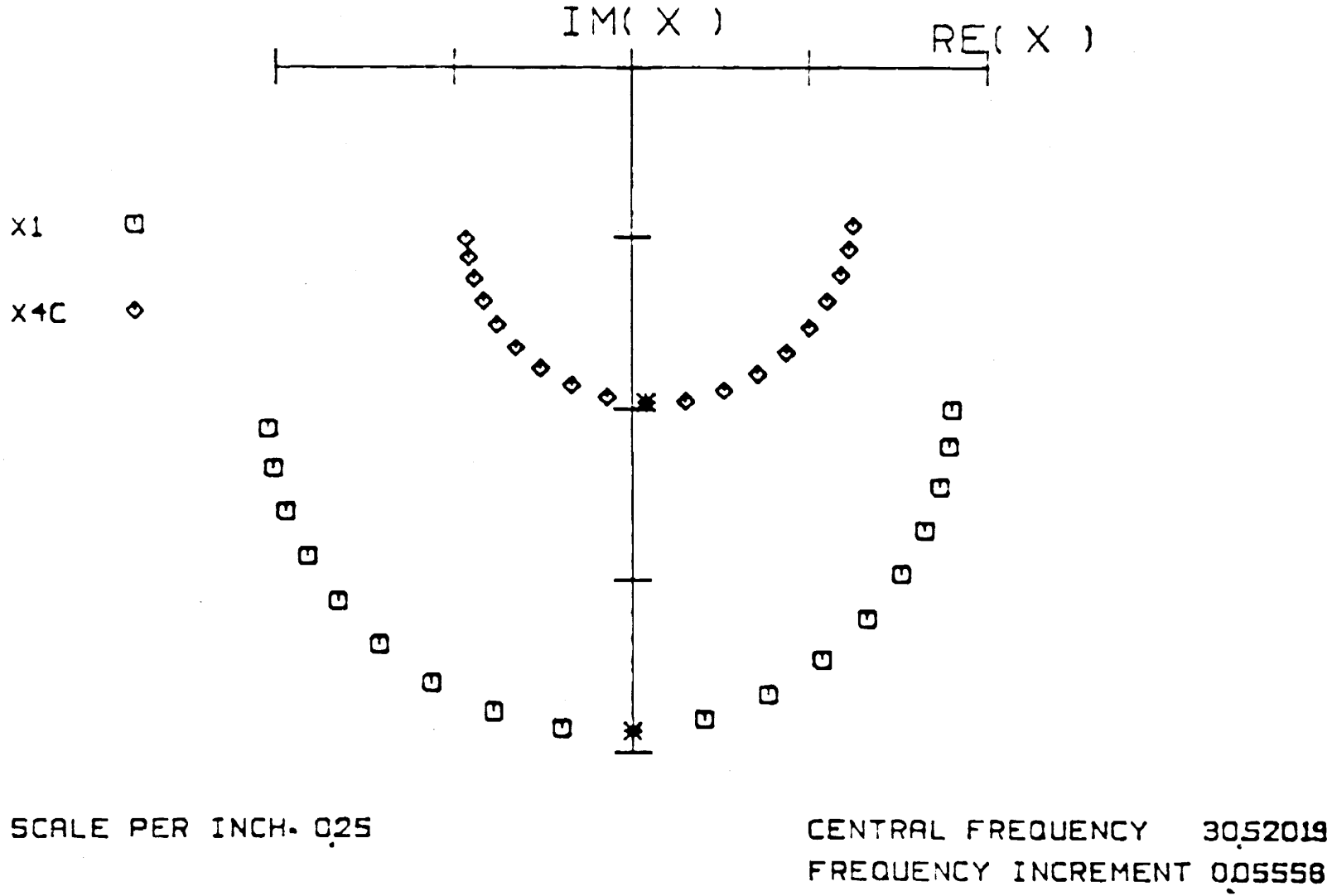

Figure 34. Co-quad Response in Mode 3 for Excitation at Nodes 1 and 3.

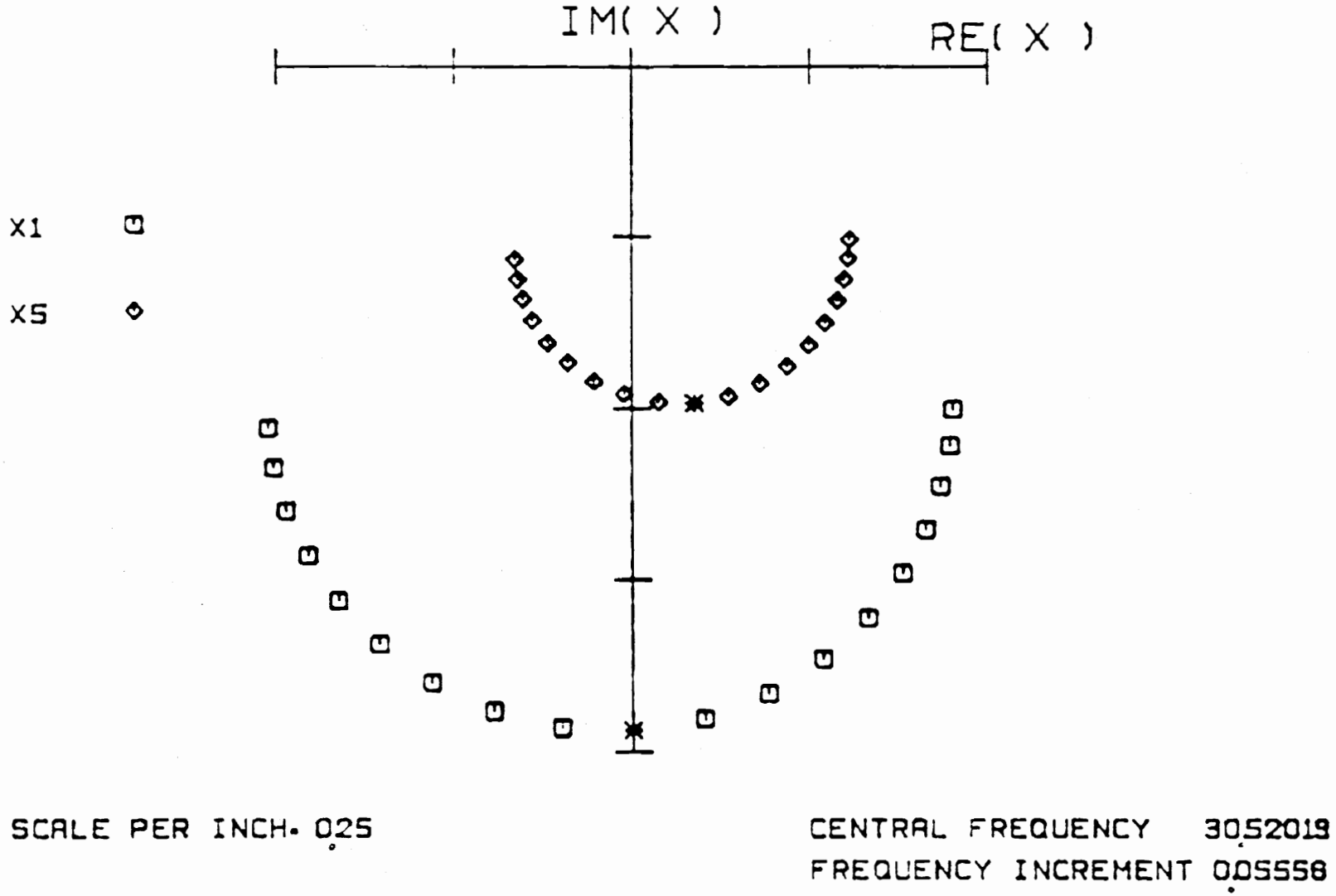

Figure 35. Co-quad Response in Mode 3 for Excitation at Nodes 1 and 3.

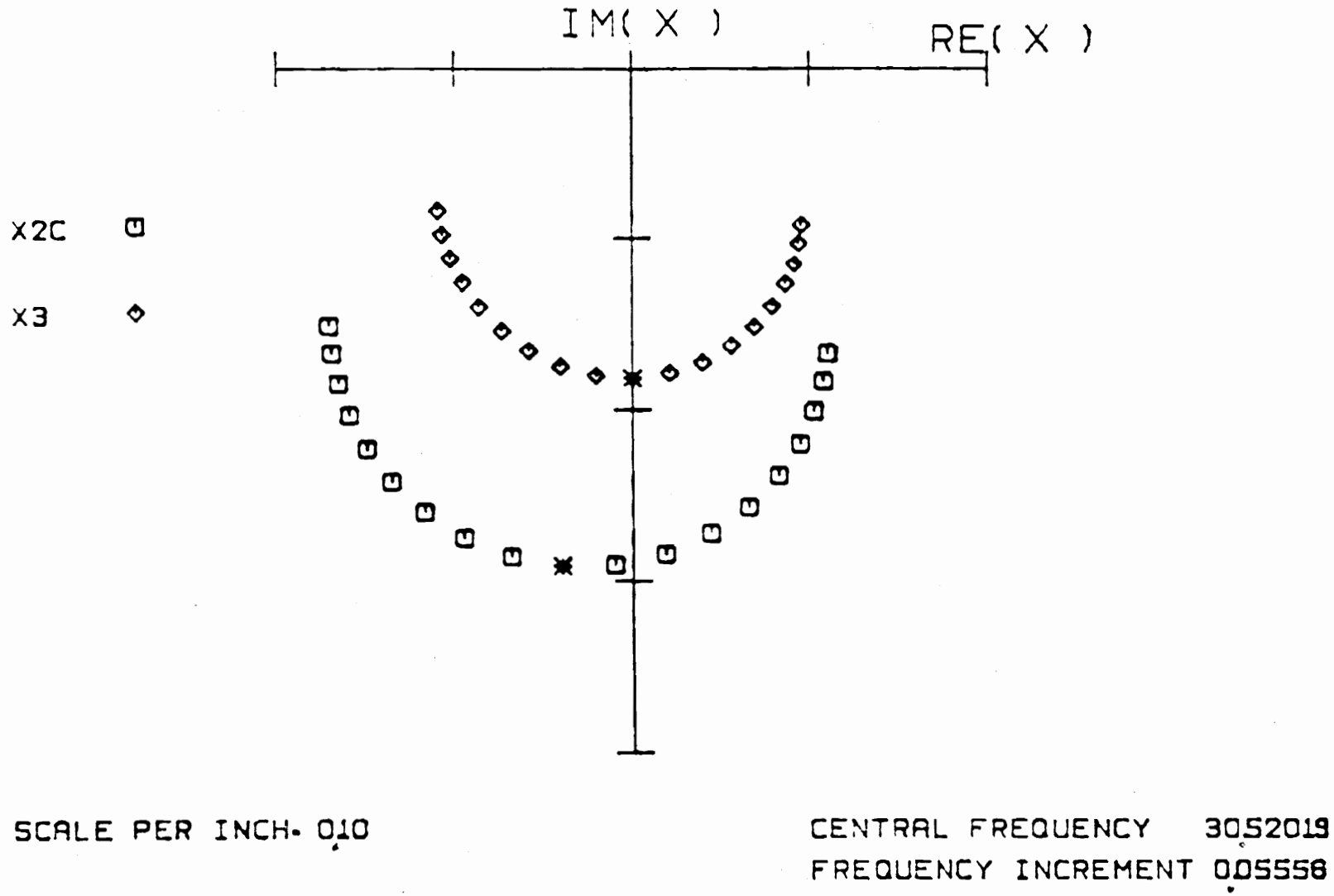

Figure 36. Co-quad Response in Mode 3 for Excitation at Nodes 1 and 3.

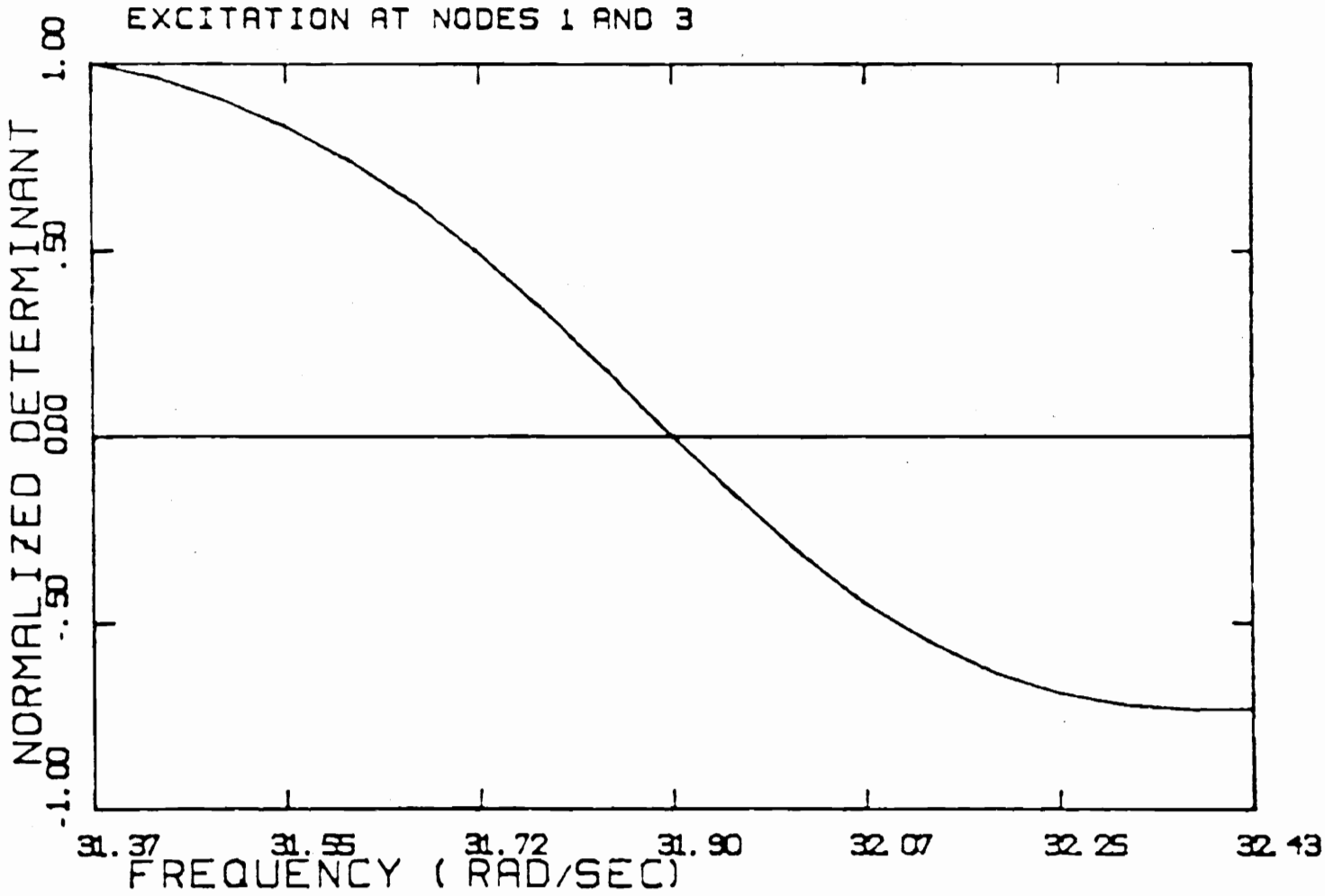

Figure 37. D(ω) for Excitation at Nodes 1 and 3, 31.37 rps. to 32.43 rps.

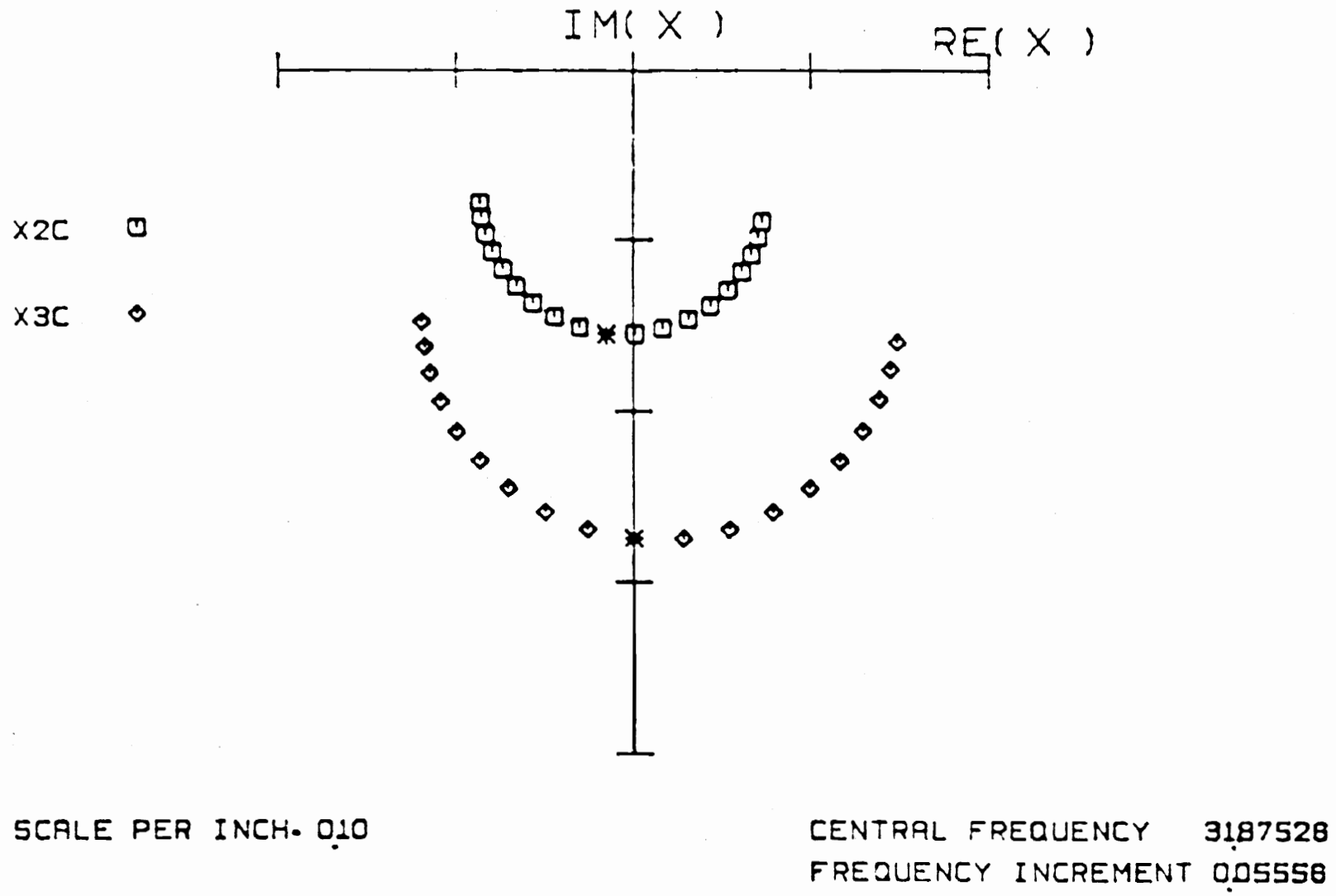

Figure 38. Co-quad Response in Mode 4 for Excitation at Nodes 1 and 3.

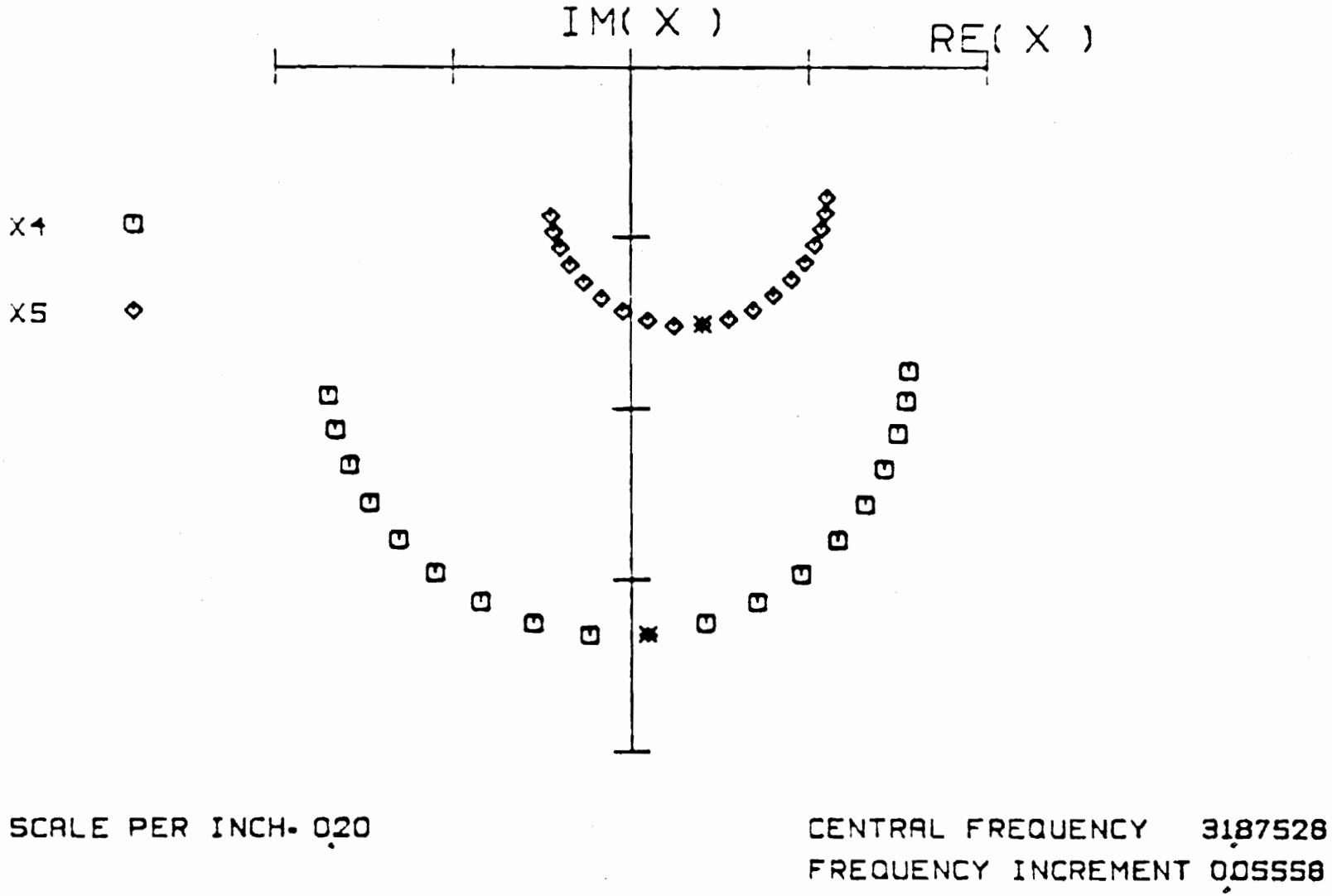

Figure 39. Co-quad Response in Mode 4 for Excitation at Nodes 1 and 3.

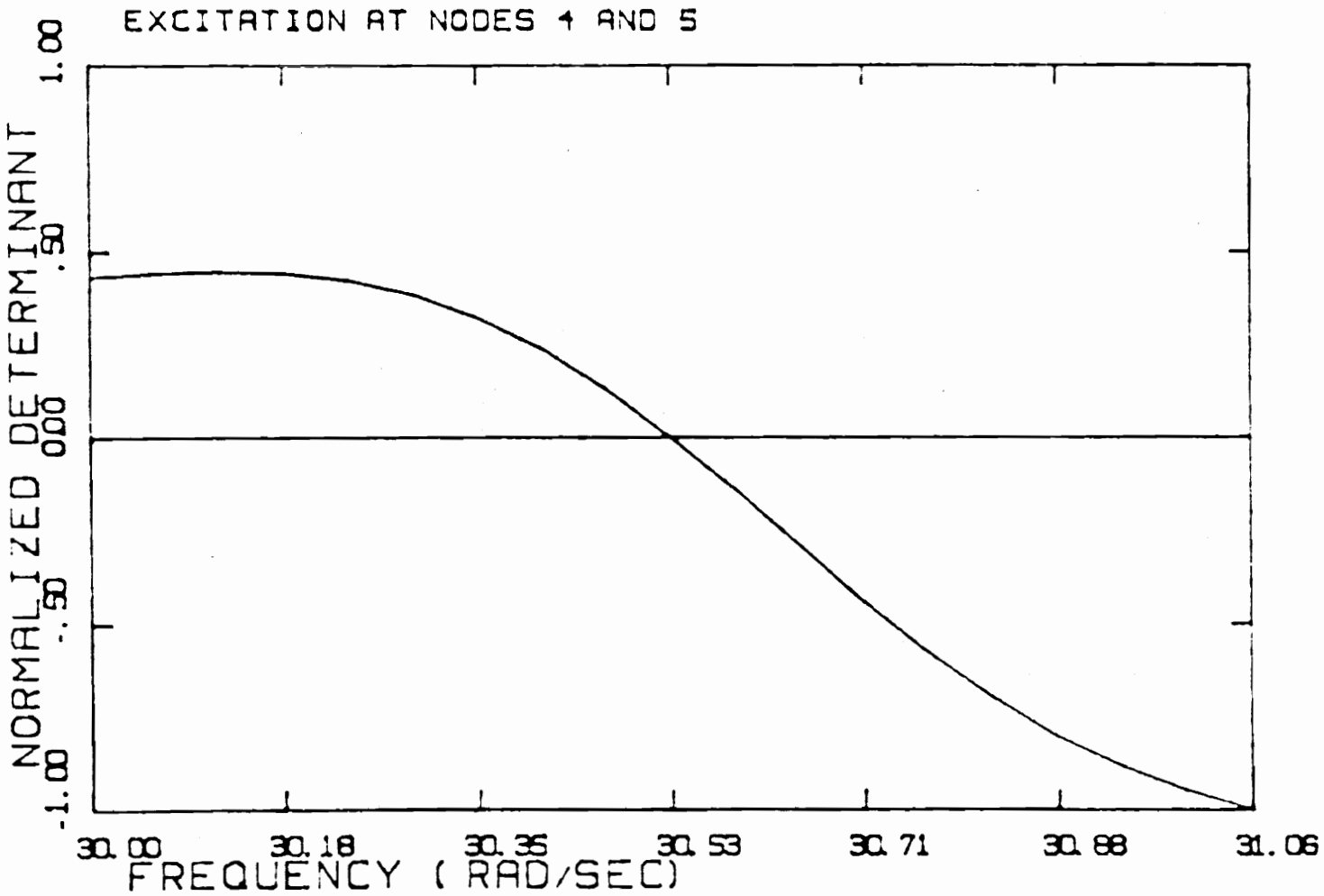

Figure 40. D(ω) for Excitation at Nodes 4 and 5, 30.00 rps. to 31.06 rps.

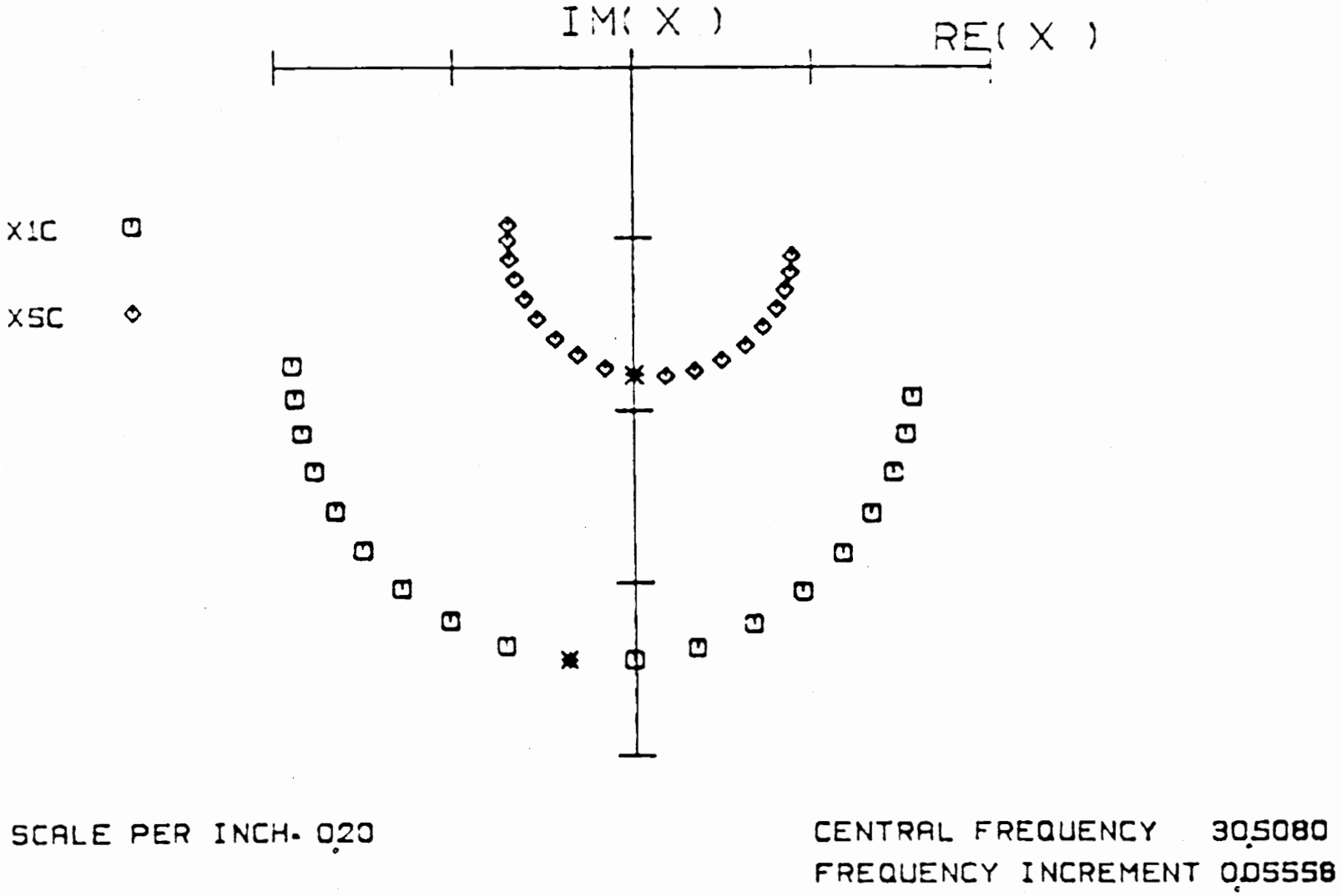

Figure 41. Co-quad Response in Mode 3 for Excitation at Nodes 4 and 5.

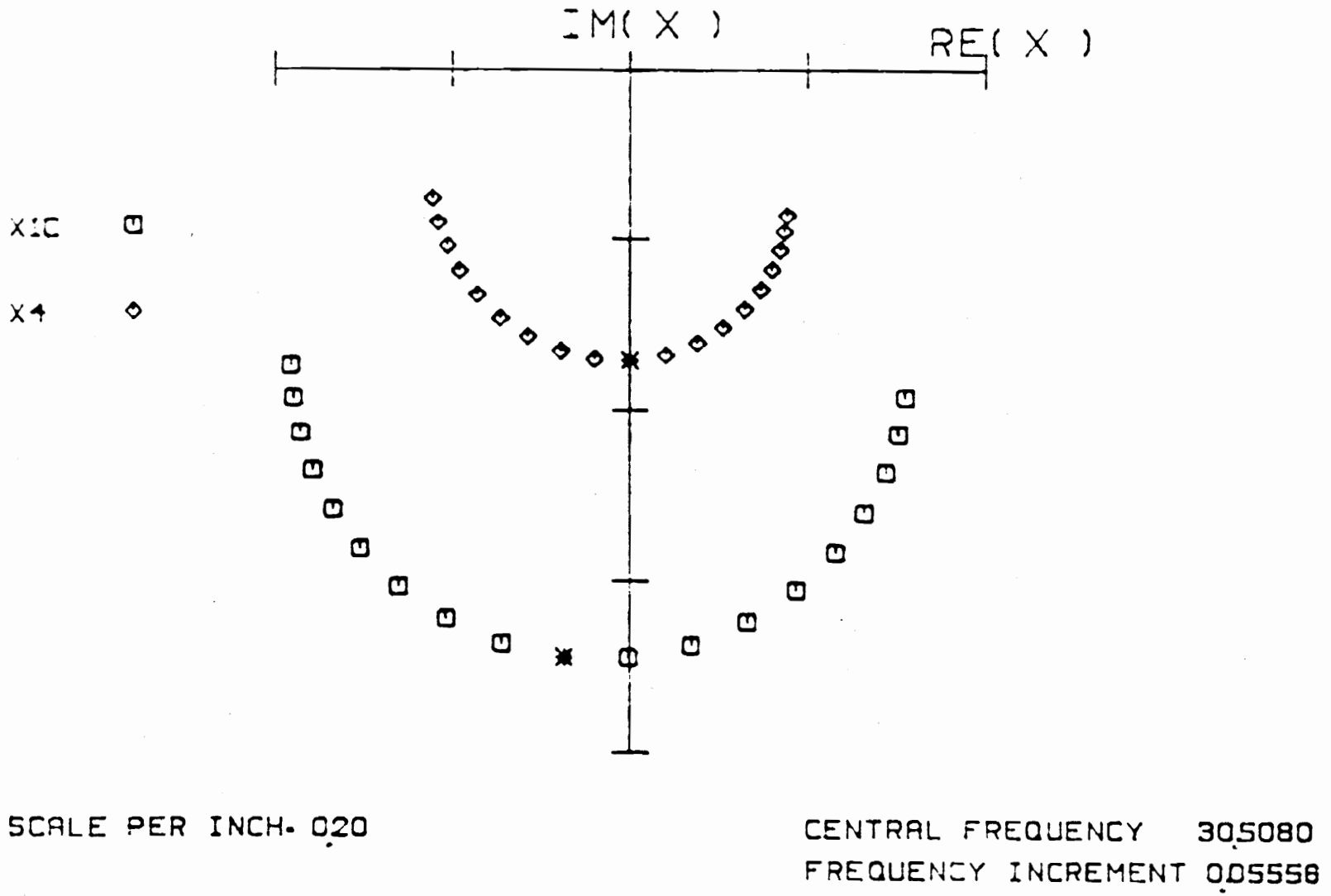

Figure 42. Co-quad Response in Mode 3 for Excitation at Nodes 4 and 5.

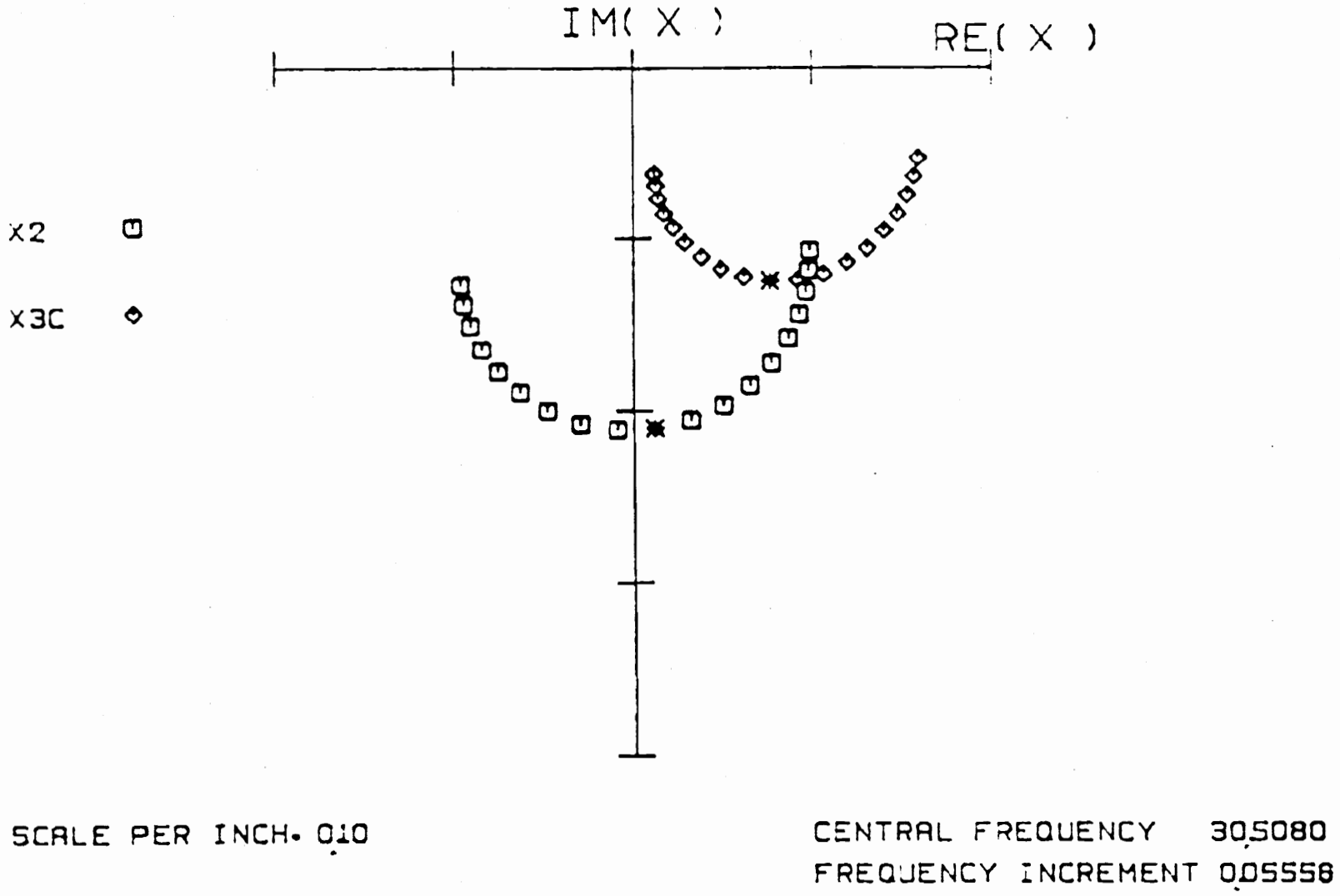

Figure 43. Co-quad Response in Mode 3 for Excitation at Nodes 4 and 5.

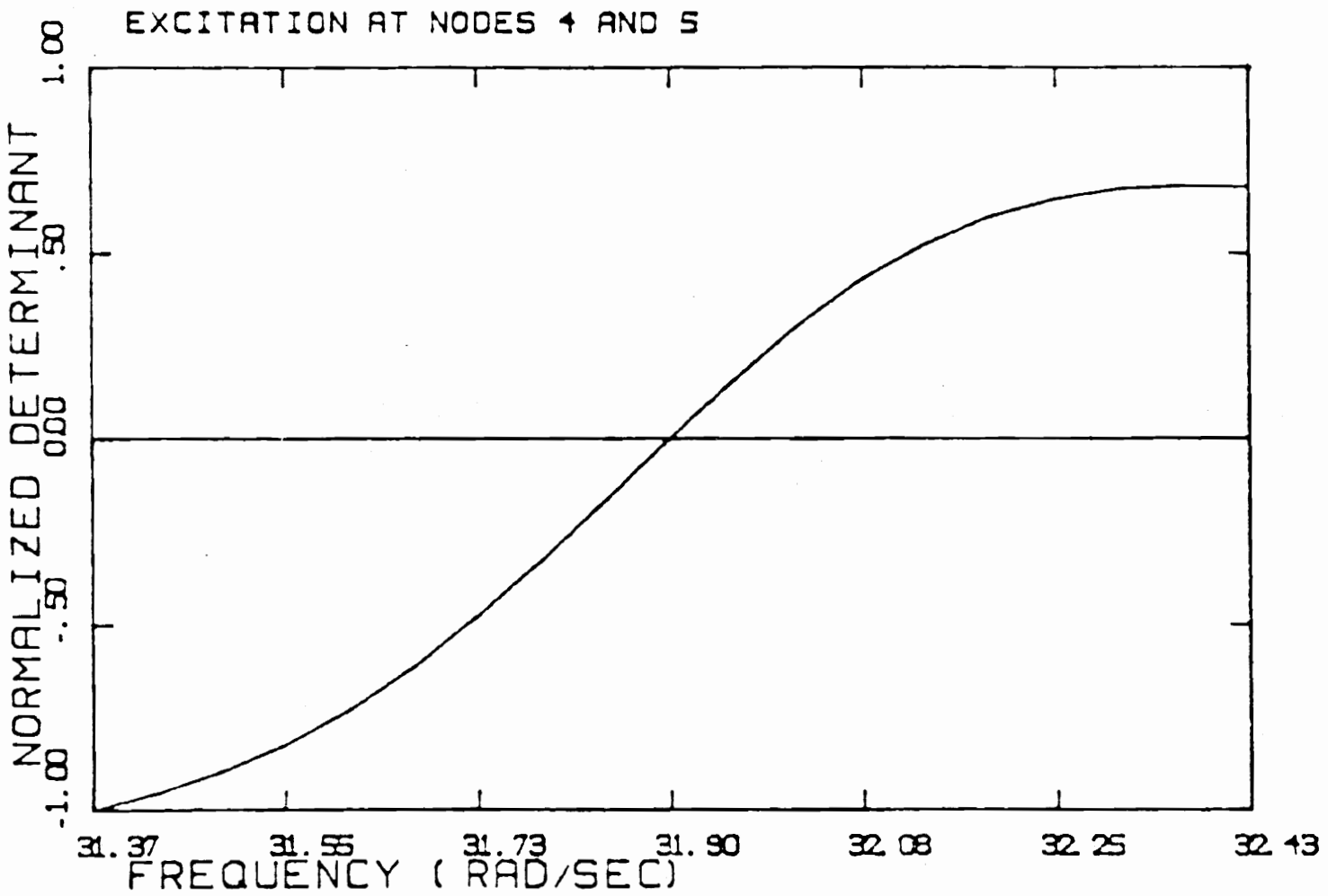

Figure 44. D(ω) for Excitation at Nodes 4 and 5, 31.37 rps. to 32.43 rps.

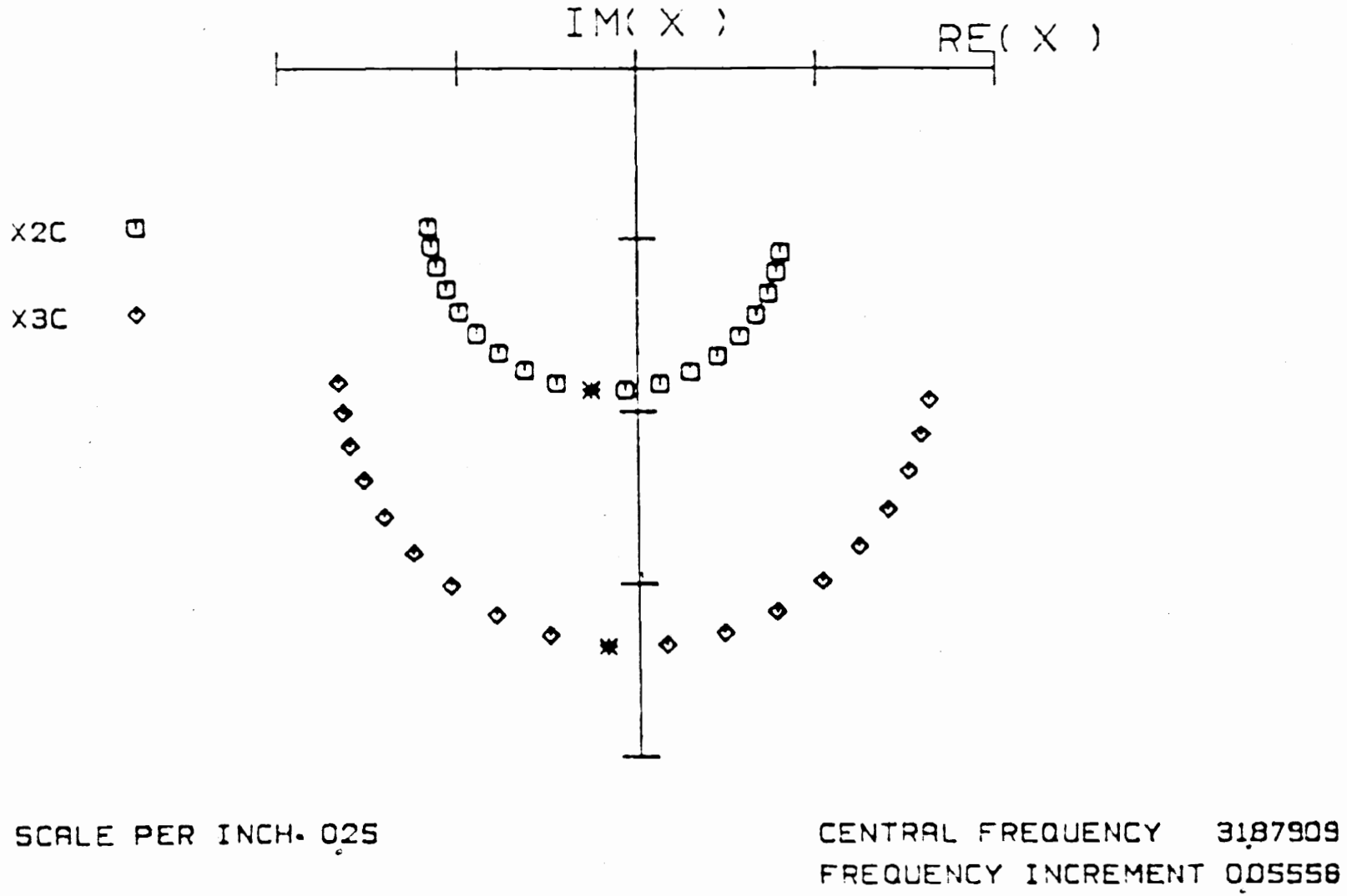

Figure 45. Co-quad Response in Mode 4 for Excitation at Nodes 4 and 5.

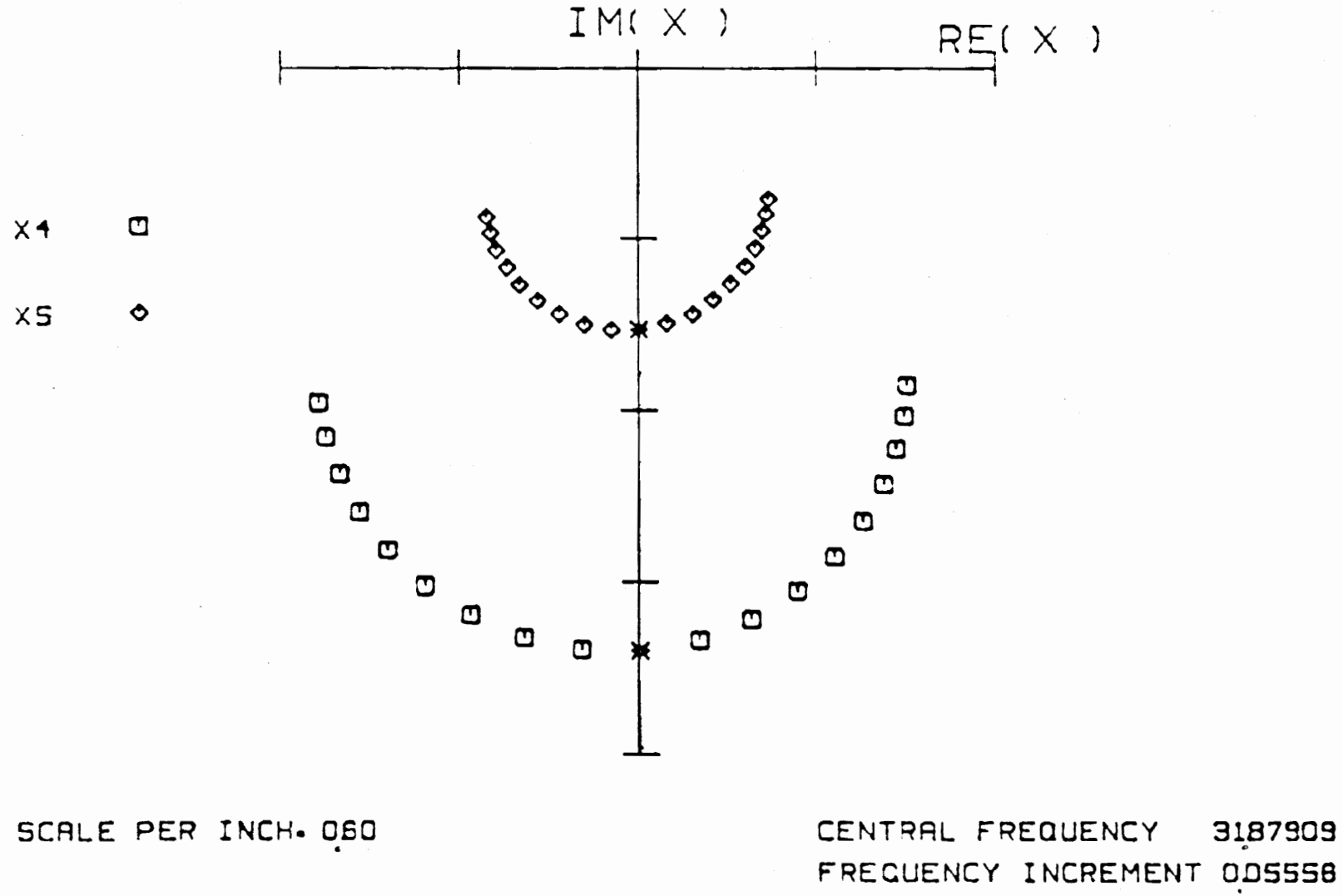

Figure 46. Co-quad Response in Mode 4 for Excitation at Nodes 4 and 5.

APPENDIX A

Description of the Computational Software Package

The programs in the software package were developed for use with the IBM Conversational Monitoring System (CMS), and were written in the FORTRAN IV programming language, for use with the FORTRAN LEVEL G compiler. To provide for the best possible use of CMS, and to provide the maximum in user program control, the software was designed to incorporate interactive input of data and operational instructions. This allows the user to determine certain important data during the actual computations, and to supply the data to the program with the aid of written instructions which inform the user of the data required. In addition, the interactive nature of the programs allows the user to evaluate the computed data and then to make a decision of whether more computations, or a certain operation is desirable.

The program RMSYS calculates the natural frequencies and the normalized mode shapes of the structure, and with this data, generates the generalized mass and damping matrices. The program requires the input of the mass and stiffness matrices of the structure, and the constants of proportionality which define the damping matrix. These constants are defined in Equation 9 of Section II. RMSYS uses a general eigenvalue solution routine to solve the free vibration equation of motion, given in Equation 4, for the natural frequencies and mode shapes. The program then uses Equations 7 and 10 to generate the generalized mass matrix and the generalized damping matrix. The output of the program includes the generalized mass and damping

matrices, the natural frequencies, and the normalized mode shapes of the system. This data is used as input for the program VIBE.

The program VIBE determines the response characteristics of the structural system under forced excitation. Included in these characteristics are the resonant frequency and the force-amplitude distribution for each mode of the structure while under excitation at a given number of degrees of freedom. Also, the coincident and quadrature displacement response and the modal energy ratios for each mode are calculated. With the input from the RMSYS program, VIBE uses Equation 18 to calculate the transfer function matrix at each frequency in a wide-band sweep. The normalized determinants of the transfer function matrices are calculated using procedures discussed in Appendix B, and the determinants are plotted as a function of frequency. This plot indicates the resonant frequency values at the crossings of the zero-determinant axis. The program then establishes the exact value of the zero-crossing frequencies with a convergence procedure, which is described in Appendix B. With the frequency value determined, the program uses an eigenvector solution routine to solve Equation 16 for the force-amplitude distribution vector. The force vector is then used in Equation 14 to calculate the coincident and quadrature response for a narrow-band frequency sweep around the resonant frequency, and the response is plotted in an Argand plane plot for use in the determination of modal quality. The force vector is also used in Equation 25 to determine the generalized response amplitude, which is used in Equations 27 and 32 to determine the modal kinetic and potential energies, respectively. The output of the VIBE

program includes the resonant frequencies, the corresponding force amplitude distributions, the modal energy ratios, the co-quad response data, the transfer function matrices at resonance, and the coincident determinant and co-quad response plots.

The program MODE is not a direct part of the software package which was developed to perform the modal computations, but is a program intended to perform a necessary support function. MODE was designed to alter a structure in order to develop a new structure which will have at least two closely spaced modes. The program uses the frequency derivative with respect to mass, which is calculated in Equation C-11, to estimate the change in mass which will cause two frequency values to become more closely spaced. The program uses an iterative process to estimate the frequency change with a change in mass and then to calculate the actual natural frequency and mode shape data for the altered structure. This procedure is continued until two closely spaced modes are obtained, and then the generalized modal data is calculated. The input and output of this program are exactly the same data as was described for the RMSYS program.

APPENDIX B

A. Normalization of the Coincident Response Determinant

The calculation of the coincident response determinant presents computational problems because of the tendency to produce overflows or underflows when determinants of large order are evaluated. Although a five-degree-of-freedom model was used in this study, the software is designed to handle much larger systems. It was necessary therefore to normalize not only the value of the determinant, but also the actual transfer function matrix used in the calculation of the determinant.

For a given frequency, ω_j, within the wide-band sweep, the transfer function matrix, $[A_R]_j$, is calculated. This matrix is then examined for the element with the largest absolute value, $(a_{max})_j$, and the matrix is normalized to this value.

$$[(A_{R\ norm})]_j = (1/(a_{max})_j\ [A_R]_j \tag{B-1}$$

The determinant of this normalized matrix is then calculated using the Banachiewicz-Cholesky-Crout method, as described in Korn and Korn (Reference 10),

$$D_j = [(A_{R\ norm})]_j \tag{B-2}$$

This entire procedure is repeated for all of the frequencies in the wide-band sweep.

With the maximum values of the transfer function matrices and the corresponding determinants of the normalized matrices calculated, the

largest absolute value in the set of matrix element maximums, a_{max}, is determined, and the corresponding determinant is defined to be the maximum determinant, D_{max}. Then the intermediate values of normalized determinant, $(D_{norm})_j$, are calculated

$$(D_{norm})_j = ((a_{max})_j/a_{max})^n(D_j/D_{max}) \quad , \tag{B-3}$$

where n is the order of the coincident response determinant. The determinants defined by Equation B-3 are then normalized to the largest absolute value for use in a coincident response determinant plot as a function of the frequency.

B. Isolation of the Resonant Frequency

The exact value of the resonant frequency indicated by the zero-crossing of the determinant plot is seldom included in the frequency values of the wide-band sweep. In order to determine the exact value of the resonant frequency, a forward difference Newton-Raphson convergence procedure is used. The frequencies on each side of the zero-crossing are located by the sign change of the determinant, and these frequencies are used as the starting point for the convergence procedure.

Using the two starting frequencies and corresponding determinants, the slope of the crossing, D', is calculated by

$$D' = (\omega_j - \omega_{j-1})/(D_j - D_{j-1}). \tag{B-4}$$

The slope is then used in the calculation of the next frequency to be used in the convergence procedure

$$\omega_{j+1} = \omega_j - (D_j/D'). \qquad \text{(B-5)}$$

Then the normalized determinant of the transfer function matrix for this frequency is calculated using the procedure described in Part A. The calculation of the local slope, the frequency, and the determinant is continued until either the determinant or the frequency change approaches sufficiently close to zero.

APPENDIX C

Frequency Derivative Derivation

In order to establish the desired closely spaced modes, it was necessary to make changes in the structure. These changes could be made in the size of the mass at certain nodes, or they could be made in the characteristics of the beams. The beams might be altered in the length, or the cross-section, or the material used. Both of these types of changes would effect the natural frequencies of the system. The simplest alteration would be in the mass values, as these values are used directly in the eigenvalue solution of the equations of motion. The use of the stiffness parameters would be more difficult because the process for establishing the stiffness matrix is fairly complicated, and more so in this case because of the condensation procedure. It was therefore decided that the alteration of the natural frequencies would be accomplished using changes in the mass values.

Alteration of the mass values in order to force closely spaced modes requires some form of analytic approximation to study the effects of the mass changes without actually solving the eigenvalue problem. Using the equations of motion for the free vibration system, an evaluation of the derivatives of the frequency with respect to the mass, as described by Zarghamee (Reference 11), was found to yield a reasonable linear approximation of the effect of the mass change on the frequency.

Beginning the calculations with the fundamental equation for the j^{th} natural mode of the system,

$$(-\omega_j^2)\ [m]\ \{\phi\}_j + [k]\ \{\phi\}_j = \{0\}\ , \tag{C-1}$$

and evaluating the derivative of the equation with respect to one mass element, m_i, a usable equation results.

$$-2\ \omega_j\ (\partial\omega_j/\partial m_i)\ [m]\ \{\phi\}_j - \omega_j^2\ [\partial m\ /\partial m_i]\ \{\phi\}_j$$

$$- \omega_j^2\ [m]\{\partial\phi/\partial m_i\}_j + [k]\ \{\partial\phi/\partial m_i\}_j$$

$$+ [\partial k/\partial m_i]\ \{\phi\}_j = \{0\}. \tag{C-2}$$

It is clear that the stiffness matrix is not a function of the mass values, therefore

$$[\partial k/\partial m_i]\ \{\phi\}_j = \{0\}\ . \tag{C-3}$$

Introduce several useful matrix relations.

$$[-\omega_j^2\ [m] + [k]]\ \{\phi\}_j = \{0\}\ , \tag{C-4}$$

$$\{\phi\}_j^T\ [-\omega_j^2\ [m] + [k]]^T = \{0\}^T \tag{C-5}$$

$$[-\omega_j^2\ [m] + [k]] = [-\omega_j^2\ [m] + [k]]^T \tag{C-6}$$

$$\{\phi\}_j^T\ -[\omega_j^2\ [m] + [k]] = \{0\}^T \tag{C-7}$$

Pre-multiplying Equation C-2 by $\{\phi\}_j^T$, and applying the matrix relations of Equations C-4 through C-7, results in a derivative equation

in the form

$$(-2\omega_j)\ (\partial\omega_j/\partial m_i)\ \{\phi\}_j^T\ [m]\ \{\phi\}_j\ -$$

$$\omega_j^2\ \{\phi\}_j^T\ [\partial m/\partial m_i]\ \{\phi\}_j\ =\ 0\ . \qquad \text{(C-8)}$$

Since the mass elements are independent, the derivative of the mass matrix with respect to a certain mass element will yield a matrix with only one non-zero unit element. Therefore,

$$\{\phi\}_j^T\ [\partial m/\partial m_i]\ \{\phi\}_j\ =\ \{\phi_i\}_j^2\ . \qquad \text{(C-9)}$$

Substituting Equations C-9 and 7 into Equation C-8, the derivative of the frequency with respect to a mass element is easily derived.

$$(\partial\omega_j/\partial m_i)\ (-2\omega_j)\ M_j\ -\ \omega_j^2\ \{\phi_i\}_j^2\ =\ 0 \qquad \text{(C-10)}$$

$$\partial\omega_j/\partial m_i\ =\ -\ (\omega_j/2)\ \{\phi_i\}_j^2/\ M_j \qquad \text{(C-11)}$$

Having defined an expression for the derivative of a natural frequency value with respect to a given mass element, the results can be applied to finite alterations in the mass to approximate the effect of such changes on the natural frequencies.

VITA

The author was born in Syracuse, New York, on January 20, 1952, and is one of two children. He received his secondary education in a parochial high school in South Amboy, New Jersey, graduating in June of 1970.

That June he entered Virginia Polytechnic Institute and State University. He graduated with a Bachelor of Science degree in Aerospace and Ocean Engineering in June of 1974. In June of that year he joined the Aerospace and Ocean Engineering Department at the same university as a graduate student.

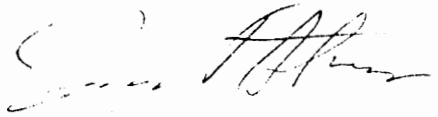

A NUMERICAL SIMULATION OF MULTIPLE-SHAKER MODAL TESTING

by

Joseph F. Stafford

(ABSTRACT)

A system of software has been developed for the simulation of structural dynamic modal testing by the method of steady-state sinusoidal excitation by discrete shakers. An analytical method commonly known as Asher's Method was employed to optimize the shaker force-amplitude distributions for the purpose of isolating individual modes of vibration. The method involves the use of transfer functions of the structure to determine the natural frequencies and force-amplitude distributions. Each force-amplitude distribution was used in the calculation of the coincident and quadrature displacements for the associated modes of vibration. Narrow-band frequency sweeps were used to determine the purity of isolated modes through the use of coincident-quadrature response plots in the Argand plane. In addition, modal energies of partially isolated modes were examined for the effects of interfering modes, again as a measure of modal purity.